

Addis Ababa University

College of Natural and Computational Sciences

School of Earth Sciences

Evaluation of Remote Sensing Based Surface Energy Balance System (SEBS) Algorithm for Estimation of Evapotranspiration in Eastern Ethiopia

A Thesis Submitted to the School of Graduate Studies of Addis Ababa University, for Partial Fulfillment of the Requirements for the Degree of Master of Science in Remote Sensing and Geoinformatics

By

Getachew Workineh

Advisor – Dr. Getachew Berhan (PhD)

Co-advisor – Dr. Dessie Nedaw (PhD)

May 30, 2016

Addis Ababa

CERTIFICATION

This is to certify that the thesis entitled as ***Evaluation of Remote Sensing Based Surface Energy Balance System (SEBS) Algorithm for Estimation of Evapotranspiration in Eastern Ethiopia*** is an authenticated work carried out by Getachew Workineh under our guidance and supervision. This is the actual work done for the partial fulfillment of the award of the Degree of Master of Science in Remote Sensing and Geoinformatics from Addis Ababa University, Addis Ababa.

Dr. Getachew Berhan
Signature_____
Department of Earth Science
Addis Ababa University
Addis Ababa
Date: May 2016

Dr. Dessie Nedaw
Signature_____
Department of Earth Science
Addis Ababa University
Addis Ababa
Date: May 2016

Addis Ababa University

School of Graduate Studies

This is to certify that the thesis prepared by Getachew Workineh entitled as ***Evaluation of Remote Sensing Based Surface Energy Balance System (SEBS) Algorithm for Estimation of Evapotranspiration in Eastern Ethiopia*** is submitted in partial fulfillment of the requirements for the Degree of Master of Science in Remote Sensing and Geoinformatics complies with the regulations of the university and meets the accepted standards with respect to originality and quality.

Signed by the Examining Committee:

Dr. Getachew Berhan	_____	_____
Advisor	Signature	Date
Dr. Dessie Nedaw	_____	_____
Advisor	Signature	Date
_____	_____	_____
Chairman	Signature	Date
_____	_____	_____
Examiner	Signature	Date
_____	_____	_____
Examiner	Signature	Date

Acknowledgements

At this moment I am indebted to acknowledge people who contribute to realize this study. Firstly, two of my advisors Dr. Getachew Berhan (major study advisor) and Dr. Dessie Nedaw (co-advisor) have been with me to provide constructive comments and insights on overall thesis process starting from proposal development to final draft submission.

Without financial support I got from German Academic Exchange (DAAD) it is impossible for me to cover my stepident and tuition fee to have fellowships in Addis Ababa University and accomplish this study. For applying DAAD in-country scholarship, the contribution of my sister Zegeyesh Taye, it is time to thank her who has helped me through relentless advice and appreciation. Efrem Armide (Zeki) you have been together with me from the very beginning to accomplishment of this study through securing me housing and other costs in Addis, thanks too much! I am also indebted for Mr. Gedamu Amare and Mr. Getachew Bayable for their contribution during the course work and research proposal development.

In due course of the study, my wife Estehiwote Aynalem is with me through shouldering overall responsibility of managing our home. Thanks sweet heart!

Then Ethiopian National Meteorological Service Agency for providing me meteorological data, NASA earth observation center who avail MODIS and land data assimilation datasets and European space agency to freely let me access surface energy and evapotranspiration product that I utilized for ET modeling and comparative analysis respectively. I want to thank school of Earth Sciences and Remote Sensing and Geoinformatics stream staff members for securing lab facility and unreserved support respectively. Am also indebted to thank my teacher Mr. Gezu Shimelse for comments on proof read of the thesis. Lastly, not least, I always acknowledge unreserved inspirations and collaboration I receive from my friends. Really they are niece academic people of whom ever I met.

Abstract

The basic objective of this study is evaluating remote sensing based SEBS model to estimate evapotranspiration in eastern Ethiopian landscape. The study has utilized cloud free MODIS level 1B images for dry season and other composites for wet season analysis. In the preprocessing phase raw MODIS scenes are converted to reflectance and radiance; brightness temperature is estimated; water vapor is estimated using ratio technique and atmospheric correction is undertaken by using SMAC model. After these, bio-physical parameters for SEBS model are estimated. Integration of these datasets with downward surface short web flux energy, sun-satellite geometry data and other meteorological data, surface energy fluxes and ET have been estimated. For comparative analysis, ET is estimated from 18 ground based meteorological observations using FAO-PM technique and composited Meteosat Second Generation (SAF MSG) ET product is utilized. Results have showed that in study site at the dry season SEBS model yields mean ET values that range from 3.74(±1.54) to 4.05(±1.72) mm day^{-1}. At the summer season, mean ET values range from 2.9(±1.7) to 3.8(±2.2). These values vary across the land cover classes in the study area. Undertaken comparative analysis showed that SEBS model underestimates ET value than FAO-PM and overestimates ET value than SAF MSG ET product. Though this is a general trend, there exist hybrid pattern in different parts of eastern Ethiopia. In the dry season, SEBS brought proxy values with FAO-PM and SAF MSG products at areas that have better vegetation cover. In most arid and semi-arid expanses of the study site, SEBS has brought extremely underestimated values than FAO-PM values while with SAF MSG, there is better coinciding values though not with similar manner. In the summer season, with advent of vegetation greenness regeneration following summer rain, SEBS model has brought values greater than dry season estimates in arid and semi-arid environment. The model is also sensitive for aerodynamic roughness length derivations. Therefore, the study can argue that though SEBS provide good ET estimates, it can be affected by vegetation characteristics and aerodynamic roughness length derivations. Accordingly, comparison of SEBS results with direct measurements, precautions while deriving roughness length and further model sensitivity study for other model inputs is recommended.

Key words: SEBS model, Evapotranspiration, Remote sensing, FAO-PM, Eastern Ethiopia

TABLE OF CONTENTS

Acknowledgements i

Abstract ii

TABLE OF CONTENTS iii

LIST OF TABLES vi

LIST OF FIGURES vii

LIST OF ACRONYMS viii

CHAPTER I: INTRODUCTION 1

1.1. Background 1

1.2. Statement of the Problem 2

1.3. Objective of the Study 4

1.3.1. General Objective 4

1.3.2. Specific Objectives 5

1.4. Scope of the Study 5

1.5. Significance of the Study 5

1.6. Limitations of the Study 6

1.7. Organization of the Thesis 6

CHAPTER II: LITERATURE REVIEW 7

2.1. Concept of Evapotranspiration 7

2.2. Quantification of Evapotranspiration 7

2.2.1. Simple Empirical Models 8

2.2.2. Residual Models 8

2.2.3. Inferential Models 12

2.3. SEBS for Evapotranspiration 12

2.4. Remote Sensing Based Evapotranspiration Estimation in Ethiopian Landscape 14

CHAPTER III: Materials and Methods 17

3.1. Description of the Study Area 17

3.1.1. Location 17

3.1.2. Climate and Agro-ecology 18

3.1.3.Geology and Soils 19

3.1.4. Vegetation and Topography 20
3.2. Methods 22
3.2.2. Re-projection and Format Conversion of MODIS Level 1B Product 23
3.2.3. Raw to Radiance and Reflectance Conversion 24
3.2.4. Brightness Temperature Computation 25
3.2.5. Atmospheric Water Vapor Content Estimation 25
3.2.6. Atmospheric Correction of MODIS Level 1B Bands 27
3.2.7. SEBS Model Biophysical Input Variables Parameterization 29
3.2.8. Estimation of Evapotranspiration & Surface Energy fluxes 32
3.2.9. Estimation of Reference Evapotranspiration by FAO-Penman Method 37
3.2.10. Spatial Interpolation of FAO Penman-Monteith by Ordinary Kriging 38
3.2.11. Comparative Analysis of SEBS and FAO-Penman ET Results 39
CHAPTER IV: RESULTS AND DISCUSSION 43
4.1. Preprocessing Phase Results 43
4.1.1. Surface Reflectance Characteristics 43
4.1.2. Brightness Temperature 44
4.1.3. Water Vapour Content 44
4.1.4. Analyzing Impacts of Atmospheric Correction 46
4.2. Analysis of Derived Variables for SEBS Model 49
4.2.1. Surface Albedo 49
4.2.2. Normalized Difference Vegetation Index (NDVI) 53
4.2.3. Leaf Area Index (LAI) 55
4.2.4. Surface Emissivity 56
4.2.5. Surface Temperature 57
4.2.6. Fraction of Vegetation Cover 61
4.3. SEBS Based Energy Fluxes and Evapotranspiration 62
4.3.1. SEBS Based Energy Fluxes 62
4.3.2. SEBS Based Evaporative Fraction 65
4.3.3. SEBS Based Daily Evapotranspiration 68
4.4. SEBS Model Results Comparative Analysis 74
4.4.1. FAO-Penman Evapotranspiration 74
4.4.2. MSG Evapotranspiration 75

4.4.3. Comparative Analysis of SEBS Model Results 79
4.4.4. SEBS Model Sensitivity Analysis 84
CHAPTER V: CONCLUSION AND RECOMMENDATIONS 87
5.1. Conclusion 87
5.2. Recommendations 89
References 91
APENDICES 111

LIST OF TABLES

3.1:	Description of selected meteorological stations	23
3.2:	Radiance bands and associated weighting functions	27
3.3:	Emissivity computations across different land cover characteristics	31
3.4:	Land cover classes and associated roughness length values	34
4.1:	Mean brightness temperature of MODIS band 31 and 32	44
4.2:	Descriptive statistics of Atmospheric water vapour	45
4.3:	of SMAC model on MODIS reflectance bands	47
4.4:	Statistical test of SMAC model impacts on MODIS reflectance bands	49
4.5:	Descriptive statistics of surface albedo across study area	50
4.6:	Descriptive statistics of LAI of the study site	55
4.7:	Association of NDVI and fraction of vegetation cover with LAI	56
4.8:	Correlation matrix to show association of land surface temperature with other surface parameters	58
4.9:	Mean land surface temperature across different land cover classes	59
4.10:	Surface energy fluxes at the study site	63
4.11:	Energy fluxes across different land cover classes	64
4.12:	Descriptive statistics of SEBS based evaporative fraction	66
4.13:	Mean evaporative fraction at different land covers classes	67
4.14:	Descriptive summary of SEBS based daily evapotranspiration	68
4.15:	Descriptive statistics of MSG evapotranspiration	76
4.16:	Correlation analysis of SEBS model results with FAO-PM and SAF ET values	82
4.17:	Sensitivity of SEBS model for land cover related inputs	85
4.18:	Statistical test for SEBS model sensitivity analysis	86
4.19:	SEBS model sensitivity for aerodynamic roughness length across land cover class	88

LIST OF FIGURES

3.1:	Location map of the study site in Ethiopia national boundary	17
3.2:	Land cover characteristics of the study area	21
3.3:	Methodological flowchart of the research process	42
4.1:	MODIS surface reflectance characteristics across different land cover class	43
4.2:	Amount of atmospheric water vapour (gm cm^{-2}) of the study site	46
4.3:	Impacts of SMAC model on MODIS reflectance bands	48
4.4:	Surface albedo characteristics	51
4.5:	Surface albedo characteristics across land cover characteristics	52
4.6:	NDVI characteristics across land cover class	53
4.7:	Spatio-temporal characteristics of NDVI at the study site	54
4.8:	Variations of surface emissivity across land cover classes	57
4.9:	Land surface temperature variability in the study site	60
4.10:	Fraction of vegetation cover of study site for different DOY	62
4.11:	Interaction of H and LE across different land cover class at different DOY	65
4.12:	SEBS based daily evaporative fraction of the study site	67
4.13:	Histogram showing pattern of evapotranspiration in the study site	70
4.14:	Spatial characteristics of SEBS based evapotranspiration	71
4.15:	Daily SEBS based mean evapotranspiration across different land cover classes	72
4.16:	*In-situ* based FAO-PM evapotranspiration in mm d^{-1}	75
4.17:	SAF MSG based evapotranspiration value across land cover classes	77
4.18:	Figure 5.19: SAF MSG based evapotranspiration of the study site	78
4.19:	Point based comparison of SEBS ET with SAF MSG & FAO-PM for dry season	79
4.20:	Comparison of randomly selected SEBS, FAO-PM and SAF MSG ET	82
4.21:	Comparative analysis of SEBS with FAO-PM results in June 15, 2015	84

LIST OF ACRONYMS

AERONET	Aerosol Robotic Network
ATCOR	Atmospheric and Topographic Correction Model
CSA	Central Statistical Agency
ESA	European Space Agency
DOS	Dark Object Subtraction
DNs	Digital Numbers
Etcalc	Evapotranspiration Calculator
EDRI	Ethiopian Development Research Institute
ESA	European Space Agency
IFPRI	International Food Policy Research Institute
FAO-PM	Food and Agricultural Organization-Penman Monteith
GLDAS	Global Land Data Assimilation System
HDF	Hierarchical Data Format
HDISC	Hydrologic Data Disc
NMSA	National Metrological Service Agency
IIRS	Indian Institute of Remote Sensing
ILWIS	Integrated Land and Water Information System
LAI	Leaf Area Index
LISS	Linear Imaging Self Scanning Sensor
LSA	Land Surface Analysis Facility
MODIS	Moderate Imaging Spectrometer
MRTSwath	MODIS Reprojection Tool Swath
MoARD	Ministry of Agriculture and Rural Development
MSG	Meteosat Second Generation
MSGToolbox	Meteosat Second Generation Toolbox
NASA	National Aeronautics and Space Administration
NWRC	National Water Resources Commission
NetCDF	Network Common Data Form
NDVI	Normalized Difference Vegetation Index
QGIS	Quantum Geographic Information System
SAF	Surface Analysis Facility
SEBS	Surface Energy Balance System
SEVERI	Spinning Enhanced Visible and Infra-Red Imager
SMAC	Simple Model for Atmospheric Correction
SRTM	Shuttle Radar Topographic Mission
TOA	Top of Atmospheric
URL	Universal Resource Locator
USAID	United States Agency for International Development

CHAPTER I: INTRODUCTION

1.1. Background

An estimated result of evapotranspiration is reported as basic input for regional and global water balance and primary productivity study models (Vorosmarty, *et al*., 1998; Ruhoff *et al*., 2014) and assessment of carbon dioxide assimilation in to biosphere (Jasechko *et al*., 2013). Annually as provided in Trenberth *et al*. (2006), evapotranspiration demands 73,000 km^3yr^{-1} amount of water. In precipitation deficit areas it causes water stress by consuming more than 90% of radiative energy reaching the surface (Jasechko *et al*., 2013). As it was presented in Ukkola and Prentice (2013), though it varies with climatic situation and surface characteristics, considerable amount of water is lost through evapotranspiration. Globally, 60% of precipitation reaching the surface is consumed by evapotranspiration (Bala *et al*., 2013). In some parts of global arid environment, loss of water via evapotranspiration accounts greater than 90% of precipitated water. According to Zhang *et al*. (2010) on their analysis accounts from 1983 to 2006, globally terrestrial ecosystems account long-term annual average of 539.3 mm yr^{-1} evapotranspiration rate with error deviance of 9.1 mm yr^{-1}. In some climatic conditions and surfaces like water body and tropical forest biomes it is reported as evapotranspiration exceeds 1400 mm $year^{-1}$ while global arid and semi-arid environment is reported with less amount of evapotranspiration. In Ethiopian landscape, a study done by Ketema and Merkel (2009) in Dire Dawa and its surrounding has reported as evapotranspiration consumes 75% of precipitation tipping into the surface. Similarly, in Northern Tigray Illala watershed, a study by Teklebirhan *et al*. (2012) has reported 81% evapotranspiration consumption form available precipitated water.

In some studies like Zhang (2009), because of changes in vegetation and drought episodes, there is decreasing evapotranspiration and increasing environmental stress. Therefore, characterization of space based regional evapotranspiration is a principal component of environmental evaluation in arid environment (Ma *et al*., 2014).Taking the urgency of effective water management and optimal planning for sustainable world, it demands quantitative estimation of evapotranspiration (Yang *et al*., 2014). Though, current remote sensing technology is to its fore front to accurately estimate surface energy fluxes between earth's surface, sun and the atmosphere, accurate estimation of energy flux within the surface, which is part of evapotranspiration estimation, is

still a concerted research environment as it needs the account of intricate systems in energy balance exchange (Liou & Car, 2014).

Taking its relevance in various practical fields for planning and decision making, energy balance estimations especially evapotranspiration has been made by using classical *in-situ* based observations and analysis methods. This can be practical for smaller watersheds or field level studies (SAF PUM, 2015) but for larger spatial extent it is difficult and sometimes impractical. With the advent of remote sensing, the state-of-the-art in data acquisition and analytical techniques are being sophisticated as geospatial data demanded to generate energy budget is acquired at intended pixel level. This advent of remote sensing technology has resulted in sophisticated data acquisition of surface physical, hydro-meteorological variables and surface characteristics within desired spatial extent that have improved hydrological modeling (Kumar & Reshmidevi, 2013). As a result of system complexity and utilization of different dataset, there is no a single standard measure of evapotranspiration (Wosenu & Assefa, 2013). Within the spectrum of estimation methodologies and wider available datasets that are resulted from remote sensing applications, Surface Energy Balance System (SEBS) (Su, 1999 & 2002) is found the potential methodology for estimating model variables that are used for estimating evapotranspiration (Gibson *et al*., 2013). Taking its potentialities, like its scale invariant character while yielding results with promising accuracy and incorporation of surface and aerodynamic roughness characteristics explicitly (Su, 2007), SEBS model has been reported as it is repeatedly utilized for teaching and research issues, it is also simultaneously noted its serious sensitivity that calls concerted research activity to test it under different landscapes. That is why this study is undertaken in eastern Ethiopia which is a broad geographic region with diverse agro-ecology and landscape.

1.2. Statement of the Problem

What signifies the relevance of this study is a wide array of practical applications that demand evapotranspiration as an input for planning and decision making. As it was summarized by Ambrose and Sterling (2014), regional scale knowledge about evapotranspiration pattern helps better understanding of hydrological, climatic and carbon cycle interactions. In addition to these, estimated evapotranspiration is used as premier variable for many practical applications like drought assessment (Wondimagegn, 2006) prediction and early warning (Tinebeb, 2012;

Tewelde, 2012), environmental stress and vegetation monitoring (Cristobal *et al*., 2011; Henok *et al*., 2014; Senay, 2015), crop growth and yield simulation (Casa & Ovando, 2012), water resources management and crop water management for irrigation (Jia *et al*., 2007), root zone volumetric soil moisture content estimation (Hain *et al*., 2009), soil and water conservation planning (Morgan, 2005), environmental water availability (Hernandez *et al*., 2014) and resource assessment (Gibson *et al*., 2009). With these range of functionalities, for a long period of time and even today, evapotranspiration is being estimated by using models that consume datasets collected from conventional *in-situ* measurements. But this is extremely tough in areas where there is *in-situ* measurement data scarcity like eastern Ethiopia. In general, as stated by Wosenu and Assefa (2013) and specific to Ethiopian case (Tenalem, 2003), remotely sensed distributed hydrological models are recommended tools to estimate evapotranspiration in areas where there exists scarcity of *in-situ* hydro-meteorological variable observation or completely impractical to measure.

The basic argument why this study is proposed and done in eastern Ethiopia is that, the study area is characterized by diverse vegetation, climatic and topographic pattern, but still there is no any predictive study undertaken that can quantify evapotranspiration conditions except at some northern extension of the study site (southern part of Awash watershed). In other way, though there are various concerted studies that have utilized other evapotranspiration estimation models in other parts of Ethiopia, it is done only in small watershed level by using remote sensing based imagery with coarse temporal resolution which is difficult for frequent monitoring of evapotranspiration. Though it is difficult to put concrete limitations of these studies, it can be certain to claim as because of coarse temporal resolution they utilize, it hinders their applicability for practical applications that demand daily or dekadal data sets like drought monitoring, vegetation growth and stress assessment and crop water requirement at different growth stages. In addition to these, as it was recommended by Li *et al*. (2008) and further claimed by McCabe and Wood (2006), in places where there is no significant vegetation contrasts (not in field or small watershed scale) within the broader region, MODIS data set can provide a reasonable temporal resolution for evapotranspiration and energy balance estimates at regional scale. This can resolve the drawbacks of high spatial resolution satellite datasets to provide frequent images with low cost (Liou & Kar, 2014). Contrary to this, a study by Cristobal *et al*. (2011) has claimed the drawbacks and inaccuracies in utilizing coarse spatial resolution remote sensing images for

estimation of evapotranspiration at heterogeneous landscape. Taking these contradicting arguments, this study can fill the gap at eastern Ethiopia mixed landscape by comparing SEBS model result, FAO-Penman ET and SAF LSA ET values. The basic argument why SAF MSG ET values selected for comparative analysis is their capability of generating evapotranspiration at any weather conditions even at temporal resolution less than a day (SAF ATBD, 2010) and similar aerodynamic roughness length derivation process with SEBS model.

More importantly, taking *in-situ* based meteorological data scarcity in the study site, using remote sensing based ET estimation is unquestionable choice. This is ascertained in the study site where this research is done; there are only 19 stations within the study site with full datasets used for reference ET estimation. Therefore, model evaluation for frequent evapotranspiration estimation from satellite data pixel wise is an essential task. Additionally, most parts of the study area is also reported as prone for recurrent drought and precipitation deficit (CSA *et al*. 2010) that demands critical studies to aide appropriate water resources management. Taking this into consideration, there is a need to estimate evapotranspiration from meteorological measurement stations; it demands big generalization from a single station, which might lead to biggest interpolation errors as point density has implications on accuracy (Zhang *et al*., 2015). Therefore, this study can fill the stated study gaps by assessing the applicability of SEBS model to yield proxy values with reference evapotranspiration values that are computed from sparsely measured meteorological stations within the study site. In this study we used MODIS daily levl1B images, model based meteorological parameters and *in-situ* measured meteorological variables with daily and hourly temporal resolutions.

1.3. Objective of the Study

1.3.1. General Objective

The general objective of this study was to evaluate remote sensing based SEBS algorithm for estimation of evapotranspiration at data scarce environment in eastern part of Ethiopia.

1.3.2. Specific Objectives

The specific objectives of this study are:

- To derive parameters used for SEBS algorithm from MODIS Level 1B calibrated products at regional scale
- To estimate evapotranspiration and energy fluxes using SEBS algorithm with integration of derived parameters and image based meteorological data, and
- To comparatively analyze capability of prepackaged SEBS for yielding proxy ET values with estimations from *in-situ* based PM-FAO ET and MSG ET product

1.4. Scope of the Study

The study has the following geographic, conceptual and methodological scopes. Geographically it encompasses broader eastern Ethiopia characterized by diverse climatic, topographic and vegetation characteristics. Conceptually, the study has re-circulated on concepts related with surface energy balance, evapotranspiration, remote sensing and spatial statistics. Methodologically, the study has integrated remote sensing based SEBS algorithm with FAO-PM ET estimation technique while incorporating statistical methods to claim final inferences claimed by the study.

1.5. Significance of the Study

If the need arises for utilization of evapotranspiration in daily practical applications in regional scale in areas like eastern Ethiopia, where there exist acute *in-situ* meteorological observation data scarcity, remote sensing based applications are prime choices. Actually there are wide array of remote sensed based ET estimation techniques that utilize a wide array of remote sensing based images as data sources. Therefore, evaluating the model performance, sensitivity and basic characteristics is mandatory as it can provide a clue on model outputs. In case of regional estimations like this study, medium to low spatial resolution data sets are a compromise for their frequent temporal resolution to generate continuous time series ET dataset. More importantly, easy data access and storage capability also increases the relevance of these datasets.

Taking these attributes into consideration, this study can have useful results that are useful for water resource management, drought monitoring, crop water requirements and resource assessment in regional scale that utilize evapotranspiration by reporting SEBS model performance. More importantly, it has tested the capabilities and stated sensitivities of SEBS

model for land cover related roughness length inputs and have thought cautions and operational ways taken into consideration while estimating evapotranspiration by using SEBS model. Therefore resource assessors, water based spatial planners and researchers can be beneficial from outputs of this study.

1.6. Limitations of the Study

While reading the outputs of this study, it should be noted that the study has the following limitations. For estimation of summer season evapotranspiration, it has utilized dekadal composites rather than daily level 1B products. These can have an implication on the quality of summer season SEBS model results as errors introduced in compositing and processing of decadal products can propagate. In addition to these, for solar zenith angle utilized there is found a gap between two consecutive MODIS swaths for geolocation files. After mosaic process it has been filled with average values. This can have also little implications of summer season SEBS model outputs.

1.7. Organization of the Thesis

The report is organized into five chapters. At the first chapter, introductory issues about the problem and justifications why the study is intended, respective objectives and research questions were presented. Scope and significance is also part of introductory chapter. At the second chapter basic conceptual and empirical literatures are reviewed to provide a clear understanding of the problem under investigation, raise issues that previous empirical studies have claimed and identify what is a real gap in the selected study site where this study has been done. In chapter three, detailed overview about the study area and methods are detailed. At chapter four methodological process adopted for the study has been tried to be presented. In chapter five, results of the study is presented with analysis and discussion by integrating findings of previous studies. Chapter six presents conclusions and recommendations of the study. In addition to stated components, this thesis is also comprised with some ancillary sections like list of tables, list of acronyms, acknowledgement and lists of reference materials cited in the study.

CHAPTER II: LITERATURE REVIEW

2.1. Concept of Evapotranspiration

Evapotranspiration is the simultaneous loss of water from the ground, open water surface and vegetation with the account of available energy and moisture (Allen *et al*., 1998). Though similar definition is brought by Oliver (2005), it has been tried to conceptualize evapotranspiration into potential and actual states. Potential evapotranspiration is a combined amount of maximum water loss if sufficient moisture and energy is assumed with consideration of atmospheric and vegetative characteristics (Yang, 2015) while actual one is observed amount of water loss under existing conditions. In most real cases, actual evapotranspiration less than potential evapotranspiration and it is rare case where actual and potential evapotranspiration is equal. As evapotranspiration is combined state, it is governed by various environmental variables like energy and moisture availability, vegetation characteristics that is plant type and growth stage and rate of turbulent diffusion further influenced by aerodynamic characteristics of wind (Balogun, 1974) and management and environmental conditions (Allen *et al*., 1998). More importantly, it is also controlled by available energy reaching the surface and atmospheric characteristics like temperature and specific humidity (Petropoulos *et al*., 2014). During characterization of evapotranspiration, it is difficult to explicitly identify either it is evaporation or transpiration especially from surfaces with different level of vegetation cover (Wang *et al*., 2011). A study that has been undertaken exclusively on rate of land evaporation by Harris and Robinson (1916) has claimed amount of available moisture, soil capillarity and texture, wind speed up to some gradient, duration of exposure for sun energy and net radiation and soil salinity are found the determining critical factors.

2.2. Quantification of Evapotranspiration

According to Wosenu and Assefa (2013), there are two methods of quantifying evapotranspiration. These are measurement and estimation. As detailed in Petropoulos *et al*. (2014) evapotranspiration can be directly measured through evaporation pans, atmometers, evapotranspirometers and lysimeters while indirectly it can be measured through methods like Bowen Ratio, Eddy Covariance and sentilometres. Because of the basic theme of this study is on remote sensing based estimation of evapotranspiration, at this review section due emphasis has given for estimation techniques. By considering data requirements and estimation process into

account, Wosenu and Assefa (2013) have elicited a number of mechanisms into three groups, *viz*, simple methods, complex and remote sensing based methods. As it is clearly stated in Courault *et al*. (2003), estimation of evapotranspiration is vested in partitioning of energy balance terms in order to estimate latent heat of flux which is energy left to initiate evapotranspiration.

With sophistication of remote sensing based techniques and continuous research in evapotranspiration estimation, there is plethora of estimation mechanisms that use different models with respective assumptions. In some studies like Li *et al*. (2009) and Nouri *et al*. (2013), for simplicity of having comprehensive overview on mechanisms estimation, models are segregated into three classes. These are simple empirical methods, residual techniques and indirect inferential approaches. The basic difference of these mechanisms is based on their model assumptions, data requirement and the way how they derive sensible heat flux after deriving surface and aerodynamic characteristics and surface temperature gradient (Karimi & Bastiaanssen, 2015).

2.2.1. Simple Empirical Models

Simple empirical methods or regression based models assume that evapotranspiration can be estimated by considering surface and near surface atmospheric temperature gradients (Li *et al*., 2009). As it was clearly stated in Kalma *et al*. (2008), basically evapotranspiration is estimated by accounting daily latent heat flux and net radiation coupled with temperature gradients. As it was provided by Nouri *et al*. (2013), while considering temperature gradient as principal model variable, they also utilize surface characteristics that influence energy partitioning like albedo, fraction of vegetation cover and leaf area index. At this continuum of modeling approach, surface is considered as single layer and multiple layers especially for soil surface where its gradient can affect amount of evapotranspiration (Wang *et al*., 2011).

2.2.2. Residual Models

Residual methods estimate evapotranspiration as residual of energy (net radiation) partitioning into sensible heat flux, latent heat flux and soil heat flux that accounts the remaining energy consumed to evaporate that amount of water. As it was clearly reviewed in Li *et al.* (2009), residual techniques were also divided into single source and two source models based on the assumption they propose the surface resistance while generating sensible heat flux. This also entails the way how surface resistance is assumed and parameterized (Barbagallo *et al*., 2009).

Single source models assume the surface as uniform without segregating energy budgets of canopy and soil alone while dual source models consider vegetation height and canopy characteristics in affecting aerodynamic roughness characteristics by creating double resistance surface.

Among single source residual evapotranspiration models, Surface Energy Balance for Land (SEBAL), Surface Energy Balance Index (SEBI), Simplified Surface Energy Balance Index(S-SEBI), Surface Energy Balance System (SEBS) and Mapping Evapotranspiration at High Resolution with Internalized Calibration (METRC) are prominent ones. Even these models are also under similar continuum of single source models, they are also greatly varied in terms of data demand, on model assumption and mechanisms how they derive sensible and latent heat fluxes. Based on comparative analysis brought in Wossenu and Assefa (2013), METRIC and SEBAL model derive sensible heat flux from the surface and near surface temperature gradient by assuming it as uniform even in heterogeneous surfaces while they vary in terms of their assumption on selecting and valuing hot and dry anchor pixels, selection of reference evapotranspiration surface to upscale instantaneous to daily evapotranspiration values and derivation of albedo. In addition to these, SEBS varies from both by its capability to atmospheric similarity theory and surface stability parameters in an extended and explicit way (Su, 1999). According to a statement presented in Allen *et al*. (2011), though MERIC and SEBAL are relatively accurate in their estimation capacity, in comparative terms, they are highly scale variant in nature that their applicability is more of at reasonably smaller areal extent than SEBS and ALEXI model can do. Additionally, their requirements of extremely trained expertise with knowledge of vegetation characteristics, physics of radiation and high quality weather data for reference crop evapotranspiration estimation constrained their wide applicability.

More importantly, SEBS is unique from others by its ability to explicitly consider evaporative fraction at limiting cases. Roerink *et al*. (2000) have also stated unique characteristics of S-SEBI model from SEBS, SEBAL and METRIC. As per this, it generates sensible and latent heat flux solely from remote sensing based images. This is done by computing maximum and minimum temperature from reflectance values. If the model assumption is fulfilled, which is uniform climatic characteristics of the field, it is reported as the model can bring precise evapotranspiration results. As a result, it is advantageous over other methods as it does not

demand meteorological data and did not assume extreme hot and dry pixels are fixed and constant along the scene like METRIC and SEBAL. If done with good processing and iterative procedures in a sound way, it is reported extremely simpler than SEBAL model (Santos *et al*., 2010). One thing that made S-SEBI similar with SEBAL and METRIC is that, it implements the concept of evaporative fraction and anchor pixel model but it does not assume the values of anchor pixels are fixed values across the scene (Roerink *et al*., 2000; Santos *et al*., 2010). The basic assumptions of SEBAL that proposes the existence of extreme contrasts at a given field (both wet and dry places) and selective terrain characteristics (level terrain) (Li *et al*., 2009) can raise its reliability for areas with rugged topography and considerably similar climatic and vegetative characteristics.

As per detailed review provided about their assumptions, advantages and disadvantages in Li *et al*. (2009) and Liou and Kar (2014), each model has its own strengths that are familiar for specific region of interest, data demand that fits availability situations and drawbacks that hinder the utility of the model as per intended. Therefore, the utilization of any model for specific purpose depends on our centerpiece assumption we propose, surface and climatic characteristics, the data on our hand and technical capacity of the analyst while the model demands firm image analysis and statistical computing. Taking this argument into consideration, some studies have been made to test sensitivities of some models for inputs while deriving flux terms. To exemplify, Timmermans *et al*. (2013), Gibson *et al*. (2013) have made detailed investigations on sensitivity of SEBS for input variables related to land cover, aerodynamic roughness length and excess resistance for heat transfer.

As explicitly stated in Huntingford *et al*. (2000), the dual source models assume a dual characteristics of above and in-canopy resistance for heat and momentum transfer which is limitations of single source models. One of explicit model from dual source continuum is Atmospheric Land Exchange Inverse (ALEXI) that partitions surface radiance temperature into soil and in-canopy temperature (Anderson *et al*., 2007). By integrating time dependant nature of surface temperature gradient and atmospheric planetary boundary characteristics, the model has reduced the effort of collecting ancillary meteorological data related to atmospheric characteristics (Anderson *et al*. 1997). Like the SEBS model, it accounts atmospheric similarity theory to derive aerodynamic characteristics and further to compute sensible heat flux (Anderson

et al., 2011). It is also reported as resilient for temperature related noises introduced while computing time dependant temperature gradient. More importantly, it is reported as less reliant on instantaneous temperature gradient that it is found robust for evapotranspiration and surface flux determination from geostationary satellite images (Anderson *et al*., 2012). As stated by Anderson *et al*. (2011), the model has a synergistic character to utilize the better spatio-temporal capabilities found at different imagery by image fusion and sharpening method. ALEXI has also reduced errors related with atmospheric correction and surface emissivity derivation (Li *et al*., 2009). The better merit of the model especially in data scarce environments where *in-situ* measurement is impractical or dataset is inconsistent, it is ideal mechanism as it needs no meteorological data (Anderson *et al*., 2011).

Though ALEXI is reported advantageous having not demanding *in-situ* meteorological dataset, mandatorily it needs geostationary satellite observations that can image the surface at least two times per day at the morning and noon time to generate time integrated surface and atmospheric temperature gradient. This constrains its applicability at the field and watershed level unless sharpened from high spatial resolution satellite images. To overcome this limitation, spatio-temporal up-scaling of moderate and coarse resolution evapotranspiration to Landsat thermal spatial resolution scale (60 meters) can be done by Atmospheric Land Exchange Inversion Disaggregation (DisALEXI) model through integration of Landsat thermal band (Anderson *et al*., 2012). Though it does not yield reasonable intended results, the disaggregation to Landsat multispectral spatial resolution (30 meters) has been done (Anderson *et al*., 2004).

As it was claimed by Lu *et al*. (2014), dual source models have a better capability in estimating evapotranspiration in divers vegetation cover by partitioning evapotranspiration into evaporation and transpiration. While sharing similar model assumptions, a study done by Kustas (1990) has claimed the better performance of single source model under arid and semi-arid vegetative ecosystems. On extended study made by Kustas *et al*. (1996), while double source models perform sounding results in energy flux estimation both at mixed landscape and somehow uniform to moderate landscape sound, single source models fail to give reasonable results at mixed landscape with different canopy structure. Though the study claimed the better performance of dual source models, it has also showed the sensitivity of dual source model for vegetation related surface roughness characteristics which is a caution taken into consideration

while modeling energy fluxes at mixed landscape. In contradiction to this, Huntingford *et al*. (2000) and Tang *et al*. (2013) have claimed related performance of both models but in absolute terms Tang *et al*. (2013), have stated the outperformance of two source models over single source models while Huntingford *et al*. (2000) have recommended synergetic utilization of single source models for inter-comparison and model calibration. In relation to comparative analysis of performance of one and two source models, findings of Colaizzi *et al*. (2012) can brought a clue on the impact of seasonal characteristics of vegetation and surface cover. They found that the performance of stated models depends on the season and vegetation characteristics.

2.2.3. Inferential Models

The third group of remote sensing based evapotranspiration estimation is indirect or inference approach. As stated by Nouri *et al*. (2013), models under this continuum generate evapotranspiration values from vegetation coefficients and reference evapotranspiration. As it was inferential, evapotranspiration is inferred from combined vegetation characteristics and crop coefficients. A crop characteristic is generated from remote sensing based data sets while reference evapotranspiration is computed from meteorological data. Huntington and Allen (2010) have implemented indirect estimation methods with utilization of reference evapotranspiration and crop coefficient to determine actual evapotranspiration and water demanded for irrigation purpose. Though they found reliable results, the derivation process is too long. As reported by Tsouni *et al*. (2008), inferential mechanisms are claimed as they utilize complex models. The caution to be taken while utilizing inferential evapotranspiration estimation models that use crop coefficients, as was stated by Ortega-Farias *et al*. (2009) is that, many of crop coefficient values reported in literatures are derivatives of other empirical models and more of general. Therefore, unless calibrated for specific local conditions, it can cause uncertainties in derived evapotranspiration values. As these kinds of models explicitly incorporate surface roughness and stomatal resistance for heat transport which is difficult parameter, they inferred from vegetation growth stage (using concept of phonology) (Courlault *et al*., 2003).

2.3. SEBS for Evapotranspiration

Surface Energy Balance System is a model that is explicitly based on portioning of available energy that reaches the earth for physical process and estimates evapotranspiration as a residual

of these processes (Karimi & Bastiaanssen, 2015).Though there are various surface energy balance estimation models, SEBS has its own unique characteristics and propositions. As it was provided in Su (2002), basically the model needs three sets of datasets for its full functionalities. These are land surface related variables that are generated from remote sensing based data include surface temperature, emissivity, surface albedo, aerodynamic roughness characteristics fraction of vegetation cover and leaf area index; meteorological measurements taken at referrence height that include specific humidity, pressure, wind speed and temperature; and surface radiation downwelling short and longweb radiation fluxes. From these variables, dwonwelling surface energy fluxes can be either direct inputs or modeled values can be used. Taking the emanating errors and related uncertainties while modeling it is recommended to use its directly sensed or measured input (Gibson *et al*., 2013). Using the stated sets of inputs SEBS model has three basic tools to derive evapotranspiration. These are tools to parameterize surface physical variables, a model to derive surface roughness characteristics and an extended model that determines evaporative fraction at wet and dry limit (Su, 2002).

What made SEBS an appropriate remote sensing based evapotranspiration estimation technique is its ability to estimate evapotranspiration at extreme dry and wet cases in order to reduce uncertainties associated with surface temperature or other model inputs, vivid mechanism to generate surface roughness values rather than using constant values and does not need to select any anchor wet and dry pixel having prior knowledge of the area like SEBAL and MTRIC models while generating sensible heat flux (Liou & Kar, 2014). More importantly, because of SEBS is spatial scale independent (Su, 2009), it is used from small scale local field level to regional scale evapotranspiration and energy flux estimations (Jia *et al*., 2003, Jia *et al*., 2012) over heterogeneous landscape (Lu *et al*., 2012). More importantly, the model is suitable for all satellites which measure under visible, near infrared and thermal bands which increase its wide applicability to utilize a wide array of remote sensing based imagery for the intended objective (Jia *et al*., 2012). As per this Landsat Multispectral Scanner(MSS) at semi-arid Iran plateau (Matinfar & Soorghali, 2014) and Landsat Thematic Mapper and Enhanced Thematic Mapper (Liu *et al*., 2007), Advance Along Track Scanning Radiometer (AATSR) and Medium Spectral Resolution Imaging Spectrometer (MERIS) on agricultural areas of Nile delta (Elhag *et al*., 2011**)**, MODIS data at heterogeneous surface (Lu *et al*., 2012); Advanced Space borne Thermal Emission and Reflection Radiometer (ASTER) at Tibetan Plateau of China (Ma *et al*., 2014)

have estimated evaporative fraction and evapotranspiration by using SEBS model and Liang (2003) has generated land albedo parameters of the surface.

Though SEBS has been stated with stated advantages, it has also reported with some limitations. As was reviewed in Li *et al*. (2009), it needs too many parameters and complex procedures to derive sensible heat flux. It has also reported sensitivities for model inputs while generating flux terms like sensible heat flux and evapotranspiration. Among these, Gibson *et al*. (2011) have investigated sensitivity of prepackaged SEBS algorithm for surface heterogeneity and surface and near surface temperature gradient. The study has also shown the deviations occur while up-scaling instantaneous (evaporative fraction) to daily evapotranspiration which is the main game of the model. Similarly, Gokmena *et al*. (2012) have revealed as SEBS model overestimates evapotranspiration values which emanates from under estimation of sensible heat flux at arid-and semi arid environment. The study has also recommended integrated utilization of soil moisture while deriving sensible heat flux term before running SEBS model. Contrary to this, Ma *et al*. (2014), has reported reliable agreement of SEBS evapotranspiration values with ground based filed measurements in regional scale. This contradicting arguments show as there need calibration of the model output values rather than simply claiming the results.

2.4. Remote Sensing Based Evapotranspiration Estimation in Ethiopian Landscape

Though the primary intention of remote sensing evapotranspiration estimation is not model evaluation at the Ethiopian landscape, evapotranspiration has been estimated by remote sensing based models. One of detailed studies undertaken by Tenalem (2003) has implemented the SEBAL model to investigate evapotranspiration pattern at Ethiopian Central Rift Valley and adjoining highlands. The study has reported spatial variability of evapotranspiration at the study site especially by taking environmental conditions like albedo, surface temperature and surface and ground water input into the lakes, there is spatial variability in evapotranspiration even in lake water surface. The existing surface hydrological flux characteristics that include evapotranspiration and heterogeneity in surface cover characteristics are reported to affect temperature characteristics of the area (Tenalem, 2004). With comparative analysis of conventional methods and remote sensing based SEBAL model at Lake Region of Central Ethiopian Rift Valley, Assefa *et al*. (2009) have done detailed study. As per their study a SEBAL model that is ingested with Landsat datasets is reported to give reasonable results with Penman

Monteith method but SEBAL is reported to underestimate evapotranspiration at continental dry areas, which shows the need for validation after analysis of evapotranspiration from remotely sensed data.

With proximate wide area extension to the stated studies at preceding paragraph, Enku *et al*. (2014) have estimated evapotranspiration at Upper Blue Nile watershed of Fogera wetlands by using SEBS Model with integration of MODIS level 1B products and processed decadal composites. In addition to estimation of ET by using remote sensing based SEBS model, they have compared with conventional Penman Monteith (PM) evapotranspiration values as way of validating the model outputs the stated landscape. In connection to this, SEBS and PM based evapotranspiration values has shown similar trends but in wet season SEBS based values outnumber while in dry season PM based values outnumber which is attributed with soil moisture and biomass characteristics that deviate with seasonal conditions. With integration of MODIS products and ground based meteorological data sets Alebachew (2009) has estimated evaporation at Lake Tana with spatial extent less than Assefa *et al*. (2009) and Enku *et al*. (2014) studies. The study has yield reasonable values that are with proxy values of evapotranspiration as that of Penman Monteith values. When speaking in absolute terms, remote sensing based energy balance model is reported to underestimate evapotranspiration values than ground based approach. Though the prime goal of Tinebeb (2012) study is evaluation of SEBS model, it has been tried to estimate evapotranspiration by using remote sensing SEBS model and statistical comparisons has been made to validate models capability by using FAO-Penman reference evapotranspiration with utilization of in-situ meteorological datasets in spatial extent of Amhara Regional State. As per her study, remote sensing based SEBS model that have utilized MODIS and SPOT vegetation products with supportive meteorological variables has brought proxy values with conventional FAO-Penman values.

After reviewing these issues in Ethiopian landscape it is logical to put identified gaps of which this study is expected to fill. Eastern Ethiopia has heterogeneous topography, vegetation characteristics and related climatic patterns but large extent of the study site is semi-arid and arid environment. Except at some sub-watershed level, distributed hydrological modeling approach by using conventional method to estimate evapotranspiration like Teklebirhan *et al*. (2012), there is no detailed studies done in eastern Ethiopia. In other words some studies that has utilized

SEBS model like Tinebeb (2012) has not tested the sensitivity of SEBS model for some input parameters like land cover related roughness characteristics, land surface temperature, stability correction terms of which this study is expected to fill after estimating regional evapotranspiration using SEBS model.

CHAPTER III: Materials and Methods

3.1. Description of the Study Area

3.1.1. Location

Geographically, the study area is found within 3°32'56" and 9°52'8" North Latitude and 39°9'43" and 48°0'0" East Logitude. The study site is presented in Figure 3.1.

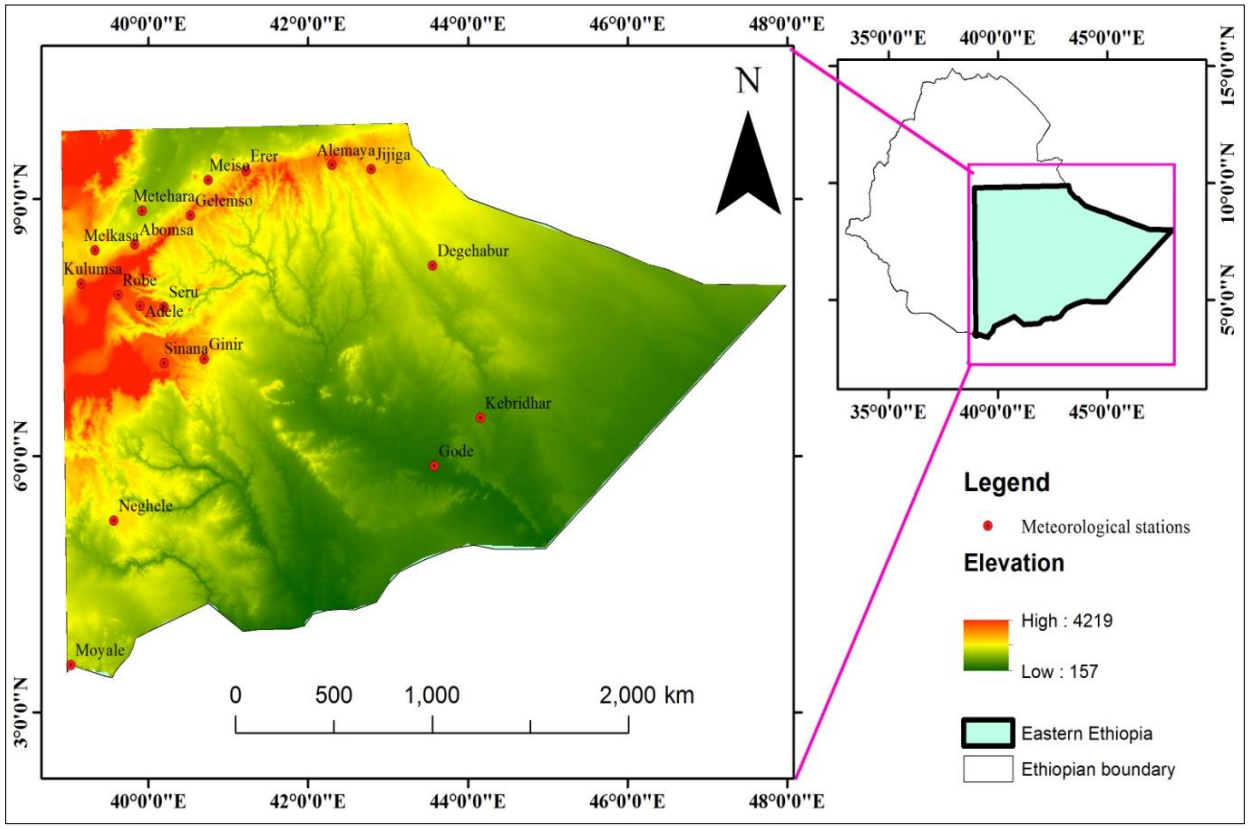

Figure 3.1: Location map of the study site in Ethiopia (*Source: Own manipulation based on CSA et al. (2006) & SRTM data*).

The geographic extent of the study site encompasses the whole area stated as eastern Ethiopian census division in *Atlas of Ethiopian Rural Economy* (CSA *et al*. 2006). As it was presented there, in its relative position the study site covers eastern and south eastern Ethiopia. Its eastern and southern extreme shares an administrative boundary with western part of Somali Land and Kenya. The northern part of the study site is part and parcel of Afar Regional State while to its west the study site has been stretched upto Arsi and Bale to eastern marigions of Central Ethiopian Rift Valley. The southern tip of the area is boardered by north western Kenya. It has large areal expansion of around, which encompasses whole Somali Regional State, little southern

tips of Afar and some part of eastern Oromia Regional State until the eastern marigins of Central Ethiopian Rift Valley. It has a total area* of 461,398 km^2.

3.1.2. Climate and Agro-ecology

The study area is characterized by varied agro-ecological and climatic situations. Taking CSA *et al*. (2007) as a frame of reference, it incompasses from a drought prone pastoral and agro-pastoral lowlands to afroalpine climatic situations. According to Ethiopian traditional agro-climatic classification, the study site has experienced four agroclimatic situations. Eastern and northern part of the study site is characterized by *bereha* (desert) and *kolla* (tropics) agro-climatic situations. *Dega* and *Woinadega* agro-climatic situation is a dominant climatic situation for some highland areas like Hararghe Highlands and some eastern marigions of Central Ethiopian Rift Valley which covers rugged mountain tops and hilly areas. Even though it is not too large, there are also areas which experience *wurch* and *kur* agroclimatic situations (CSA *et al*., 2006., CSA *et al*., 2007). As Ethiopian Ministry of Agriculture and Rural Development(MoARD) sophisticated 18 agro-climatic classifications vested in CSA *et al*. (2006), vast expanses of eastern Ethiopian lowlands have experienced hot to warm arid and hot to warm humid climate. In a more norrow way than this, as per Ethiopian Development Research Institute (EDRI) social accounting matrix agro-ecological classification presented in CSA *et al*. (2007), eastern Ethiopia has three agro-ecologies *viz*, eastern low land pastoral areas, drought prone highlands and moisture reliable cereal growing areas. Belete *et al*. (2014) have reported that, the study area is basically comprised of Genale-Dawa, Wabishebele and Ogaden watersheds and some southern extensions of Awash watershed with diverse hydro-metreological characteristics.

The rainfall pattern and amount of rainfall in the study site is reported as erratic, sporadic and scanty that, especially, vast areas in its eastern and northern margins get an annual rainfall less than 400 milimetres that only a time span less than two months experience a precipitation amount greater than 100 milimetres. Except some parts, annual rainfall is less than 800 milimetres in most low land areas. As a result, most of the eastern lowland areas of Afar and Somali, which are part of this study site are unsuitable for rainfed crop production because of precipitation deficincy (CSA *et al*., 2006). In some highland patchs of the study site like eastern

* *the area is computed by using ArcMap*

margins of Central Rift Valley, Hararghe Highlands and some watersheds like Dechato around Dire Dawa city, highly concentrated and erosive rainfall has caused flash floods that devastatingly damage human lives and livestock, different crops and properties (CSA, 2013). More than its meagre amount, rainfall is also characterized by high seasonal variability that, three fourth of the study site has shown a coefficient of variability more than 50 percent (CSA *et al*., 2006; CSA & IFPI, 2013). This variability is found a chronic risk of production for farmers whose livelihoods depended on rainfed agriculture and pastoralism without alternative means of living (CSA *et al*., 2006; CSA, 2007).

With such kind of scarce rainfall pattern, most parts of eastern Ethiopia is characterized by prevalnce of extreme temperature that work to create precipitation deficit and hydrologic disturbances. As per CSA (2013), some parts of noth east and eastern lowlands of the country has experienced extereme maximum temperature. It has been stated as it cause negative implications for plant and animal physiological activities, hinders normal growth and development of plants and resulted in heat stress to menace animal productivity through reduced feed and dry matter intake. The interactive impact of higher temperature and rainfall precipitating for a short period of time has highly reduced the areas length of growing period (CSA & IFPRI, 2013). Majority of the areas in the northern, eastern and east central part have a length of growing period less than 60 days. Here it can be argued as such kind of implications have negative repurcussions on agricultural water management, agricultural productivity and sustainability of rural livelihoods.

3.1.3.Geology and Soils

As it was present in geological map of Ethiopia which is compiled by Mengesha *et al*. (1996), Eastern part of Ethiopia is mostly dominated by late Palaeozoic, Mesozoic and Cenozoic continental and marine sediments. The northern and eastern part of the study area is characterized by presence of paramount geologic faults, late and early to late Juriasic formation of lime stone, shale and sandston (it was also stated in NWRC, 1972) mixed with precamberian formations of granulite and migmatite with minor metasedimentary gneisses. Its eastern and some east central part has a geological structure of Eocene formations. Additionally, as per Natinal Water Resources Commission (NWRC, 1972), in areas along the main road from Asbe Teferi (Chiro) to Kulbi, there is a geological formation of tertiary basalt trap series. Additionally,

as presented in Ethiopian Geological Survey and Ministry of Mines (2009), having recognized the pedological and geological charateristics in combination, some parts of eastern Ethiopia have highest clay potential to extent they can support bricket and cement production. As per the report Melka Jebdu, Haromaya, Hamaresa and Gelemso were found potential clay sites of eastern Ethiopia.

As per Ethiopian pedological map presented in CSA *et al*. (2006) and CSA and IFPRI (2013), the study site is dominated by various soil types that simultanously vary with physiography and climatic characters of a site. The northern extremes and highland areas around the eastern marigins of Central Ethiopian Rift Valley are dominated by Leptosols, Cambisols, Vertisols and Luvisols. These soils are characterized by their acidic nature that they experience nutrient deficiency and presence of high exchangeable aluminium which leads to toxicity. Liming, continous fertilization and addition of macro nutrients is recommended to realize desired agricultural production from these soils (Macías *et al*., 2008). Vertisols are heavy clay soils from a sandy parent material; crack when dry and stick when wet. Ethiopian vertisols are extremely velnerable for problem of waterlogging because of their poor drainage characteristics (CSA& IFPRI, 2013) that they need moisture respnse farming for potential production. Despite the fact that it need curious water and moisture management, these soils are highly fertile for cereal, cotton and pasture land (Spaargaren, 2008). For that matter the undertaken study can contribute its part in estimating water demand for evapotranspiration.

Its eastern extreme around the low lands of Somali and its east central part is dominated by Calsisols and Gypsisols. These are alkaline soils which are common in deasert areas and its adjacent vicinity; they support xerophytic vegetative types and ephemeral grasses that they well support halophytic vegetation types (Chesworth *et al*., 2008) and in Ethipian eastern lowlands they have low agricultural potential (CSA & IFPRI, 2013). There are also Luvisols in some patchs of souhern and south eastern portion of the study area where precipitation is reliable than arid areas with good agricultural potential (CSA *et al*., 2006).

3.1.4. Vegetation and Topography

Floristic types and characteristics is varied simultanously with variabilities in other biophysical characteristics like climatic, edaphic and physiographic characteristics of a given geographic region. As eastern Ethiopia is characterized by divers agroecology, soil and physiography its

vegetative characteristics is also hetrogenous. As per this, by taking broad vegetation categories and their spatial destribution presented in Zerihun (1999), in the study area there are seven broad vegetation classes ranging from desert to afroalpine vegetation. The northern, eastern and east central part of the study site is dominated by open xerophytic woodland vegetation. The area is dominated by desert and semi-desert ecosystem vegetation that the flora has developed high xeromorphic adaptation; trees and shrubs have developed dwarf growth with small, sclerenchymatic or pubescent leaves (USAID, 2008). In relation to vegatation characteristics, to give some clue, a land cover map of the area is presented in the following Figure 3.2.

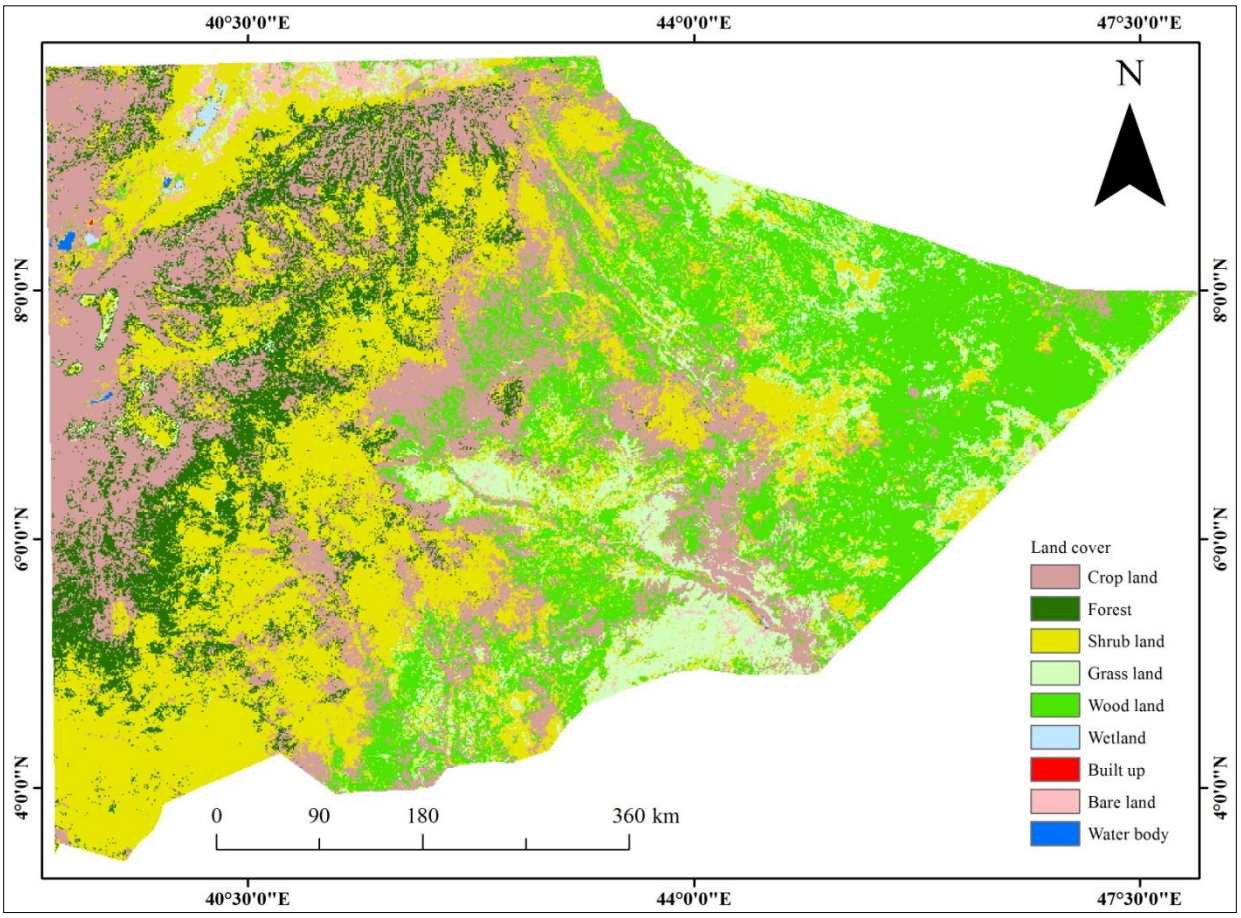

Figure 3.2: Land cover map of the study area (*Source: European Space Agency, 2009*).

The highland areas like western marigin of Bale Mountains and Hararghe Highlands exhibit Afroalpine and Subafroalpine, moist and dry evergreen montane forests, montane savana and montane evergreen thicket and scrub vegetation. To this its spatial distribustion, the tree cover characteristics of eastern Ethiopia is very low. As a map prepared by CSA *et al*. (2006), by using data generated from medium resolution satelite image, shows as vast expanses of eastern

Ethiopia is experiencing a tree cover of less than 5 percent while the western part of eastern Ethiopia including some of its highland patchs have experience moderate to higher tree cover.

3.2. Methods

3.2.1. Meteorological Dataset Preparation

As it was stated implicitly stated on objective section, the study has consumed two types of data sets. These are remote sensing based products and meteorological data sets. One thing to be noted here is meteorological data set is also composed of two components. The second component is collected from ground based meteorological observation stations by Ethiopian National Meteorological Service Agency (NMSA). The first one is collected from international climate data archives (detailed is given at succeeding subtitles). For meteorological data, its completeness has been checked for the DOY under analysis. The data set is collected for days with similarly synchronized with satellite overpass of the area of which the date chosen for analysis purpose. The compiled data is made ready at excel and coded in processing software that is ET calculator.

Meteorological data set available on global databases that provide it in different spatio-temporal scale has been downloaded taking the date of satellite overpass into account. Then format and coordinate system conversion has been undertaken. There is also specifying area of interest from global coverage either during download or format conversion and coordinate transformation phases.

Ground meteorological observation stations are chosen primarily based on data type availability for Penman-Monteith analysis technique and spatial location. Accordingly, 23 level one and level two meteorological stations are selected by using their full database archived at NMSA available on line at (*see the URL cited below on table footnote)*. Their full description is presented on Table 3.1.

Table 3.1: Description of selected meteorological stations

Meteorological Station	Location(degree decimals) Lat	Long	Meteorological Station	Location(degree decimals) Lat	Long
Abomsa	8.4666	39.8333	Jijiga	9.3500	42.7900
Adele	7.7505	39.9017	Kebridhar	6.4400	44.1600
Alemaya	9.4000	42.3000	Kulumsa	8.0096	39.1553
Arsi Robe	7.8756	39.6222	Meiso	9.2243	40.7537
Degehabur	8.2200	43.5600	Melkassa	8.4000	39.3300
Eerer	9.3300	41.2200	Metehara	8.8586	39.9190
Gelemso	8.8093	40.5250	Moyale	3.5500	39.0300
Ginir	7.1300	40.7000	Negele	5.2400	39.5700
Gode	5.8800	43.5800	Seru	7.7358	40.2025
			Sinana	7.0800	40.2000

Note: values approximated to fourth digit
Source: Compiled from ENMSA Web Portal[1]

3.2.2. Re-projection and Format Conversion of MODIS Level 1B Product

Level 1B MODIS products are provided with hierarchical file format (HDF) format which is not as such compatible to easily read and undertake analysis on GIS related platforms like ArcMap and ILWIS softwares. In addition to this, the image has global sinusoidal projection system, which is difficult to use at regional and local analysis and mapping operations. More importantly, full scene of an image is too large for analysis operation that, there should be extraction of region of interest of which the study is going to be undertaken. Therefore, coordinate re-projection, extraction of region of interest and format conversion is undertaken by using MODIS Reprojection Swath Tool (MRTSwath Tool), which is open source geospatial software. Concerning detailed description and the software itself, it can be possible to access release notes and user manuals from [URL][2]. At the outset of the study, though it is proposed to use level 1B products both for dry and wet season, presence of cloud contamination at the study site has created a challenge for summer season. Therefore, for summer season the study has utilized processed composites. The images selected for dry season is four MODIS scenes from year 2013 (DOY 20 & 27) and from year 2014 (DOY 10 & 32) based on clarity of the image scenes from cloud contamination. As cloud obstructs the image to provide clear information about the surface, care has been taken to select cloud free scenes. In addition to cloud cover characteristics,

[1] *http://www.ethiomet.gov.et/stations/information*
[2] *https://lpdaac.usgs.gov/tools/modis_reprojection_tool*

the existence of meteorological data for validation at the day of the year when image is taken has also taken into consideration. For summer season Leaf Area Index (LAI), fraction of vegetation cover, land surface temperature and albedo we have utilized decadal composites of MSG products. NDVI is taken from Spot Copernicus program PROBAV-V decadal composite. These products are chosen because of their accuracy reported at its validation process and atmospheric correction model utilized – Simplified Model for Atmospheric Correction (SMAC), which is similar with this study utilized for processing MODIS level 1B products for dry season analysis (Smets *et al*., 2015; Wolters *et al*., 2014). Emissivity is computed through formulations presented in Valor and Caselles (1996) by using its empirical relationship with fraction of vegetation cover. As per this 2014 DOY (165, 195, 226 and 257) were taken. Format conversion and re-projection is done using MSG toolbox and QGIS NetCDF browser. The remaining datasets are similar with dry season datasets.

3.2.3. Raw to Radiance and Reflectance Conversion

Level 1B product are accessed in the form of coded electromagnetic signal or digital numbers (DN) and conversion of DN to radiance and reflectance terms is mandatory to undertake any further analysis. This is done by using radiance and reflectance rescaling and offset values given in its metadata. The metadata of MODIS HDF data format is accessed by using HDF viewer, which is also open source software. Overall functionalities, the platform and its user manual have been accessed from [URL][3].

Conversion of raw digital count to reflectance values is done by using the following formulae as stated in Toller *et al*. (2006);

$$R = S(\lambda - O) \tag{3.1}$$

while R is top of atmospheric reflectance, S is reflectance scale, λ is reflectance Digital Number(DN) of MODIS data and O is reflectance offset term which all are accessed from the metadata of the image by using HDF viewer. Similarly, the conversion of raw DN to radiance is also done by using radiance rescaling factor and radiance offsets as:

$$Rd = Rs(\lambda r - Ro) \tag{3.2}$$

[3] *https://www.hdfgroup.org/products/java/hdfview/*

Where Rd is top of atmospheric radiances, *Rs* is radiance rescaling factor, *Ro* is radiance offset and λr is radiance DNs of the MODIS bands In addition to reflectance and radiance digital counts sensor and sun geometry related count bands given in geolocation file (sensor zenith and azimuth angle bands and sun zenith and azimuth angle bands that are downloaded as geolocation file in association with MODIS level 1B products). Conversion of these geolocation sun-sensor geometry files is done similar to reflectance and radiance terms by using rescaling terms given in header file of MODIS level 1B HDF image. The stated overall operation is undertaken by utilizing prepackaged SEBS module preprocessing sub-module provided in ILWIS.

3.2.4. Brightness Temperature Computation

Before performing any computation and analysis operation on MODIS radiance bands related with temperature, it should first converted to top of the atmosphere brightness temperature (Yale Center for Earth Observation, 2014). As per this, radiance value is converted to brightness temperature by using Planks formulae which is presented in Pinheiro *et al*. (2007) as:

$$T_b = \frac{c_2}{\lambda_c \log\left(\frac{c_1}{\lambda_c^5 \pi L_r} + 1\right)} \tag{3.3}$$

T_b is brightness temperature of the given band central web length, λ_c is the sensors central web length for band 31 and 32 while c_1 and c_2 are blackbody constants ($c_1 = 1.19107 \times 10^8$ Wμm^4 and $c_2 = 1.43883 \times 10^4$ μm K) and L*r* is band 31 and 32 radiance values. These blackbody principle which works under the assumption of uniform emissivity has also been used for the conversion of Landsat thermal band to brightness temperature by some projects like (Landsat Project Science Office, 2002; Waters *et al*., 2002) and empirical studies like Qin *et al*. (2001).

3.2.5. Atmospheric Water Vapor Content Estimation

To undertake atmospheric correction of MODIS reflectance bands using Simplified Method for Atmospheric Correction (SMAC) model, data concerning some critical variables under radiative transfer like atmospheric water vapor content is critical model variable. Therefore, water vapor content is generated from radiance bands. There are various mechanisms to generate water vapor content from MODIS radiance values. From these the most prominent and repeatedly used techniques were split window and ratio methods (Li *et al*., 2003; Sobrino *et al*., 2003; Moradizadeh *et al*., 2008). In addition to these techniques, regression method and triangle slope

methods (Kaufman & Gao, 1992; Zhang *et al*., 2008) are also mechanisms used to estimate water vapor content in the atmosphere. To the operationalization this study, water vapor content is retrieved by using a ratio technique. Principally, this technique uses one no-absorption window band and other absorption bands while they pass at the same time at the same atmospheric conditions (Sobrino *et al*., 2003; Moradizadeh *et al*., 2008). As argued by Sobrino *et al*. (2003), this approach is advantageous over other stated techniques as it is resilient for noise emanated from statistical errors of bands, dynamic nature of atmospheric components and heterogeneities in surface conditions (reflectance and roughness parameters of the surface).

As it was clearly given in Sobrino *et al*. (2003) and further investigated by Moradizadeh *et al*. (2008), absorption channels selected for this operation are radiance band 17, 18 and 19 while window channel is radiance band 2 of MODIS level 1B data set and sometimes channel five is also used as comparative window channel. They have described the proportion between absorption channels and one window channel as follows:

$$G_i = \frac{B_i}{B_2} \tag{3.4}$$

where G_i are ratios of B_i (i^{th} band in this case with bands 17, 18, and 19 of MODIS radiance bands with band 2 radiance band). According to their simulation result, by using stated proportions on Eq. 4.4, the water vapor content and sensitivity of each absorption channel varies and is presented on the following regressive equations.

$$W_{17} = 26.314 - 54.434G_{17} + 28.449G_{17}^2 \tag{3.5}$$

$$W_{18} = 5.012 - 23.017G_{18} + 27.884G_{18}^2 \tag{3.6}$$

$$W_{19} = 9.446 - 26.887G_{19} + 19.914G_{19}^2 \tag{3.7}$$

Weighted average of three absorption bands water vapor content is generated by using weighting functions as:

$$\sum_{i=17}^{19} f_i W_i \tag{3.8}$$

where, f_{18} to f_{19} are weighting function derived by using the following empirical relationship

$$f_i = \frac{\eta_i}{\sum \eta_i} \tag{3.9}$$

where η_i can be derived as $\eta_i = \frac{|\Delta\tau_i|}{|\Delta W|}$ where ΔW is the difference between the maximum and minimum water vapor content, $\Delta\tau_i$ is the difference between the transmissivities in maximum and minimum atmospheric water vapor content obtained from i^{th} band. Though simulated results presented in Sobrino *et al*. (2003) and Moradizadeh *et al*. (2008) deviate in small amount, the following values has been used for the this study.

Table 3.2: Radiance bands and associated weighting functions

	Channel		
Coefficients	B17	B18	B19
$\boldsymbol{\eta_i}$	0.062	0.147	0.115
$\boldsymbol{f_i}$	0.192	0.453	0.355

Source: Sobrino et al. (2003)

And finally the water vapor estimation equation is become as:

$$W = 0.192W_{17} + 0.453W_{18} + 0.355W_{19} \quad (3.10)$$

3.2.6. Atmospheric Correction of MODIS Level 1B Bands

Any signal sent to the surface from space by satellite sensors and reflected back to it can be affected while it made any interaction with the atmosphere. The primary intention of any atmospheric correction is to compensate these interfering atmospheric effects on the quality of remotely sensed images (Lu *et al*., 2002; Hadjimitsis *et al*., 2010). This lets to meet the objective of obtaining faithful parameters from satellite imagery (Hareef, 2013). As proved from studies like Cihlar *et al*. (1997) and Hareef (2013), there is a significant impact of atmospheric interference on the quality of remote sensed images for practical applications like vegetation indices and energy balance estimation, which the prime business of this study.

Taking this into consideration, to account the impacts of atmosphere (this term is inclusive for ozone concentration, aerosol optical thickness, and atmospheric water vapor content); Simplified Method for Atmospheric Correction (SMAC) model has been implemented on visible reflectance channels. As per detailed description given by Rahman and Dedieu (1994), this technique is found applicable for many geostationary and meteorological earth observation satellites that have large-field-of-view. More importantly, it is reported as advantageous over other methods that it is

extremely quick (Parodi, 2007) and does not use pre-calculated look up tables for correction purposes. As detailed on the stated paper, this kind of atmospheric correction model utilizes some parameters related with radiation absorption and scattering like ozone content, aerosol optical depth, water vapor and sensor specific correction parameters. As justified with comparative analysis done by Norjamaki and Tokola (2007), the model is possibly logical than a frequently used methods, which are quick and simple like Dark Object Subtraction (DOS) technique as it incorporates the various model variables related with atmospheric characteristics while the image scene is taken as model variable.

Comparative to other radiative transfer models like ATCOR (Richter & Schlifer, 2015), it is relatively found quick and user friendly. In other words though some studies like Hajj *et al*. (2008) report one of the relative methods, Pseudo Invariant Target method, outperforms radiative transfer models like SMAC, it is found tiresome and needs a reference master image and time series slave images with identifiable homogenous features for comparison. As per these, it is semi-empirical model implemented when the analyst can have atmospheric characteristics other than an image under analysis. More importantly, it has been underlined that, SMAC is a straightforward technique while users are expected to work with large amount of time series historical data (Rahman & Dedieu, 1994), which increases its relevance for MODIS daily calibrated raw data atmospheric correction purpose.

SMAC model explicitly accounts gaseous transmittance of both incoming and outgoing radiation, albedo characteristics, aerosol and rayleigh scattering while combining sensor viewing and sun zenith and azimuth angles (Rahman & Dedieu, 1994; Proud *et al*., 2010). Therefore, in a comprehensive way, prepackaged ILWIS based SMAC sub-module needs four data sets that account these parameters, *Viz*, data related with band specific top atmospheric reflectance channel; sensor specific coefficient file which contains continental and desertic atmospheric models designed for specific sensor calibration (Shoko *et al*., 2015) which is downloaded from an open source based repository[4], data related with atmospheric characteristics (aerosol optical thickness, ozone layer concentration, surface pressure and atmospheric water vapor content), sun satellite geometry related data sets which are geolocation files (Solar and viewing (sensor) zenith and azimuth angles). Geolocation files are extracted from MODIS dataset, aerosol optical

[4] *http://52north.org/downloads/category/82-smac*

thickness and ozone layer concentration datasets has been compiled from National Aeronautics and Space Administration (NASA) website[5] and surface pressure is generated by using elevation pressure relationships stated in Ferreira *et al*. (2012) from Global Land Data Assimilation System (GLDAS) reference height pressure products data set, which is archived at NASA DISC Hydrology Data and Information Services Centre (HDISC) website[6] while atmospheric water vapor is computed as a preprocessing operation of the SEBS prepackaged algorithm. For the matter of assessing the effect of atmospheric correction on the bands, reflectance values after and before atmospheric correction has been compared. The comparison has been made by descriptive and inferential statistical methods. Descriptively the mean reflectance value of bands after and before correction has been presented in a tabular and graphical form while inferentially the significance of atmospheric correction is tested by using paired-samples t-test (Till & Williams, 1987; Burt *et al*., 2009). This is a kind of test used to compare the variances of the means of the same variable before and after some occasions (Pallant, 2007). For this study, the variability of reflectance value scores before and after SMAC atmospheric correction. For this purpose, 500 randomly selected samples have been extracted from similar locations. This statistical analysis has been done by using Statistical Package for Social Sciences (SPSS) version 20.

3.2.7. SEBS Model Biophysical Input Variables Parameterization

SEBS is a remote sensing based residual surface energy balance estimation technique where majority of its core variables are derived from other primary inputs as a preprocessing of model parameters. As per these, land surface albedo, Normalized Difference Vegetation Index (NDVI), surface emissivity and aerodynamic resistance are variables which are derived from primary radiance and reflectance values derived from MODIS level 1B products, sensor specific coefficients and meteorological variables.

3.2.7.1. Surface Albedo Estimation

After overall format conversion and coordinate transformation, atmospheric correction and raw to radiance and reflectance conversion, surface albedo is computed to serve as one of core model variable in SEBS algorithm. As it was given in Liang (2001), surface albedo using level 1B MODIS products is generated by using the following regressive model.

[5]

[6] *http://disc.sci.gsfc.nasa.gov/hydrology/data-holdings*

$$\alpha = 0.160b_1 + 0.291b_2 + 0.243b_3 + 0.116b_4 + 0.112b_5 + 0.018b_7 - 0.0015 \quad (3.11)$$

where, α is surface albedo, b_1 to b_7 were MODIS band 1, 2, 3, 4, 5, and 7, which are atmospherically corrected reflectance bands. One thing to be noted here is that, during generation of surface albedo by using SEBS prepackaged module, there need a sensor specification to ingest the necessary bands.

3.2.7.2. NDVI, Vegetation Fraction, Leaf Area Index and Emissivity Estimation

Normalized Difference Vegetation Index is one of the variables used to estimate surface emissivity, emissivity difference and vegetation proportion. As per this, NDVI can be computed from MODIS level B products by using reflectance band 1 and 2 as red and near infrared bands respectively as was stated in King *et al*. (1992) and Peng *et al*. (2013);

$$NDVI = \frac{NIR - R}{NIR + R} \quad (3.12)$$

Where NDVI is normalized difference vegetation index, NIR is band 2 and R is band 1 MODIS level 1B products which are near infrared and red reflectance bands. This is done by using ILWIS scripting environment. Fraction of vegetation is a basic input for calculation of surface emissivity, soil heat flux and roughness length for heat transfer which further is used to compute sensible heat flux (Gibson *et al*., 2011). It is computed using NDVI and vegetation cover empirical relationship as given in Wang *et al*. (2008) and Lu *et al*. (2012):

$$F_v = \frac{(NDVI - NDVI_{min})^2}{(NDVI_{max} - NDVI_{min})^2} \quad (3.13)$$

where, F_v fraction of vegetation cover, $NDVI_{min}$ is taken as 0.2 below it is surface devoid of vegetation and $NDVI_{max}$ is taken as 0.5, above it is a surface fully covered by vegetation.

Especially in regional studies where there exists mixed vegetation landscape similar to a study site where this study is undertaken, it is advisable to use empirical relationships of vegetation indices and Leaf Area Index (LAI) other than directly using land cover dataset. As it was investigated by Wang *et al*. (2005), MODIS LAI is strongly explained by its NDVI values though it was warned the time of the year when the image is taken should take into consideration. Taking these into consideration, Leaf Area Index (LAI) is estimated from NDVI values as given in (Parodi, 2007):

$$LAI = \sqrt{\frac{NDVI(1+NDVI)}{(1-NDVI)}} \tag{3.14}$$

where, LAI is Leaf Area Index and NDVI is Normalized Difference Vegetation Index resulted from prior operation stated above. This is done by using Map calculation sub-module operation through ILWIS scripting.

Taking computed NDVI values, it is possible to generate surface emissivity values by using empirical relationship between NDVI and surface emissivity as presented in Sobrino *et al*. (2003) and Wang *et al*. (2008). By segregating a surface based on vegetation coverage and NDVI value relationship into three categories as land devoid of vegetation (NDVI less than 0.2), surface characterized by partly vegetation and non-vegetated (NDVI between 0.2 and 0.5 inclusive the limit values) and fully vegetated ground (where NDVI greater than 0.5), emissivity has been iteratively computed as follows.

Table 3.3: Emissivity computations across different land cover characteristics

Surface vegetation type	Emissivity ($\boldsymbol{e}$)	Emissivity difference ($\boldsymbol{ed}$)
Devoid of vegetation	$0.9832 - 0.058b_1$	$0.0018 - 0.06b_1$
Mixed cover type	$0.971 + 0.018\,F_v$	$0.006(1 - F_v)$
Full cover vegetation	$0.990 + ed$	$ed = 0.005$

Source: Taken from Sobrino et al. (2003)

3.2.7.3. Land Surface Temperature Estimation

One thing to be noted here is that brightness temperature at top of atmosphere is different from land surface temperature. As justified by Mao *et al*. (2005), land surface temperature computation can be done by accounting two essential land and atmospheric parameters (transmittance and emissivity). Therefore, land surface temperature is estimated as a function of brightness temperature, surface emissivity, emissivity deference and atmospheric water vapor content. It is estimated by using an empirical relationship given by Sobrino *et al*. (2003) as:

$$T_s = T_{b31} + 1.02 + 1.79(T_{b31} - T_{b32}) + 1.2(T_{b31} - T_{b32})^2 + (34.83 - 0.68W)(1 - e) + ed(-73.27 - 5.19 * W) \tag{3.15}$$

where, T_s is land surface temperature, T_{b31} and T_{b32} are brightness temperatures computed from band 31 and band 32 respectively, W is atmospheric water vapor content, e is surface emissivity computed to the prior step and ed is emissivity difference similarly computed to the prior steps.

3.2.8. Estimation of Evapotranspiration & Surface Energy fluxes

Basically evapotranspiration and other flux terms like evaporative fraction, soil heat flux, and latent heat flux are estimated from surface energy balance. As it was presented in Su (2002) and consecutively in Lu *et al*. (2012), an incoming and outgoing energy is expressed in the form of surface energy balance system as:

$$R_n = G_0 + \lambda E + H \tag{3.16}$$

where, R_n is net radiation, H is sensible heat flux, λE is latent heat flux (λ is latent heat of vaporization and E is actual evapotranspiration) and G_0 is soil heat flux.

By using the above equation as frame of reference, net radiation can be estimated from parameterized remote sensing based variables by using an equation given in Allen *et al*. (1998) and Su (2002) as:

$$R_n = (1 - \alpha)R_{swd} + \varepsilon \mathrm{R}_{lwd} - \varepsilon\sigma T_s^4 \tag{3.17}$$

where α is surface albedo, ε is land surface emissivity, $\mathrm{T_s}$ is land surface temperature, R_{swd} is downwelling short wave radiation, R_{lwd} is downwelling long wave radiation and σ is Stefan – Boltzmann constant which is $5.6710^{-8} Watt\, m^{-2} K^{-2}$. As it was recommended by Su (2002) and Gibson *et al*. (2013), downward short web radiation is advisable to use its direct input other than using modeled value. Therefore, the study has used Meteosat Second Generation products delivered at Land Surface Analysis Satellite Applications Facility (LSA SAF) website [URL][7]. This data is provided in binary HDF5 file format with Native Geographic Projection (NGP). It is processed by using MSGToolbox for format transformations from HDF5 to other GIS file format, re-projection and selection of region of interest (ROI) from continental and global dataset. Concerning MSG Toolbox, it is possible to consult [URL][8].

[7] *http://landsaf.meteo.pt/*
[8] *http://landsaf.meteo.pt/staticData/LSASAF_MSGToolbox_v1.0.exe*

Only to use downward short web radiation as model input, downward long web radiation is iteratibly computed in prepackaged SEBS as was given in Parodi (2007) by utilizing a formula:

$$R_{lwd} = \varepsilon_a \varepsilon \sigma T_s^4 \tag{3.18}$$

where $\varepsilon_a$apparent atmospheric emissivity which can also routinely is computed in prepackaged SEBS module as $9.2 * 10^6 * (273.15 + T_a)^2$ where T_a is near surface air temperature. To estimate the soil heat flux, the equation and empirical relationship between vegetation fraction, soil heat flux and net radiation presented in Su (2002) is implemented as:

$$G_o = R_n[\Gamma_c + (1 - f_c)(\Gamma_s - \Gamma_c)] \tag{3.19}$$

where Γ_c and Γ_s is ratio between soil heat flux and net radiation which is 0.05 for fully vegetated surface and 0.315 for bare soil respectively (Monteith, 1973 & Kustas and Daughtry, 1989 as cited in Su (2002)) and f_c is vegetation fraction similar to F_v computed in equation 4.13. As per detailed explanations given in Bastiaanssen *et al*. (1998), if surface temperature characteristics, soil profile characteristics and diurnal soil conductivity phase difference is given due emphasis, Γ_c parameterization technique from soil heat flux and net radiation is reported sounding.

One of the basic capabilities of SEBS algorithm is its ability to incorporate surface roughness and aerodynamic resistance terms in an explicit way. To determine these parameters, prepackaged SEBS module have either optional input variable (vegetation height map 'h', surface roughness for momentum transfer map 'Z_{0m}' and zero-plane displacement map 'd_0') or iteratively produces surface roughness and aerodynamic resistance maps by using NDVI and LAI maps. This wider option has increased the flexibility of SEBS algorithm while working in mixed landscape at large geographic area where data related to vegetation height is scarce, cost inefficient and time consuming to prepare. For the operationalization of this study, the relation between zero plane displacement and surface roughness for momentum transfer is presented as was given in Su (2002):

$$z_{oh} = \frac{z_{om}}{exp\ (kB^{-1})} \tag{3.20}$$

where kB^{-1} is the inverse Stanto number which is a dimensionless heat transfer coefficient. Even though the value related with dynamic aspect of kB^{-1} term is computed with series of

equations presented in Su (2005), in prepackaged SEBS module the value is most of the time left a default value approximately to 2.5 (Ferreira *et al*., 2012) or iteratively computed. For current study it utilized a description given in Su (1999; 2002) and Su *et al*. (2001).

The roughness length z_{om} has been generated by using associated values of land cover map of the study area. The study area is too large that it needs considerable amount of time to prepare land cover map by using raw satellite image. Therefore, from available global land cover datasets, European Space Agency (ESA) based GlobCover data has been selected taking its better spatial resolution at wider geographic region and its accuracy at both global scale (Bicheron *et al*., 2008) and local scale (Bai *et al*., 2014). The data set is provided with land cover data, its legend and detailed descriptions. Within the study area, there are 15 land cover classes but it is reclassified to 9 land cover classes based on their surface roughness aggregation characteristics (Z_{0m})[9]. The roughness length values of associated land cover class were adopted from values presented in various literatures and empirical studies. As per this, the following values are adopted from available empirical literatures.

Table 3.4: Land cover classes and associated roughness length values

Land cover class (reclassified)	Z_{om} in meters
Crop land	0.05
Forest	1.2
Shrub land	0.03
Grass land	0.02
Wood land	0.5
Wetland	0.1
Built up	0.2
Bare land	0.005
Water body	0.0005

(*Source*: Troen & Peterson, 1989; Waters *et al*., 2002; Silva *et al*., n.d.; URL[10])

For the purpose of sensitivity analysis related to derivation of roughness length stated in Gibson *et al*. (2011), aerodynamic roughness length can be modeled by using its relationship with NDVI as proposed by Su and Jacobs (2001) as:

[9] *Original land cover classes and reclassified thematic classes will be given at appendices*

[10] http://www.tuuliatlas.fi/modelling/mallinnus_3.html

$$Z_{0m} = 0.005 + 0.5\left(\frac{NDVI}{NDVI_{max}}\right)^{2.5} \tag{3.21}$$

Vegetation height and displacement height for aerodynamic roughness height are iteratively computed by using Brutsaert (1982) which is cited in Lin *et al*. (2006) and Allen *et al*. (1998) as:

$$h = \frac{Z_{0m}}{0.136} \tag{3.22}$$

$$d = \frac{2}{3}h \tag{3.23}$$

One of the components within SEBS is sensible heat flux, which is energy used to heat the surface. Sensible heat flux is basically influenced by three variables, *viz*, gradient of surface and near surface temperature, wind speed and aerodynamic roughness length. Therefore, sensible heat flux has been iteratively computed by using theory of Atmospheric Similarity Layer (ASL) as was given in Su (2002):

$$\begin{aligned} u &= \frac{u_*}{k}\left[ln\left(\frac{z-d_0}{z_{0m}}\right) - \Psi_m\left(\frac{z-d_0}{L}\right) + \Psi_m\left(\frac{z_{0m}}{L}\right)\right] \\ \theta_o - \theta_a &= \frac{H}{ku_*\rho C_p}\left[ln\left(\frac{z-d_0}{z_{0h}}\right) - \Psi_h\left(\frac{z-d_0}{L}\right) + \Psi_h\left(\frac{z_{0h}}{L}\right)\right] \end{aligned} \tag{3.24}$$

where z is the height where near surface metrological variables measured, u_* is the friction of velocity which can be further computed as $\left(\frac{\tau_0}{\rho}\right)^{1/2}$, τ_0 is surface shear stress, ρ is the density of air, k is von Karman's constant which is 0.4, θ_o& θ_a are the potential temperature at the surface and potential air temperature at height *z* respectively, Ψ_m and Ψ_h are the stability correction functions for momentum and sensible heat transfer respectively, L is the Obukhov length, which further is calculated as:

$$L = -\frac{\rho C_p u_*^3 \theta_v}{kgH} \tag{3.25}$$

where g is the acceleration due to gravity and θ_v is near surface temperature and C_p is specific heat capacity. For unstable atmospheric conditions Ψ_m and Ψ_h is step wisely computed as given in Paulson (1970):

$$\Psi_m = 2\ln\left[\frac{1+x}{2}\right] + \ln\left[\frac{1+x^2}{2}\right] - 2\arctan(x) + \frac{\pi}{2} \text{ and } \Psi_h = 2\ln\left[\frac{1+x^2}{2}\right]$$
$$\text{where } x = (1 - 16\frac{z-d}{L})^{0.25} \quad (3.26)$$

One of the basic capabilities of SEBS model is its consideration of sensible heat flux at both limiting cases to determine evaporative fraction. As it was presented in Sue (2002), at the dry limit latent heat of vaporization becomes zero because of water deficiency from soil while at the wet limit evaporation takes place at its full potential and evaporation might be constrained by deficiency in available heat energy. Their relationship is presented as follows. On the dry limit:

$$\lambda E_{dry} = R_n - H_o - H_{dry} \equiv 0, \text{ or}$$
$$H_{dry} = R_n - H_o \quad (3.27)$$

And on the wet limit it has the following relationship

$$\lambda E_{wet} = R_n - H_o - H_{wet}$$
$$H_{wet} = R_n - H_o - \lambda E_{wet} \quad (3.28)$$

In addition to parameterized variables above, prepackaged SEBS algorithms needs meteorological variables related with air pressure at surface and reference height, specific humidity, air temperature and mean daily air temperature and wind speed data sets at reference height. Taking absence of these parameters at the study area with fine spatial resolution, the study has utilized three hourly GLDAS dataset with 0.25^o resolution and further re-sampled to 0.01^o. The dataset is provided in NetCDF file format. Spatial sub-setting, format conversion to Geotif (.tif) and re-sampling to intended spatial resolution has been done by using a NetCDF browser, which is a Quantum GIS (QGIS) plug-in. The mean daily air temperature has been computed by averaging GLDAS three hourly products. Pressure at surface is computed by using relationship between height and pressure as stated in Ferreira *et al*. (2012):

$$P_{sur} = P_{ref} + 23 \quad (3.29)$$

where, P_{sur} is pressure at surface and P_{ref} is pressure at reference height which is GLDAS product retrieved at 2 meters height.

In SEBS algorithm, it was assumed that the instantaneous evapotranspiration value and daily evaporative fraction is equal. Therefore, by using this assumption, the evaporative fraction is upscaled to daily actual evapotranspiration as was given by Wang *et al*. (2008) and Gibson *et al*. (2013):

$$ET_a = 8.64 * 10^7 \frac{\Lambda * \overline{R_n}}{\lambda \rho_w} \tag{3.30}$$

where ρ_w is density of water in [kgm^{-3}] and $\overline{R_n}$ is daily net radiation in [Wm^{-2}].

3.2.9. Estimation of Reference Evapotranspiration by FAO-Penman Method

As argued by Temesgen *et al*. (2014), though remote sensing based methods can provide reasonable results, it is recommended to be tested by ground observation datasets. Hence, for the purpose of validating remote sensing based SEBS model evapotranspiration value, evapotranspiration is estimated by using FAO-PM technique. The primary reason why FAO Penman-Monteith technique is opted for this study is that, it has a capability of yielding correct reference evapotranspiration values under wide range of surface characteristics and climatic conditions with consistency even when there exists data scarcity (Allen *et al*., 1998; Temesgen *et al*., 2014). It is also reported as capable of yielding consistent and accurate results at different climatic conditions (Raes, 2009).

According to vivid presentations given in FAO Irrigation and Drainage Paper 56 (Allen *et al*., 1998), reference evapotranspiration from *in-situ* meteorological data is estimated by using the following procedure as:

$$ET_o = \frac{0.408\Delta(R_n - G) + \gamma \frac{900}{T + 273} u_2 (e_s - e_a)}{\Delta + \gamma(1 + 0.34u_2)} \tag{3.31}$$

ET_o is reference evapotranspiration [mm day^{-1}], R_n is net radiation at the crop surface [MJ m^{-2} day^{-1}], G is soil heat flux density [MJ m^{-2} day^{-1}], T is mean daily air temperature at 2 m height [°C], u_2 is wind speed at 2 m height [m s^{-1}], e_s is saturation vapor pressure [kPa], e_a is actual vapor pressure [kPa], $e_s - e_a$ is saturation vapor pressure deficit [kPa], Δ is slope of vapor pressure curve [kPa °C^{-1}], γ is psychometric constant [kPa °C^{-1}].

FAO-Penman technique requires primary meteorological data related with humidity, air temperature, radiation (surrogates can also serve) and wind speed data measured at reference height. The remaining variables demanded in Eq(4.30) are their derivatives. Presenting the mechanism how every derivative model variables were estimated here might make the paper too dubious. Its functionality and detailed derivative variables computation is given in Raes (2009), Zotarelli *et al*. (2009) and Bruin *et al*. (2010) in a vivid manner.

By considering computational routines and resultant errors that might emanate if done manually, overall computation has been done by using Evapotranspiration Calculator program (ETcalc version 3.2 standalone versions or which is also integrated in CROPWAT version 8.0 as sub-module). It is an open source stand alone program that is executable at windows and other operating environments (FAO, 2012). Concerning detailed description, functionality and release notes it has been presented in [URL][11].

3.2.10. Spatial Interpolation of FAO Penman-Monteith by Ordinary Kriging

In-situ meteorological measurements were collected from dispersed meteorological stations. To create a continuous raster surface of computed evapotranspiration values, it has been done by using spatial interpolation in ArcGIS environment. The spatial interpolation is undertaken by using ordinary krigging technique from spatial analysis module of ArcGIS package as given in Hengl (2009) and Ly *et al*. (2011):

$$\hat{Z}(S_o) = \sum_{i=1}^{N} \lambda_i Z(S_i) \tag{3.32}$$

Where $Z(S_i)$ is the measured or computed value (for the purpose of this study, referrence evapotranspiration) at i^{th} location λ_i is an unknown weight for the measured value at the ith location, S_o is the prediction location while N is the number of locations where reference ET is computed. Ordinary krigging method is found the best method as it produces little root mean square error (Ly *et al*., 2011; Mair & Fares, 2011). More importantly, ordinary krigging technique enables to see the semivariogram plotes and probability maps to ascertain the model fit of prediction function (Hengl, 2009) and to have a clue on the interpolation error (ITC-ILWIS, 2001).

[11] *http://www.fao.org/nr/water/eto.html*

3.2.11. Comparative Analysis of SEBS and FAO-Penman ET Results

The comparison of estimated evapotranspiration has been done by comparing values taken randomly from the whole image in one way and segregated samples from different land use classes. After picking values from sample points, correlation analysis and coefficient of determination is computed as follows. Taking its applicability in many bivarate analysis operations, Pearson's correlation coefficient has been given in Tabachnick and Fidell (2013) as:

$$r = \frac{\sum Z_x Z_y}{N-1} \tag{3.33}$$

Where $Z_X = \frac{X_i - \bar{X}}{S}$ and $Z_Y = \frac{Y_i - \bar{Y}}{S}$. X and Y are SEBS based and FAO-Penman based evapotranspiration related values at location *i*, and S is the standard deviation of values.

As it was stated in Verhoef *et al*.(1997), in order to quantify the total variance accounted between SEBS based and FAO-penman estimated ET values, coefficient of determination which is denoted by R^2 is the square of correlation coefficient in case of linear regression model. As was stated by Mkhwanazi *et al*. (2012), coefficient of determination can bring show the total variability explained in a given model by variables. It is explained as:

$$R^2 = \{\frac{\left(\frac{1}{N}\right) * \sum[(X_i - \bar{X})(Y_i - \bar{Y})]}{(\sigma_x * \sigma_y)}\}^2 \tag{3.34}$$

Where $\sigma_x * \sigma_y$ standard deviations in estimated SEBS ET and FAO-Penman are based evapotranspiration values. And its statistical significance has been tested by setting appropriate error margin.

In addition to comparative analysis of SEBS model results with SAF MSG evapotranspiration and FAO-PM results, model sensitivity analysis for aerodynamic roughness length derivation has been undertaken. After derivation of evapotranspiration by using fixed values assigned for land cover classes and empirical relationships of NDVI, presence of significant mean difference is tested by using paired sample T test (Pallant, 2007; Burt *et al*., 2009) on SPSS.

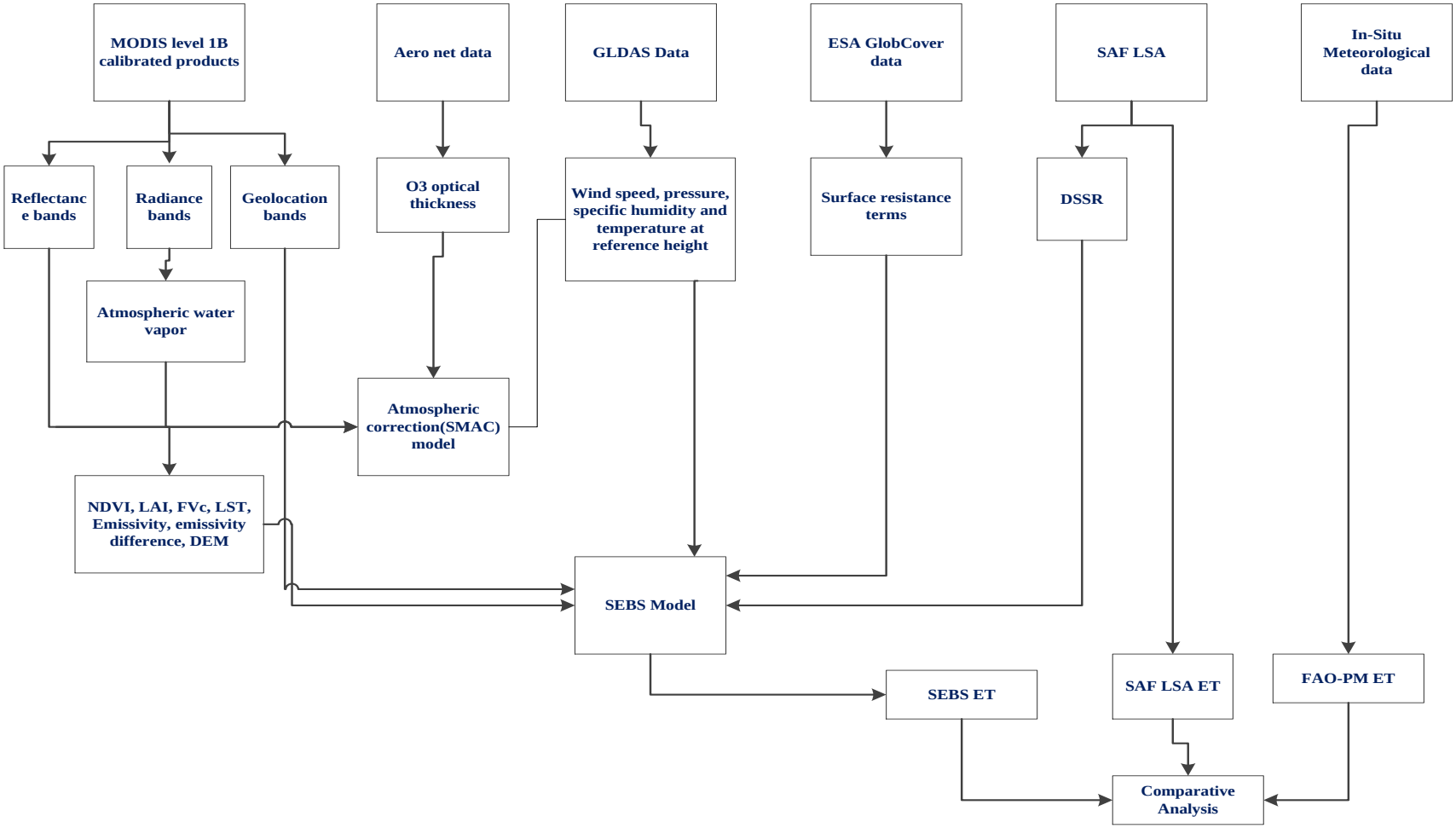

Figure 3.5: Methodological flowchart of the research process

CHAPTER IV: RESULTS AND DISCUSSION

4.1. Preprocessing Phase Results

4.1.1. Surface Reflectance Characteristics

Surface reflectance characteristics is primarily used to derive surface biophysical characteristics such as albedo and NDVI, which further are used for modeling other biophysical characteristics, surface energy flux terms and evapotranspiration. Taking this into consideration, digital counts are converted to reflectance by using reflectance rescaling and offset values. Computed values are also aggregated to different land cover classes to show how different surface characteristics respond for each MODIS reflectance bands. This is presented in Figure 4.1.

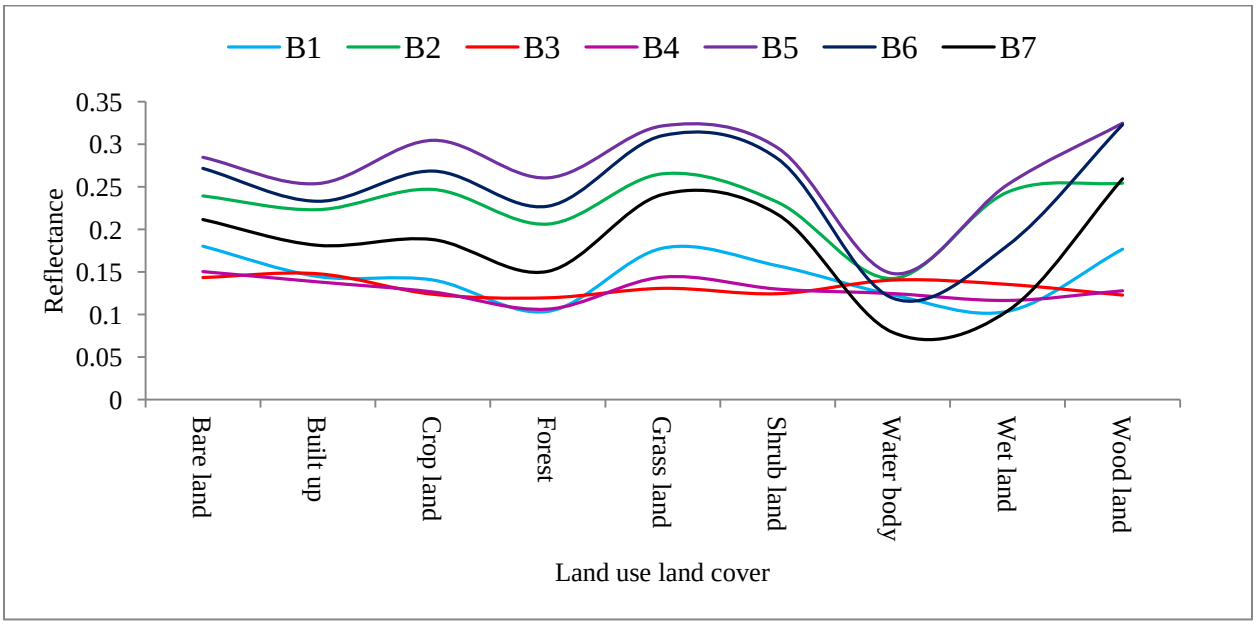

Figure 4.1: MODIS surface reflectance characteristics across different land cover class

Because of the study site have different surface cover characteristics; its response to reflectance bands at different web length is different. As shown on Figure 4.1, minimum reflectance for all reflectance bands is observed in water body followed by wetland. This is because of available water absorbs incident electromagnetic radiation. Grassland and shrub land has larger reflectance characteristics than other land cover characteristics. This reflectance pattern can vary with season when surface cover characteristics vary in reflectance condition and surface moisture availability. As presented in Trishchenko *et al*. (2002), Lillesand *et al*. (2005) and Ashraf *et al*. (2011) water body absorbs infrared bands and dry grass and bare land reflect more at this

electromagnetic band. As indicated in Figure 4.1, near infrared reflectance is not completely absorbed. This is mostly related with water turbidity (Karabulut & Ceylan, 2005) and water surface roughness because of waves (Katsaros *et al*., 1985).

4.1.2. Brightness Temperature

The brightness temperature is the temperature recorded by the sensor and is at the top of the atmosphere temperature. Brightness temperature of band 31 and 32 has been computed by using inverted blackbody temperature. The mean brightness temperature for band 31 ranges from 296.3 ^{o}K to 302.4 ^{o}K, while band 32 ranges from 296.3 ^{o}K to 301.5 ^{o}K. Overall summary of the brightness temperature is presented in Table 4.1.

Table 4.1: Mean brightness temperature of MODIS band 31 and 32

		Mean T ^{o}K		Max T in ^{o}K		Min T ^{o}K		Std.	
Year	DOY	B31	B32	B31	B32	B31	B32	B31	B32
2014	10	299.4	298.3	317.1	315.6	269.8	268.8	10.1	9.9
2014	32	299.3	297.4	317.4	314.8	275.8	275.8	10.1	9.8
2013	20	298.4	296.3	318.5	318.2	259.2	254.7	11.8	12.2
2013	27	302.4	301.5	318.5	318.1	272.2	271.8	9.5	9.7

Source: Compiled from estimated brightness temperature

This value of brightness temperature does not account for effects of surface emissivity and fraction of vegetation. Surface temperature is computed by using combined values from MODIS bands 31 and 32 brightness temperature, surface emissivity and fraction of surface covered by vegetation (*See part 4.2.5*). Similar to our study, Li *et al*. (2015) has reported that in tropical climate the brightness temperature ranges from 300 to 320°K. Similarly they have reported brightness temperature is affected by atmospheric water vapour gradient. A study by Naoki *et al*. (2010) has also attributed surface brightness temperature with surface reflectance characteristics. Therefore, in pixel which experience large brightness temperature values much radiative energy is emitted back from the surface which is a preliminary to compute surface thermal characteristics.

4.1.3. Water Vapour Content

Taking its attenuation effect on intended signal transmission across the atmosphere; water vapor is computed for the purpose of atmospheric noise correction in SMAC model. As per this, on all DOY under analysis, atmospheric water vapour content deviates from 0.39 gm cm^{-2} to 5.41 gm cm$^{-2.}$ As summary provided in Table 4.2, the water vapor content of the atmosphere during

satellite overpass varies as per surface wetness characteristics. This can be attributed to vapour yield from the surface, which is also regulated by available surface water, temperature and aerodynamic turbulence which all are vary both spatially and temporally.

Table 4.2: Descriptive statistics of Atmospheric water vapour

	Atmospheric water vapour in gm cm^{-2}			
DOY	20-Jan-13	27-Jan-13	10-Jan-14	1-Feb-14
Min	0.40	0.40	0.39	0.41
Max	3.05	3.18	5.41	5.41
Mean	1.64	1.47	2.02	1.71
Stdv	0.72	0.63	0.95	0.76

As it is presented on Table 4.2, atmospheric water has shown slight variations within days of the year the analysis has been done. In 2013, 20th and 27th DOY, the mean atmospheric water vapor content is found 1.649 and 1.475 gm cm^{-3} respectively while for 2014 10th and 32th DOY, the mean water vapour content of the study area is found to be 2.025 and 1.713 gm cm^{-2} respectively. As indicated by Mao *et al*. (2010), the default water vapour value used in MODTRAN4 atmospheric correction for MODIS bands under different atmospheres ranges from 0.3 to 3.5 gm cm^{-2}, which shows the estimated water vapor values for this study is reasonably logical. Moradizadeh *et al*. (2010) have classified atmospheres that experience amount of water vapour less than 2 gm cm^{-2} as dry atmosphere. This ascertained our study has consistent results with this classification as analysis is for winter season dry atmosphere.

Jimenez-Munoz and Sabrino (2005) have stated that, as atmospheric water vapour increases it acts to decrease both upward and downward atmospheric transmissivities. The atmospheric water content retrieved by ratio, split window and split window covariance variance technique has shown variability even results obtained by one model. If not considered at atmospheric correction of MODIS reflectance bands, it can result in considerable error in derived surface related biophysical variables from reflectance bands. As reported by Wilson *et al*. (2014), even in the clear sky the ignorance and incorporation of AOT and atmospheric water vapour has resulted large reflectance changes and deviations in resultant biophysical variables derived (specifically change in NDVI). The study has also reported the outperformance of ratio technique that results resemble with ground measurement. The availability and variability of atmospheric water vapour is largely attributed by with location, surface water availability and triggers of hydrologic phase change like wind and temperature. Figure 5.2 presents spatial variability of computed water vapour within the study site.

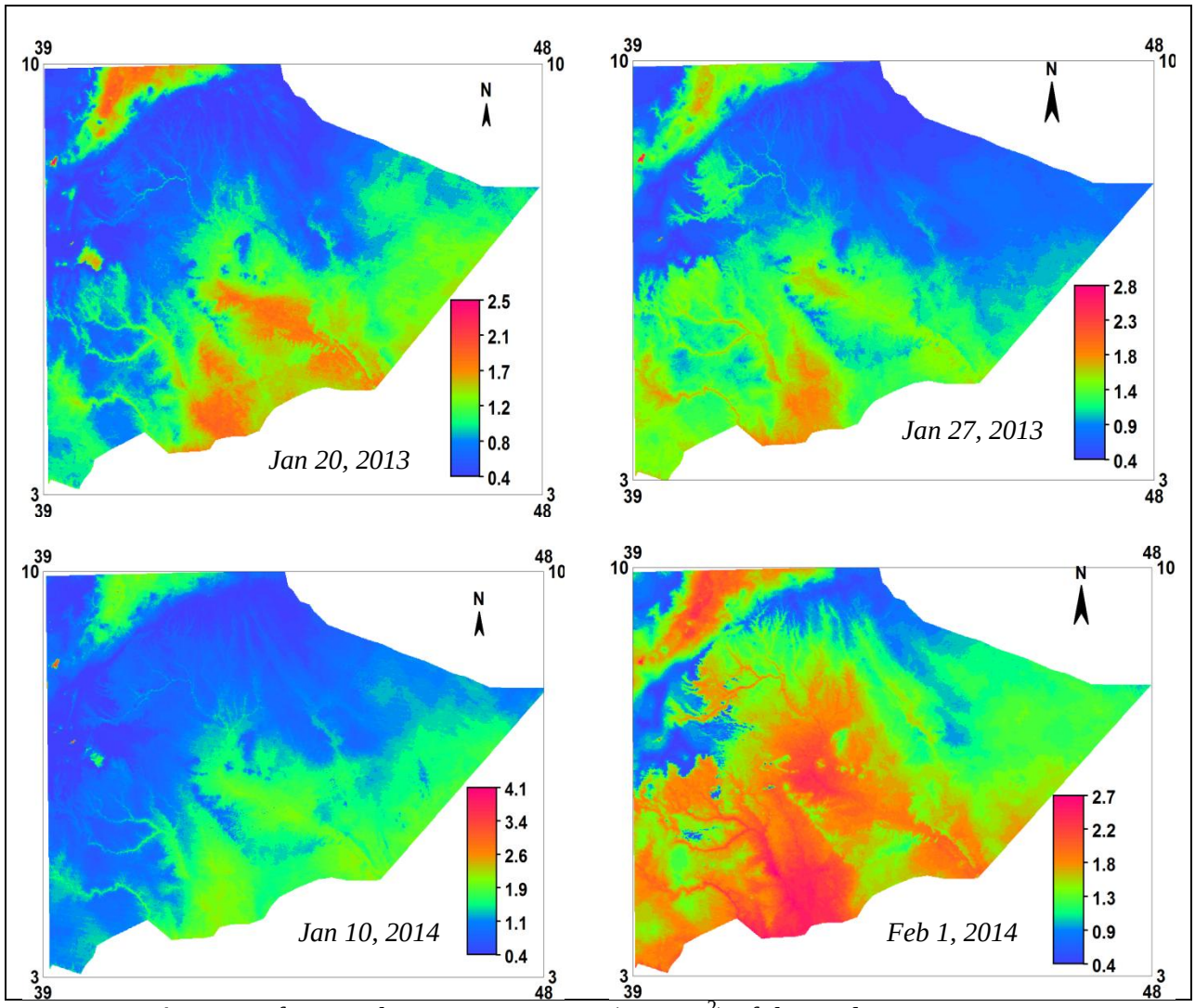

Figure 4.2: Amount of atmospheric water vapour (gm cm^{-2}) of the study area

As it was presented on Figure 4.2, larger atmospheric water vapour values has been observed in lowland areas and water body. It follows streamlines of watersheds where surface moisture yield is governed by temperature and moisture availability.

4.1.4. Analyzing Impacts of Atmospheric Correction

Though MODIS scenes for this study are cautiously selected for the days of clear sky, it is not to say the image is free from other interference on the radiative transfer of the signal. Unless undertaken atmospheric correction has not brought statistically significant changes in brightness temperature, it is better to use original atmospherically uncorrected image because atmospheric correction might bring unnecessary noise in brightness characteristics of the image.

Table 4.3: Impacts of SMAC model on MODIS reflectance bands

	DOY							
	20-Jan-13		27-Jan-13		10-Jan-14		1-Feb-14	
Band	$\sum \rho$	SMAC $\sum \rho$	$\sum \rho$	SMAC $\sum \rho$	$\sum \rho$	SMAC $\sum \rho$	$\sum \rho$	SMAC $\sum \rho$
B1	0.21361	0.17595	0.21361	0.17595	0.20523	0.15149	0.21339	0.18595
B2	0.24856	0.27387	0.24856	0.27387	0.22608	0.23375	0.25008	0.28440
B3	0.20285	0.06427	0.20285	0.06427	0.22953	0.10032	0.21753	0.06217
B4	0.19750	0.13335	0.19750	0.13335	0.19987	0.12819	0.19975	0.13764
B5	0.28299	0.33401	0.28299	0.33401	0.24365	0.27854	0.29136	0.34902
B6	0.27091	0.31589	0.27091	0.31589	0.22596	0.26004	0.27899	0.33240
B7	0.21675	0.23954	0.21675	0.23954	0.17058	0.19161	0.21820	0.25304

$\sum \boldsymbol{\rho}$ mean reflectance of the band before correction and SMAC$\sum \boldsymbol{\rho}$ is reflectance after correction

To give brief overview on the impacts of atmospheric correction, the following graph shows the impacts of atmospheric correction on MODIS reflectance bands. As it can be observed from Figure 4.3, atmospheric correction has both additive and subtractive effects. For band 1, 3 and band 4, SMAC atmospheric correction has resulted reductions in reflectance values while the remaining bands have shown increments in reflectance values. For the remaining days of the year, the analysis has been undertaken; there is a similar impact of SMAC atmospheric correction model on respective MODIS reflectance bands. Similar to findings of current study, an empirical study undertaken by Hareef (2013) that analyses atmospheric correction impacts on IIRS LISS-IV reflectance bands has reported both subtractive effects on green and red bands and additive effect on near infrared bands. An investigation done by Riihela *et al*. (2013), on Spinning Enhanced Visible and Infra-Red Imager (SEVERI) reflectance bands 1 and 2, have also reported both additive and subtractive effects of SMAC model. The magnitude of changes in corrected and uncorrected value depends on AOT and ozone layer concentration of the atmosphere. This is an indication of interactions of different atmospheric components for satellite signal, though it instance depends on the signal band width similar to outcomes of this study.

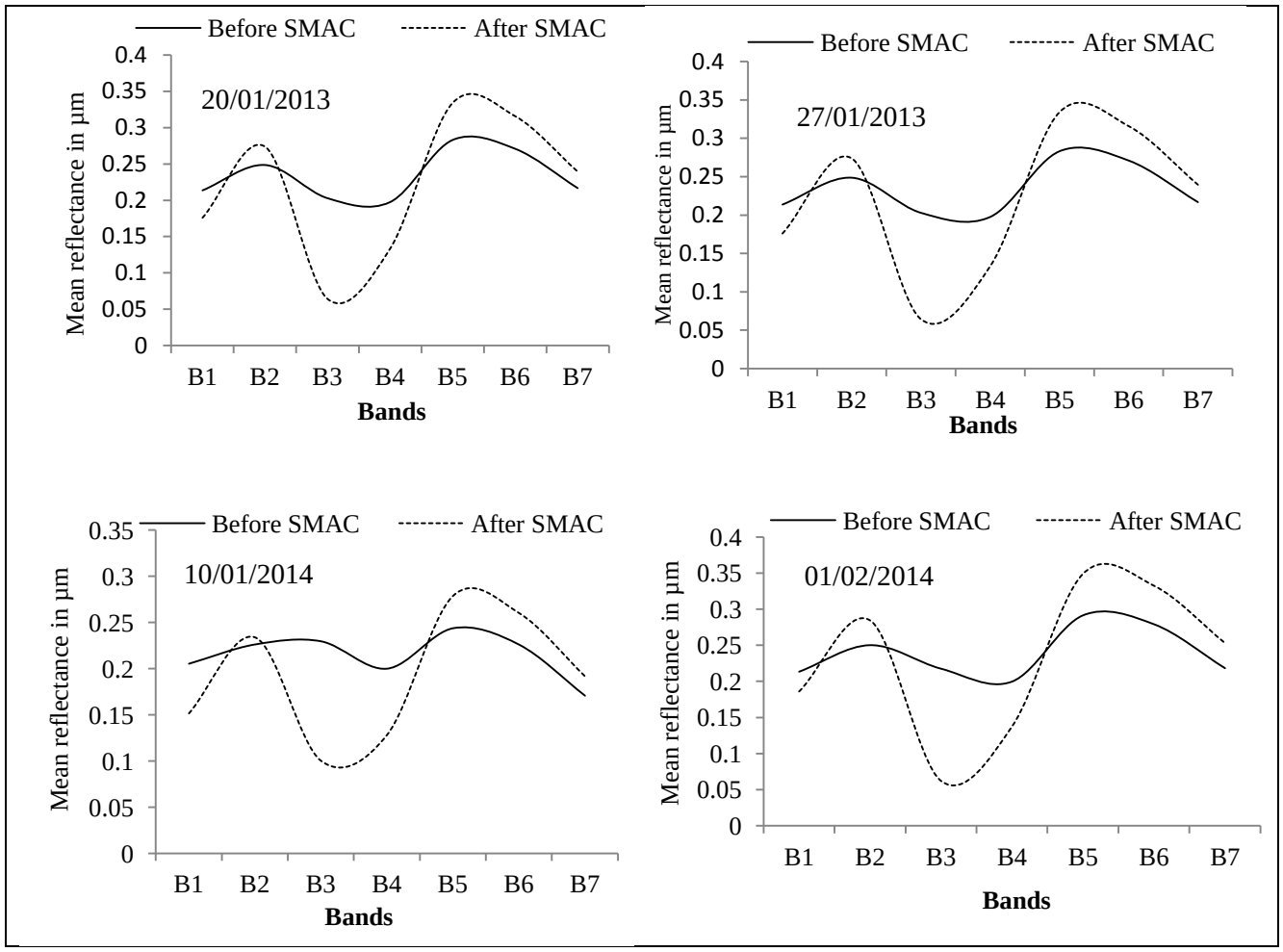

Figure 4.3: Impacts of atmospheric correction on MODIS reflectance bands

As it is presented on Table 4.3 and Figure 4.3, it is clear to have descriptive notation on the effect of SMAC based atmospheric correction on MODIS reflectance bands. For the purpose of certainly on claiming the impacts of atmospheric interference at the radiative transfer of MODIS reflectance signal, paired samples t-test on randomly taken 500 sample reflectance values from before and after atmospheric correction of each reflectance band has been undertaken. The result of analysis is presented on the following Table 4.4. The finding of this study has similar connotations with study done by Sharma *et al*. (2008) and Hadjimitsis *et al*. (2010), Hareef (2013) on IIRS P6 – LISS-IV and Landsat imagery respectively. Accordingly, the studies have reported an extreme reflectance value improvement in Landsat dataset and related land surface biophysical parameters like NDVI after atmospheric correction. In underlined way, Hadjimitsis *et al*. (2010) have claimed evapotranspiration value increments after utilization of

atmospherically corrected reflectance bands to derive variables for evapotranspiration estimation in SEBS model.

Table 4.4: Statistical test of SMAC model impacts on MODIS reflectance bands

Band	Mean difference	Standard deviation	Standard error of sample mean	T-statistic	Sig(2-tailed)
B1	0.0137742	0.0092234	0.0009223	14.93	0.00
B2	-0.007883	0.0059435	0.0005944	-13.26	0.00
B3	0.0172049	0.0050713	0.0005071	33.92	0.00
B4	0.0356100	0.013801	0.001380	25.80	0.00
B5	-0.01380	0.004727	0.000473	-29.20	0.00
B6	-0.014427	0.004723	0.000472	-30.54	0.00
B7	-0.018646	0.007711	0.000771	-24.18	0.00

As clearly presented on Table 4.4, overall bands have shown a statistically significant change at 95 and 5 percent confidence level and margin of error respectively at 499 degree of freedom (N-1) in sample means of reflectance before and after atmospheric correction. As presented in the Table 4.4, observed power of significance is too high that SMAC model has brought big improvements on MODIS reflectance bands under analysis. Therefore, for the succeeding analysis operations of which that demand reflectance bands, atmospherically corrected bands have been utilized.

4.2. Analysis of Derived Variables for SEBS Model

At this section, biophysical variables used to derive SEBS energy flux parameters and evapotranspiration has been presented. Basically analyzed surface albedo, LAI, NDVI, LST, fraction of vegetation cover and surface emissivity has been discussed. These parameters are basic determining factors in estimating energy fluxes through their conditioning effect of temperature and determining moisture availability (Billi & Caparrini, 2006).

4.2.1. Surface Albedo

An albedo, which is a ratio of reflected radiant flux to incident flux, is a parameter in controlling radiative energy portioning of between the surface and atmosphere (Schaaf, 2009). It plays a significant role in controlling net energy available for surface bio-physical processes (Dobos, 2006). Surface albedo is a variable used for various practical modeling applications (Liang, 2000), like to estimate the energy budget of the surface especially the net radiation. Presence of immense albedo can reduce available net radiation to trigger evapotranspiration (Pereira & Pires,

2011). Taking this into consideration, surface broad band albedo characteristics have been computed by using all reflectance MODIS bands. This is done to account overall broadband surface albedo on modeling process.

Table 4.5: Descriptive statistics of surface albedo across study area

DOY	20-Jan-13	27-Jan-13	10-Jan-14	1-Feb-14
Min	0	0.02	0	0
Max	0.57	0.65	0.63	0.61
Mean	0.25	0.27	0.26	0.27
Stdv	0.16	0.14	0.15	0.16

As presented values on Table 4.5 shows, the mean albedo values range from 0.25(±0.16) to 0.27(±0.16) but depending on the optical characteristics of the surface to reflect the incoming light. Extreme maximum albedo values range from 0.57 to 0.65 while the minimum albedo values range from 0 to 0.22. For existence of highly maximum albedo, it is attributed to the dryness of the surface where in the winter season the ground is left bare especially at agricultural land. As indicated in Pereira & Pires (2011), vegetation darkness associated with greenness can reduce surface albedo on vegetated surfaces. Contrary to this, in our analysis we found that, major rain fed agricultural fields is left bare and dry.

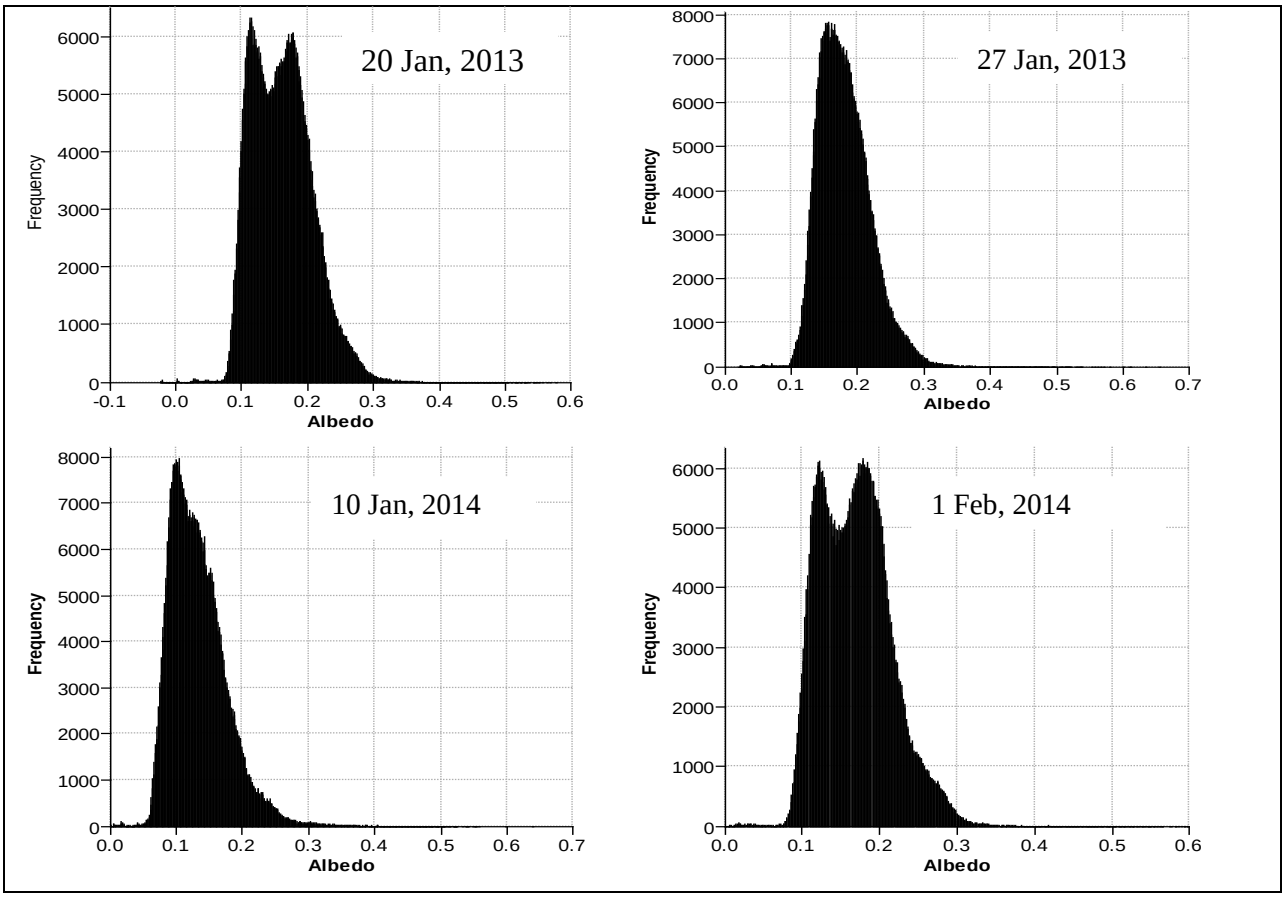

Figure 4.4: Surface albedo characteristics

As clearly presented on Figure 4.4, the maximum frequency of albedo values is found within the range of 0.05 to 0.25. The values that range to and greater than 0.3 are very few pixels which can also be attested from very low standard deviations from the mean, which is provided in Table 4.5. These pixels might be associated with some rock outcrops and built-up areas. Water body exposed for wind to have rough surface at satellite overpass time (10 AM local time where sun angle is low to moderate) can have also these outlier albedo values from the scene. One thing which should be noted here is that results presented at this study were not fixed for the study area rather surface albedo characteristics varies with local solar time and day of the year (season) (Disney, 2004), even for constant surface illumination characteristics. Though undertaken at different landscape of which current study site is done, results presented by Schaaf *et al*. (2002) have ascertained this argument. From the Julian day 129 of year 2000 to Julian day 033 of year 2001, crop land has shown lower albedo values than other land cover classes.

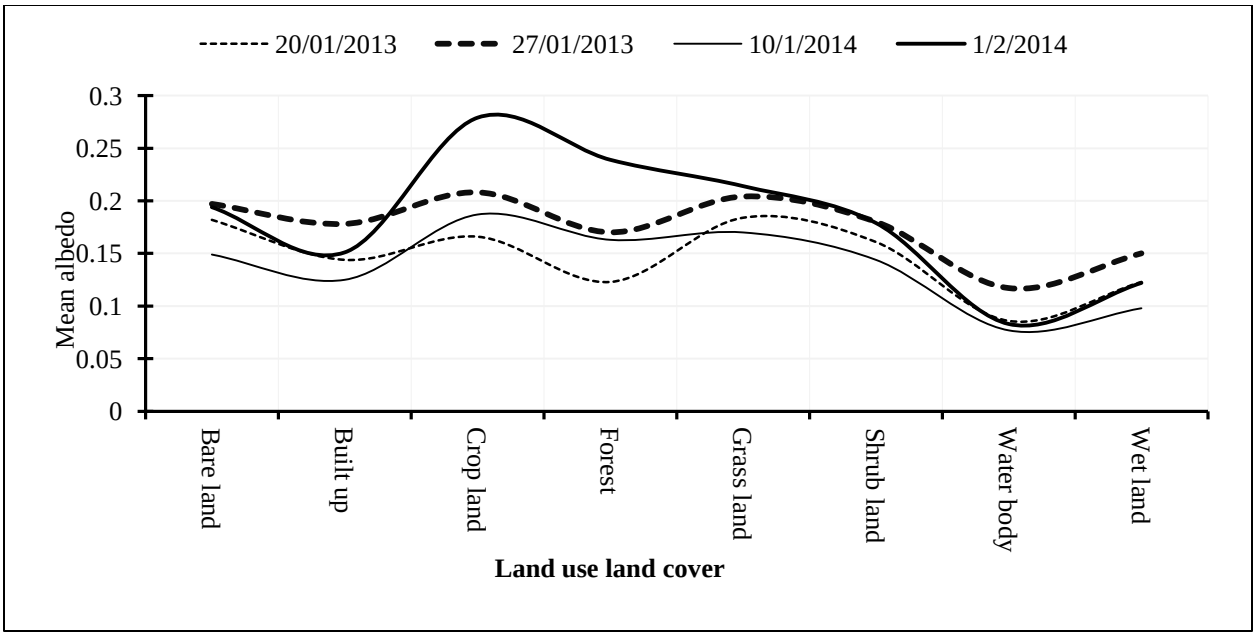

Figure 4.5: Surface albedo characteristics across land cover characteristics

As shown on Table 4.5, surface albedo varies as a function of land cover characteristics. Though it varies with days of the year, the minimum albedo is observed on water body followed by wetland, which is an indication as water body reflects minimum electromagnetic radiation. Similar to albedo values presented in Dobos (2006), which range from 0.1 to 1, current study, has also shown a minimal albedo values within this range. The variability of albedo within this range at water body is attributed to water surface roughness and angle of incident sun angle. Relatively the maximum surface albedo is observed on cropland. This is because of at the time of satellite overpass (all image is taken in dry winter season), the crop land is left either bare or covered by reflective crop residue which reflects immense amount of electromagnetic radiation. Following crop land, grass land and bare land have experienced relatively high albedo values.

As forest land has relatively better greenness and low color contrast, it has relatively moderate albedo values. Similar to this finding, though at different ecosystem with eastern Ethiopia, Moore (1976) has reported albedo contrasts between grassland (0.27 ± 0.03) and forest (0.11 ± 0.001) in the winter season. An albedo for grass land is reported to decrease in the summer season. This is because of vegetation regeneration and area covered by leaf is inversely related with surface albedo (Peng, 2015). By using this concept, Zeng & Woon (2009) have undertaken albedo based simulation model to assess expansion of sub-tropical deserts. They have reported increments in albedo and reductions in vegetation cover in areas where deserts are advancing. A

study by Fuller and Ottke (2002), has reported a strong curvilinear association between vegetation regeneration and surface albedo in western Africa. This shows that albedo varies as per vegetation canopy characteristics and species. Albedo values of built up areas in current study is lower than the surrounding land cover characteristics. This is attributed to presence of mixed vegetation in built up areas relatively greener than surrounding landscape (Taha, 1997).

4.2.2. Normalized Difference Vegetation Index (NDVI)

NDVI is a basic variable to derive various biophysical parameters as direct or surrogate variable. At this study derivation of fraction of vegetation cover, leaf area index and aerodynamic roughness length have utilized NDVI values as a basic variable. The basic assumption of this study on NDVI is that it can infer the state of vegetation condition, which is also an indication of available evapotranspiration from the land and vegetation surface governed by vegetative characteristics and available water. Observed NDVI value has also temporally vary. This is because of seasonal variability in climatic variables like precipitation that can affect seasonal vegetation greenness.

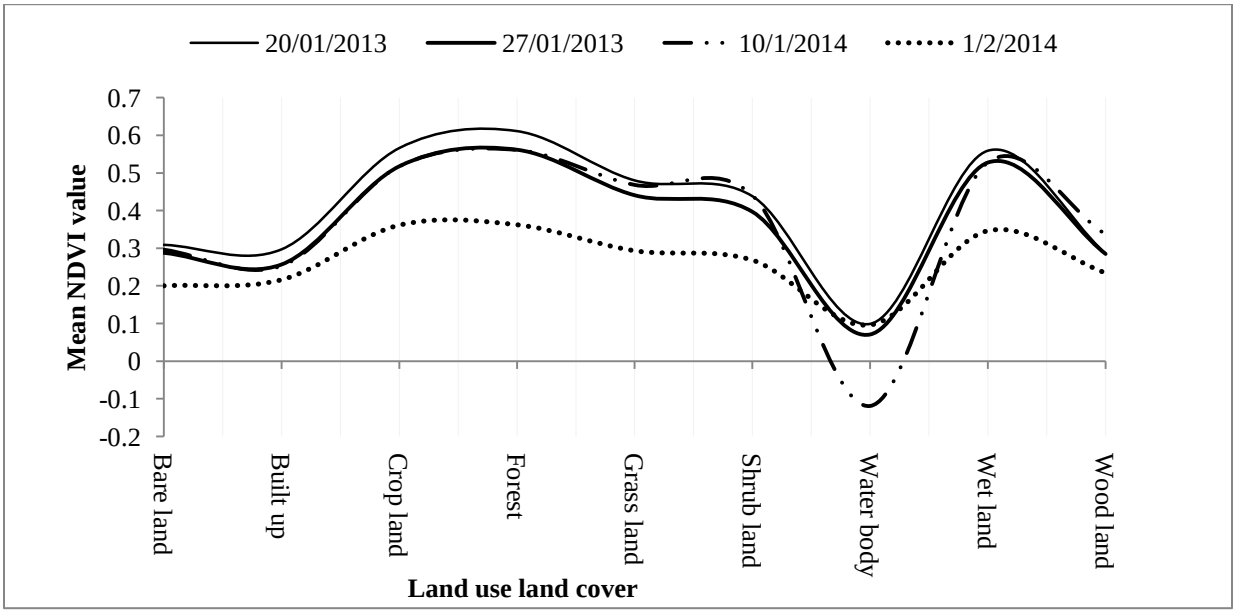

Figure 4.6: NDVI characteristics across land cover class

Depending on land cover type and day of the year, the study site has experienced variations in NDVI values. In all days of which the analysis is undertaken, the maximum NDVI value is observed in forest landscapes succeeded by wetland ecosystem. This maximum value related with these cover characteristics is related with vegetation flourishment and greenness

characteristics. As the season of satellite overpass for selected days of the year is dry winter season, cropland and grass land has shown relatively proxy NDVI values. This is resulted from dryness of grass land and dry crop residue at the crop land that can have relatively similar response for incoming electromagnetic radiation. Similarly, built-up environment and bare land have also shown relatively closer NDVI values.

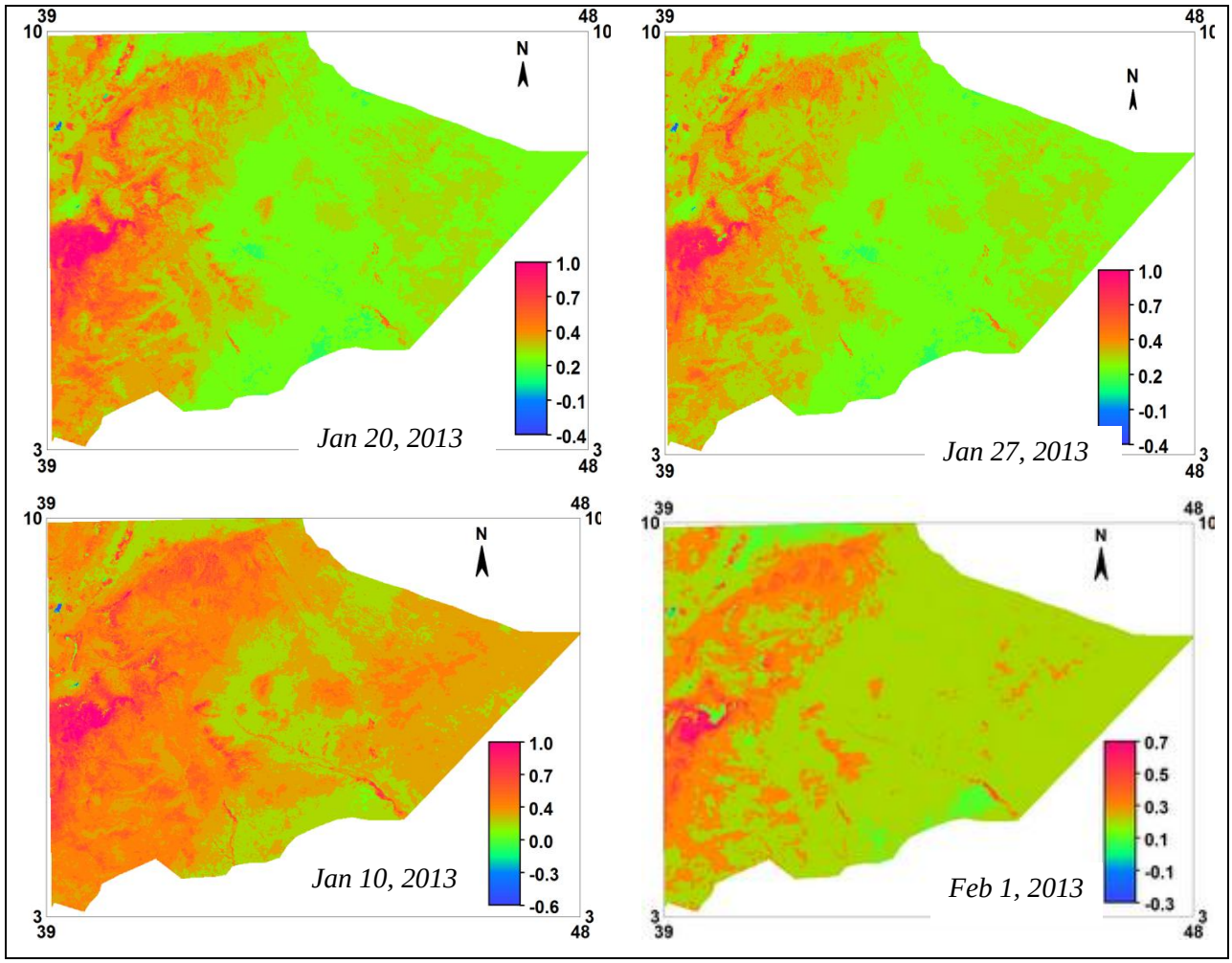

Figure 4.7: Spatio-temporal characteristics of NDVI at the study site

As per operational definition of this study a surface completely devoid of vegetation have an NDVI value 0.2 and below. As shown in Figure 4.7, bare land has shown NDVI value greater than 0.2 and slightly less than three. This connotes that the bare surface can have some leapfroggingly grown vegetation. An extremely minimum NDVI value is observed at water body. Its value is below 0.09 and for one day it downs to negative values. This is because of in the dry season where the sky is clear reflective surfaces like water and fresh snow reflect more at

red than infrared bands in one way that these surfaces experience negative NDVI values (Trishchenko *et al*., 2002). A lot unique and greater than expected is NDVI value of the built-up surface. This happens because of presence of mixed pixels that contain vegetation and built-up features, which inflates NDVI.

4.2.3. Leaf Area Index (LAI)

The LAI is one of the variable used to generate SEBS based energy flux terms and evapotranspiration in a prepackaged SEBS model. As stated in Manninen *et al*. (2009), this variable is an indication of available leaf quantity and is a measure of vegetation potential for photosynthesis, respiration, and interception of precipitating rain and other process that link the vegetation response with climate system. Therefore, LAI is an indication of surface covered by leaf and is a proxy variable to show the triggering effect on evapotranspiration. As presented in Kergoat (1998), this is happen through leaf area and canopy conductance, stomatal resistance and aerodynamic resistance. Taking different biomes as test sites, the study has claimed that interception water loss and total evapotranspiration have directly proportional relationships with LAI while soil evaporation loss decreases with increments in LAI. Transpiration loss has increased proportionally to some extent and falls with increasing LAI of the biome. Similarly, Simic *et al*. (2014) have claimed increments in forest Leaf Area Index has escalated evapotranspiration to extent it reduce ground water recharge. Taking this argument as centerpiece of reasoning as how LAI affect evapotranspiration, analyzed result of this study is presented in Table 4.6.

Table 4.6: Descriptive statistics of LAI of the study site

	DOY			
LAI	20-Jan-13	27-Jan-13	10-Jan-14	1-Feb-14
Minimum	0.00	0.00	0.00	0.00
Maximum	9.80	6.10	9.80	1.90
Mean	4.50	2.90	4.50	0.90
Std dev	2.70	1.70	2.70	0.60

For images in month of January, the maximum LAI of the study area is 9.8 and 6.1 while for February first 2014, the maximum LAI is found to be 1.9. This massive reduction in maximum LAI is related with decreasing in NDVI value, which is also attributed with reductions in vegetation greenness conditions with advent of extreme dry season. As investigated by Birky

(2001) on their linear modeling of NDVI, leaf area biomass and gross primary productivity, around 51% of variability in NDVI is explained with these variables. Observed reduction in LAI index can reduce the size of surface for transpiration resultant water usage (Pereira & Pires, 2011). Average values of LAI do also range from 0.9 in dry day of February first, 2014 while 4.5 in the mid of January when vegetation greenness is relatively better than other dry season days. Most low land parts of the study area where arid and semi arid climate dominate, has experienced a LAI value of less than 1. This is a consistent finding with a LAI and aridity gradient simulation done by Scholes *et al*. (2004). With increasing aridity gradient and decreasing rainfall amount, the LAI has shown consistent reductions with precipitation and aridity gradient. The findings of Zeng & Yoon (2009), has also reported similar feedback system between LAI, albedo and temperature to show global warming and temperature dynamics. Since 1901 in areas where LAI changed from 2.6 to 0.3, there is from 28% to 5% reductions in soil wetness, which further menace evapotranspiration. Similarly, a global synthesis review done by Asner *et al*. (2003) has reported that temperate evergreen forests, plantations and wetlands have large NDVI values while grass lands, tundra ecosystem and deserts have minimal values.

More importantly, plant canopy structure, which is partly manifested by LAI, can affect surface temperature characteristics and vegetation greenness that are the main deriving and constraining factor to initiate evapotranspiration (Han *et al*., 2004). To support firm relationship between NDVI and vegetation fraction, a correlation matrix analysis has been run and the result indicates as a LAI is a positive implication of vegetation cover and its vegetative greenness condition. There is extremely strong positive association between LAI in one hand and NDVI and fraction of vegetation cover in other hand.

Table 4.7: Association of NDVI and fraction of vegetation cover with LAI

	NDVI	LAI	F_v
NDVI	1.00		
LAI	0.97	1.00	
F_v	0.73	0.70	1.00

4.2.4. Surface Emissivity

As investigated by Brunsell and Gillies (2000), an account of surface emissivity characteristics into land surface temperature retrieval has resulted significant changes in surface temperature

values. As per this during conversion of brightness temperature into surface temperature value, surface emissivity characteristics and atmospheric water vapour should be considered. Surface emissivity varies as per thermodynamic character of the surface cover. As per this, a surface emissivity map has been presented on the following Figure 4.8.

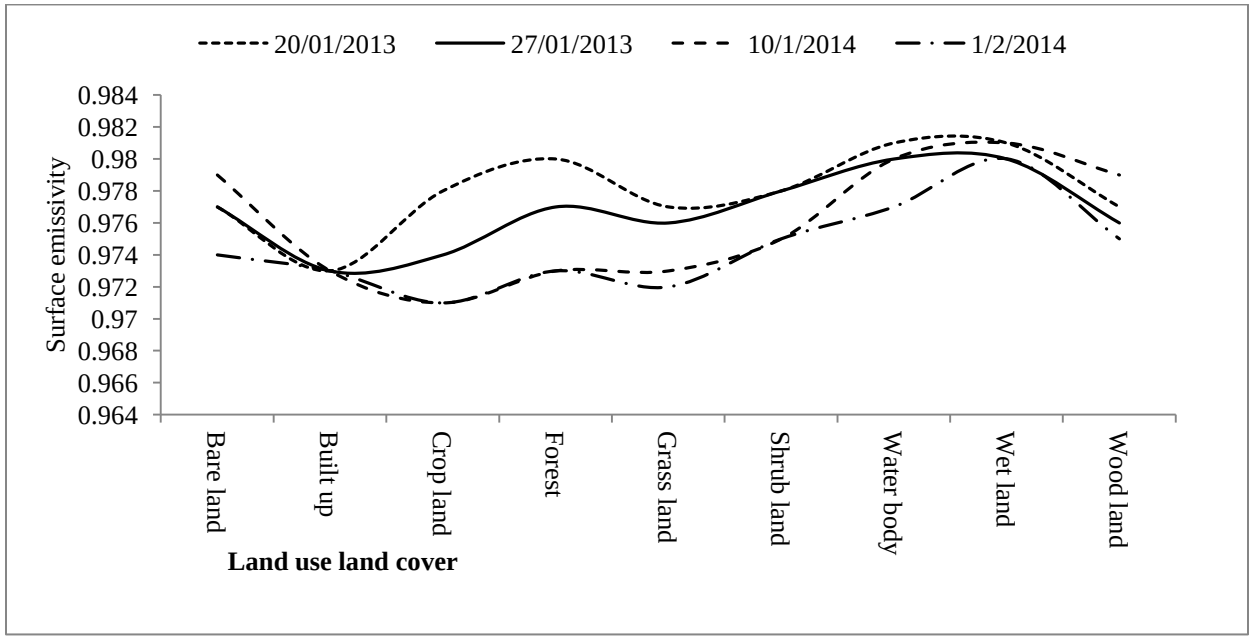

Figure 4.8: Variations of surface emissivity across land cover classes

A surface emissivity characteristic of the study site varies as per land cover characteristics. A large surface emissivity value has been observed in forest, wetland and water body. Bare land and built up has shown minimal surface emissivity followed by crop land and grass land. As stated in Petitcolin and Vermote (2002), surface emissivity is minimal at bare soil while it ranges to climax (unity) at fully vegetated surface or forestland with full canopy. Further study done by Takashima & (1987), has claimed impossibility to infer surface emissivity from level of vegetation cover especially in arid and semi-arid environment.

4.2.5. Surface Temperature

If other things remain constant, deviations in surface temperature can lead differences in evapotranspiration rate even at similar surfaces with similar biophysical characteristics. After computation of other model variables that are inputs for land surface temperature (brightness temperature, atmospheric water vapour, emissivity and emissivity difference), land surface temperature has been estimated. To provide a clear clue, the way how these variables are

associated with surface temperature is also presented by using correlation matrix of the stated variables.

Table 4.8: Correlation matrix to show association of land surface temperature with other surface parameters

Parameter	T_s	$\boldsymbol{\varepsilon}$	LAI	NDVI	*Fv*	W	$\boldsymbol{T_{b31}}$	$\boldsymbol{T_{b32}}$	$\boldsymbol{\varepsilon d}$	Elevation
T_s	1.00									
$\boldsymbol{\varepsilon}$	-0.56	1.00								
LAI	-0.15	-0.29	1.00							
NDVI	-0.22	-0.20	0.97	1.00						
Fv	-0.47	0.37	0.70	0.73	1.00					
W	-0.01	0.03	-0.08	-0.08	-0.07	1.00				
$\boldsymbol{T_{b31}}$	0.99	-0.55	-0.12	-0.19	-0.46	0.01	1.00			
$\boldsymbol{T_{b32}}$	0.99	-0.53	-0.14	-0.20	-0.45	-0.09	0.99	1.00		
$\boldsymbol{\varepsilon d}$	-0.41	0.08	0.42	0.46	0.20	0.05	-0.30	-0.32	1.00	
Elevation	-0.46	-0.05	0.53	0.56	0.43	-0.50	-0.46	-0.44	0.26	1.00

Though the primary goal of this study is not revealing factors that determine surface temperature condition, results presented on Table 4.9 below, can give a better clue to understand how surface temperature varies across space and interact with other biophysical conditions. Basically, land surface temperature has shown big positive association with both brightness temperatures of radiance bands 31 and 32 followed by land surface emissivity where coefficient of correlation is -0.56 that inversely associated with land surface temperature. Surface elevation and associated level of fraction of vegetation cover are also negatively associated with land surface temperature. The big lesson we can take from this correlation matrix table is that because of implications of surface emissivity, vegetation greenness condition (NDVI), level of vegetation cover, available atmospheric water vapour and elevation, land surface temperature can have either higher or lower thermal values than top of atmospheric (TOA) temperature based on their level of interplay. As reported by Li *et al*. (2015), land surface temperature is a brightness temperature where atmospheric effects and surface emissivity is taken into model assumption during estimation.

Table 4.9: Mean land surface temperature across different land cover classes

	Mean surface temperature in ^{o}K			
Land Cover	20-Jan-13	27-Jan-13	10-Jan-14	1-Feb-14
Bare land	309.35	311.76	310.56	310.28
Built-up	305.37	306.23	306.43	304.33
Crop land	306.24	306.22	304.16	304.25
Forest land	305.32	305.61	304.15	301.92
Grass land	309.90	310.90	307.76	309.48
Shrub land	308.62	309.49	307.32	307.34
Water body	298.73	297.12	298.44	296.68
Wet land	301.23	302.99	303.84	302.43
Wood land	310.79	311.73	308.53	310.52

As lucidly presented on Table 4.9, the land surface temperature is spatially varied across different land cover classes. The highest temperature is observed at bare land; shrub land, grass land and crop land where at the winter season have relatively similar vegetative phonological characteristics and wetness conditions. As presented in Dessie (2010), presence of high temperature results in large amount of evapotranspiration, which even farther works to reduce ground water recharge of a given area. In all days under analysis, a lowest value of surface condition is observed at water body followed by wetland where surface thermal power is conditioned by water vapour and available moisture.

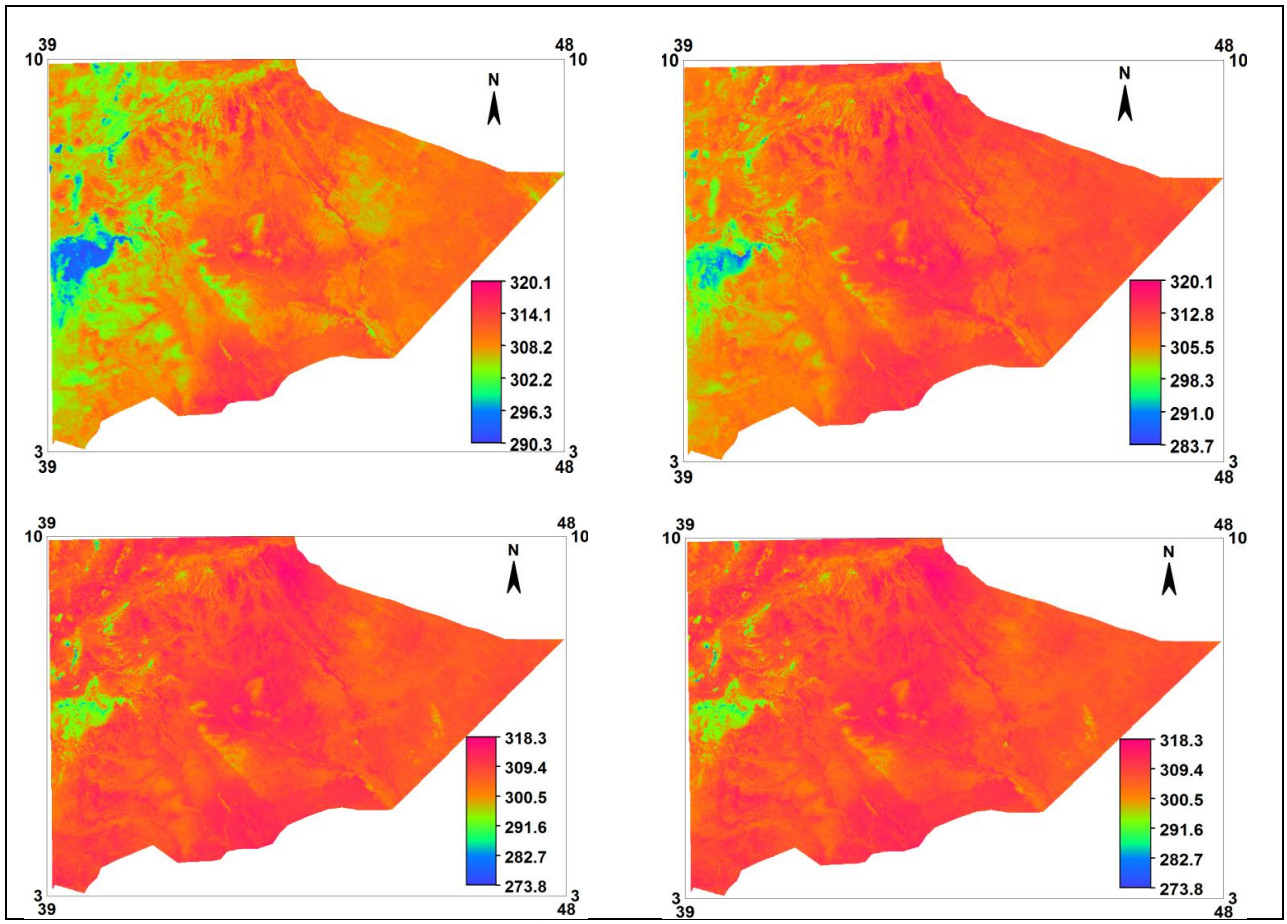

Figure 4.9: Land surface temperature (K^{o}) variability in the study site

Vegetated surfaces can have a lower surface temperature than other built up and bare land areas around arid and semi-arid areas especially city centers and thermal power plant (Sekertekin *et al*., 2015) but at current study a lot different value observed than usual temperature scenario is thermal condition of built-up areas which experienced lower temperature values. This is because of most built-up area in the study site is urban areas. To reduce prevailing heat, most urban areas in eastern Ethiopia are covered with garden and street vegetation which experience them to have relatively lower temperature conditions than surrounding arid and semi-arid rural areas. In other way, urban temperature pattern is also depends on reflective characteristics of built-up materials. If built-up areas have high albedo characteristics, it can have lower skin temperature attributed to lower absorption rate of incident radiation (Sailor, 1995; Taha, 1997). This happens as an increase in albedo of 0.01 can result an increase of blackbody temperature by 1 ^{o}K if other variables in the feedback loop remain constant (Goode *et al*., 2001). This urban temperature

pattern is mostly for dry winter season as surrounding rural area in summer season have better vegetation greenness.

4.2.6. Fraction of Vegetation Cover

Vegetation cover has a significant implication in either fostering or hindering the process of evapotranspiration. For the operationalization of this study, fraction of vegetation cover is derived from vegetation greenness condition (NDVI). As NDVI is sensitive to seasonal vegetation greenness condition, vast expanses of the study site (Figure 4.10, below) has experienced minimal vegetation fraction values. Moderate to high values of fraction of vegetation cover is observed at highland areas where relatively better forest stand exists. Lowland areas of eastern part of the study site have experienced minimal or almost zero vegetation cover. This is related with natural aridity of the area and the season when the image is taken. In arid and semi-arid environment the leaf area biomass and greenness is minimal. This can lower NDVI values (Carlson & Ripley, 1997; Birky, 2001). Therefore, as NDVI and fraction of vegetation cover have an excellent association (Barati *et al*., 2011), lower NDVI resulted in lower fraction of vegetation cover. Vegetation fraction can have an impact on surface het transfer and energy closure.

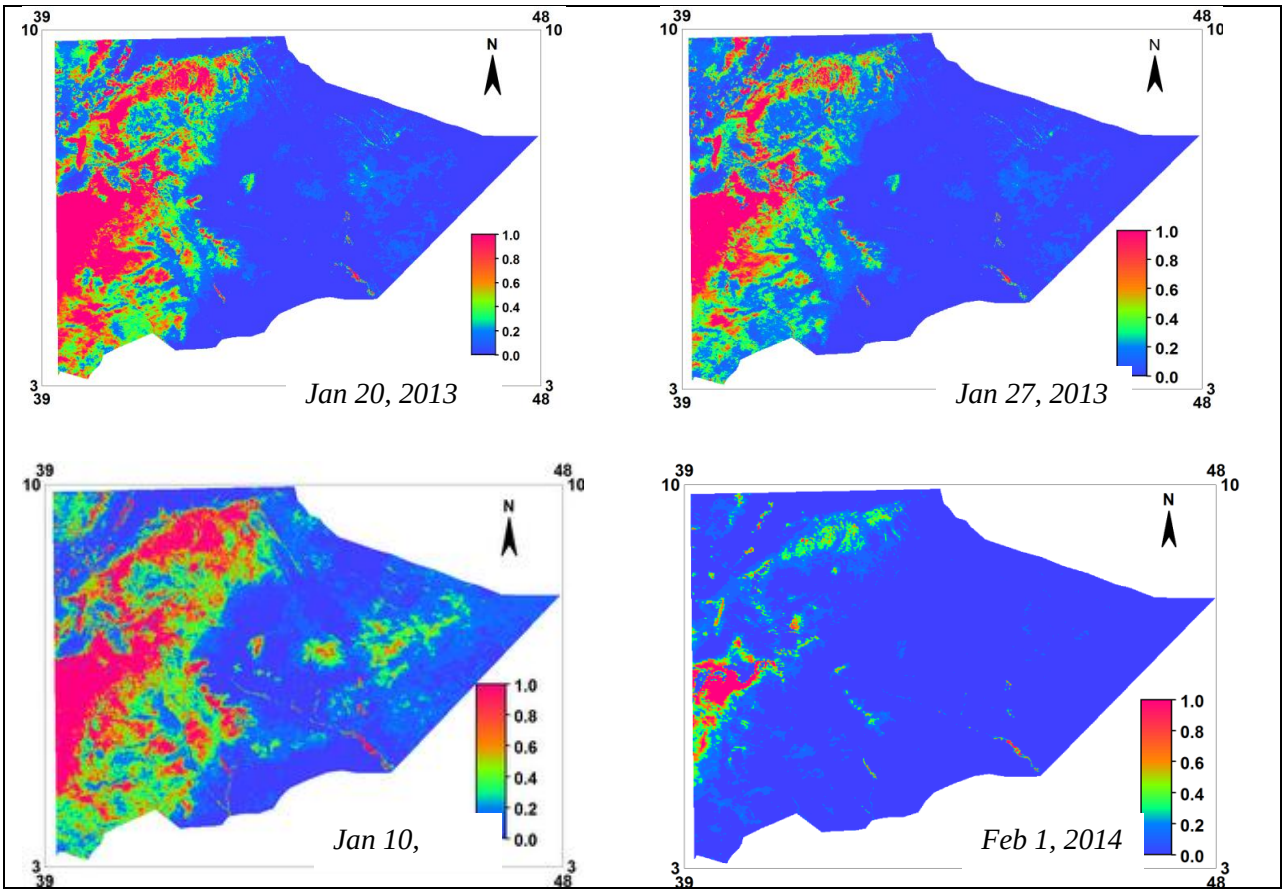

Figure 4.10: Fraction of vegetation cover of study area

4.3. SEBS Based Energy Fluxes and Evapotranspiration

4.3.1. SEBS Based Energy Fluxes

By using parameterized biophysical variables which are discussed above and other processed meteorological variables from GLDAS dataset, SEBS energy flux terms, evaporative fraction and actual daily evapotranspiration has been computed. Estimated results has been tried to be presented and discussion were provided. In SEBS algorithm, net radiation, sensible heat flux, ground heat flux and latent heat flux are basic energy partitioning variables to estimate evapotranspiration. For DOY under analysis, aggregate descriptive statistics of study area energy fluxes are given in Table 4.10.

Table 4.10: Surface energy fluxes at the study site

SEBS energy flux terms	Aggregate mean energy flux values in DOY			
	20-Jan-13	27-Jan-13	10-Jan-14	1-Feb-14
LE (Wm^{-2})	260.78	308.85	277.99	279.81
H (Wm^{-2})	184.6	199.96	186.02	162.41
G_o (Wm^{-2})	131.12	155.66	130.83	151.69
R_n (Wm^{-2})	576.50	664.47	594.84	593.91
	15-Jun-14	15-Jul-14	15-Aug-14	15-Sep-14
LE (Wm^{-2})	599.20	599.80	608.20	654.80
H (Wm^{-2})	228.10	204.80	187.20	218.50
G_o (Wm^{-2})	317.10	360.30	307.10	320.00
R_n (Wm^{-2})	1144.40	1164.90	1102.50	1193.30

As tried to be presented in Table 4.10, net radiation has shown larger values than other three energy flux terms. This is because of net radiation is the sum of latent heat of vaporization, ground heat flux and sensible heat flux which is energy used to evaporate the water from different surfaces, to heat the surface and to heat the air respectively. As results clearly shown, latent heat of vaporization, soil heat flux and ground heat flux interact in a different manner. The values and magnitude of interaction has dramatically changed in dry and wet seasons. In the wet season there is found larger latent heat fluxes and net radiation. Values presented on this table are aggregate means of the whole study area and do not elucidate the spatial variability of energy flux across different landscapes. As argued by Yan *et al*. (2014), land cover characteristics of a given spatial location can have a significant and tremendous impact on land surface energy balance exchange. This is happen because of different land cover characteristics have different heat transfer characteristics (Billi & Caparrini, 2006). Taking this into account, to have a clue for spatial variability of surface energy balance fluxes across land cover classes, energy flux are partitioned into different land cover classes.

Table 4.11: Energy fluxes across different land cover classes

DOY	Parameter (Wm^{-2})	Bare land	Built-up	Crop land	Forest land	Grass land	Shrub land	Water body	Wet land	Wood land
20, 2013	*LE*	159.69	-264.55	251.99	364.48	153.79	269.22	355.91	398.21	177.9
	H	246.83	680	211.99	122.78	283.25	200.34	109.81	89.07	384.17
	G_o	144.68	140.39	120.88	117.68	143.94	135.68	158.78	108.15	146.88
	R_n	551.2	555.84	584.86	605.29	580.98	605.24	624.5	595.43	596.84
27, 2013	*LE*	159.43	-210.72	265.98	422.84	105.7	297.53	304.94	440.3	167.02
	H	297.71	699.73	248.33	130.66	358.98	226.59	259.38	130.28	308.62
	G_o	164.69	162.2	146.49	145.82	162.03	162.01	188.37	128.26	166.69
	R_n	621.83	651.21	660.8	699.32	626.71	686.13	752.69	698.84	642.33
10, 2014	*LE*	159.69	-264.55	251.99	364.83	153.79	269.22	355.91	398.21	177.9
	H	246.83	680	211.99	122.78	283.25	200.34	109.81	89.07	272.06
	G_o	144.68	140.39	120.88	117.68	143.94	135.68	158.78	108.15	146.88
	R_n	551.2	555.84	584.86	605.29	580.98	605.24	624.5	595.43	596.84
32, 2014	*LE*	96.21	-201.99	228.22	366.76	86.37	267.59	258.78	395.59	147.5
	H	310.89	630.72	212.88	101.74	324.9	189.52	203.65	85.27	279.89
	G_o	155.04	153.42	145.98	149.81	149.68	158.1	189.6	143.18	153.72
	R_n	562.14	582.15	587.08	618.31	560.95	615.21	652.03	623.67	581.11

The interactive feedbacks between these variables are a lot intricate and are coupled with land cover characteristics, available energy and moisture characteristics. As presented in Table 4.11, surfaces that are moisture deficit such as built-up and bare land has experience higher sensible heat flux and lower latent heat of vaporization while surfaces with relatively available moisture like wetland, water body and forest cover have shown higher latent heat of vaporization and lower sensible heat flux.

On this study, an eye catching interaction among variables is patterns in latent heat of vaporization and sensible heat flux. At built-up environment where there exist both vegetation and artificial surfaces, major part of energy is portioned to heat the surface while in areas where there exist mist conditions like water body, wetland and forest land small sensible heat flux is observed. In landscapes where there is high amount of energy is partitioned to evaporate the water, little energy is portioned to heat the surface. Though the magnitude of relationship is not

equal, as observed from this study, it can be inferred as latent heat of vaporization and sensible heat flux are inversely proportional at different land cover classes. As investigated by Yan *et al*. (2014), land cover conversions alone if other things remain constant, can regulate energy flux balance of a surface especially the intricate balance between sensible heat flux, latent heat of vaporization and net radiation. Similarly, Jiang *et al*. (2014) and Ma *et al*. (2014) on their study that investigated land cover change and its implications on energy flux balance have reported that much amount of latent heat flux is observed in forest land while built-up surface has experienced minimal latent heat flux.

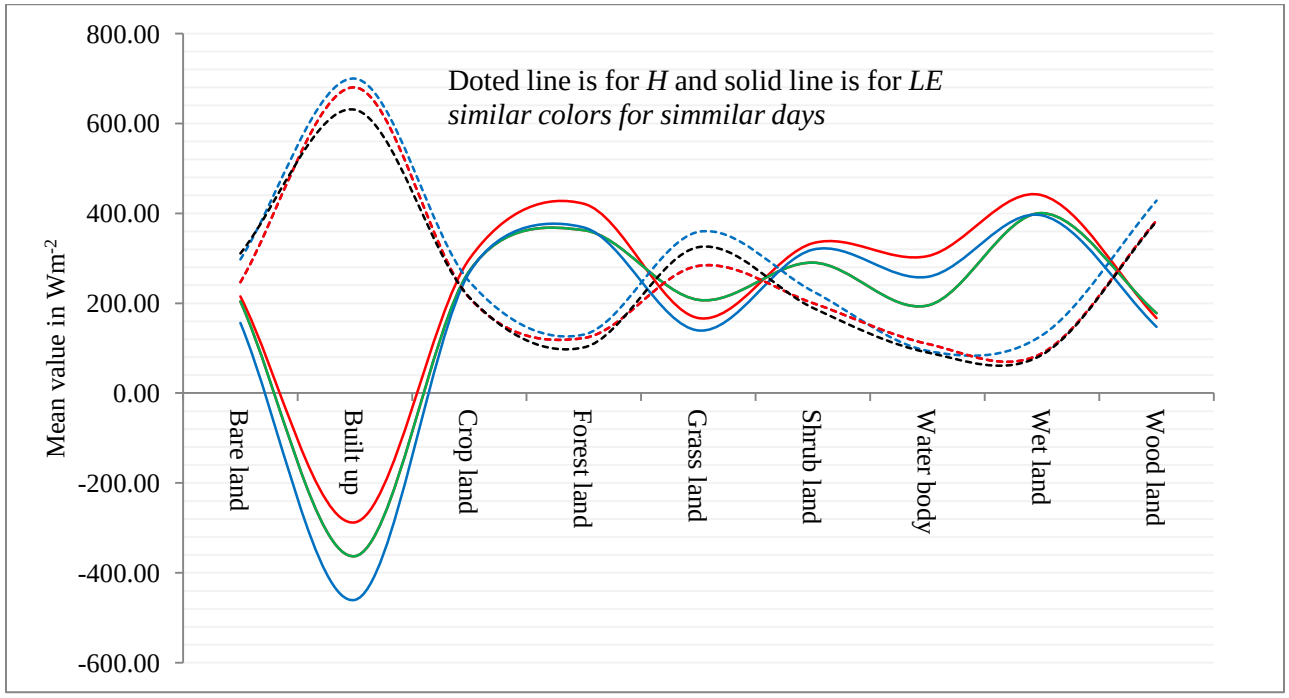

Figure 4.11: Interaction of H and LE across different land cover class at different DOY

4.3.2. SEBS Based Evaporative Fraction

SEBS model does not directly estimate daily evapotranspiration values rather by upscaling instantaneous evaporative fraction. Taking this into consideration, estimated evaporative fraction for dry season is presented on Table 4.12. The minimum evaporative fraction is found 0, which implies either overall energy is partitioned to heat the surface or evapotranspiration process is constrained by absence of available surface water. The maximum evaporative fraction observed for all day under analysis is 1, which implies unless constrained by available energy there, is potential evapotranspiration.

Table 4.12: Descriptive statistics of SEBS based evaporative fraction

Evaporative fraction (mm h^{-1})	20-Jan-13	27-Jan-13	10-Jan-14	1-Feb-14
Min	0	0	0	0
Max	1	1	1	1
Mean	0.5	0.5	0.5	0.5
Std	0.3	0.3	0.3	0.3
	15-Jun-14	15-Jul-14	15-Aug-14	15-Sep-14
Min	0	0	0	0
Max	1.3	1	1	1
Mean	0.7	0.5	0.5	0.5
Std	0.4	0.3	0.3	0.3

In remote sensing based estimation of evapotranspiration, evaporative fraction (ratio between available latent heat of vaporization to net radiation during satellite overpass) is basic for daily and grater temporal evapotranspiration estimation. Similarly, it is an indication of surface moisture availability and vegetation condition (Nutini *et al*., 2014). As stated in Peng *et al*. (2013), for the days of clear sky, evaporative fraction is constant across the day that it is used for upscaling into daily actual evapotranspiration.

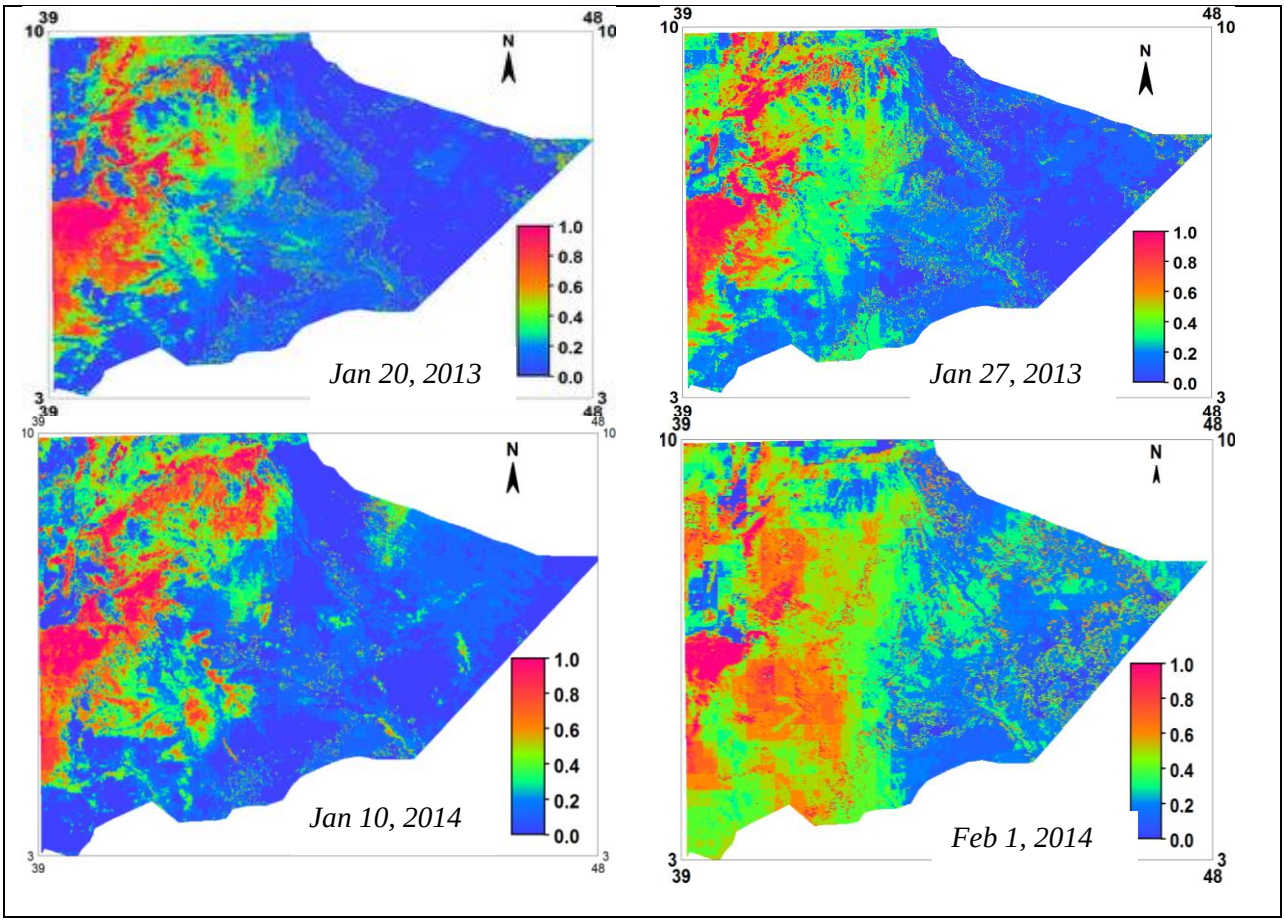

Figure 4.12: SEBS based daily evaporative fraction of the study site for dry season

With this assumption, the mean evaporative fraction of the study site across different land cover class for DOY under analysis is presented in Table 4.13.

Table 4.13: Mean evaporative fraction at different land covers classes

	Mean evaporative fraction mm hour^{-1}			
Land Cover	20-Jan-13	27-Jan-13	10-Jan-14	1-Feb-14
Bare land	0.49	0.48	0.48	0.37
Built-up	0.67	0.71	0.79	0.77
Crop land	0.59	0.63	0.63	0.61
Forest land	0.64	0.69	0.64	0.67
Grass land	0.61	0.60	0.60	0.56
Shrub land	0.60	0.62	0.60	0.64
Water body	0.68	0.76	0.62	0.75
Wet land	0.74	0.56	0.63	0.70
Wood land	0.37	0.39	0.39	0.38

Table 4.13 has brought clear spatial variability of instantaneous evapotranspiration at satellite overpass time (late morning). Large evaporative fraction is observed at wetland and water body

followed by built-up area on 2013, DOY 20 and 27 but for the year 2014 DOY 10 and 32, built-up environment has shown largest mean evaporative fraction followed by wet land and water body. For all DOY under analysis on this study, wood land followed by bare land have experienced lower evaporative fraction.

4.3.3. SEBS Based Daily Evapotranspiration

To operational definition of this study, SEBS based evaporative fraction is considered as instantaneous evapotranspiration of satellite overpass. By using this instantaneous evapotranspiration, daily actual evapotranspiration is upscaled (*see* Eq. 3.29). As presented in the table provided below, the maximum daily evapotranspiration for the study site reaches to 10 mm day^{-1} while the daily minimum evapotranspiration is found 0 mm day^{-1}. These maximum and minimum values cannot be representative of the whole study area as single pixels can have an outlier values. The mean and standard deviation is more sounding descriptive parameters. The mean evapotranspiration for the study area is 3.77 (±1.63), 3.74 (±1.54), 3.83 (±1.58) and 4.05 (±1.72) mm day^{-1} for the DOY 20 & 27 in 2013 and DOY 10 & 32 in 2014 respectively. The finding of current study is consistent with long-term monthly mean annual potential evapotranspiration results presented in Karimi *et al*. (2015). The study has reported long-term potential evapotranspiration of Awash Valley; northern extent of current study area, for months January and February is found 4.8 & 5.2 mm day^{-1} respectively. Similar to patterns of evaporative fraction, the mean evapotranspiration value of the study area has not shown big differences except its standard deviations from the mean. This can be resulted from small pixels that have large values in dry season and relatively larger number of pixels with moderate values.

Table 4.14: Descriptive summary of SEBS based daily evapotranspiration

Daily ET(mm day^{-1})	20-Jan-13	27-Jan-13	10-Jan-14	1-Feb-14
Min	0	0	0	0
Max	6.59	6.94	7.76	9.86
Mean	3.77	3.74	3.83	4.05
Std dev	1.63	1.54	1.58	1.72
	15-Jun-14	15-Jul-14	15-Aug-14	15-Sep-14
Min	0	0	0	0
Max	7	7.1	7.5	6.1
Mean	3.4	3.5	3.8	2.9
Std dev	2	2	2.2	1.7

To provide a clue on how evapotranspiration pattern has changed with seasonal vegetation regeneration and available energy, computed image histogram is presented in Figure 4.13. As shown on the figure, on DOY at the dry season, there is large frequency of pixels with smaller evapotranspiration values especially with values ranging from 0 to 3 mm while in the wet season there are frequent numbers of pixels with evapotranspiration values ranging from 3 to 5 mm. In wet season, because of vegetation greenness and surface moisture availability in the study site, there is small number of pixels with null evapotranspiration values.

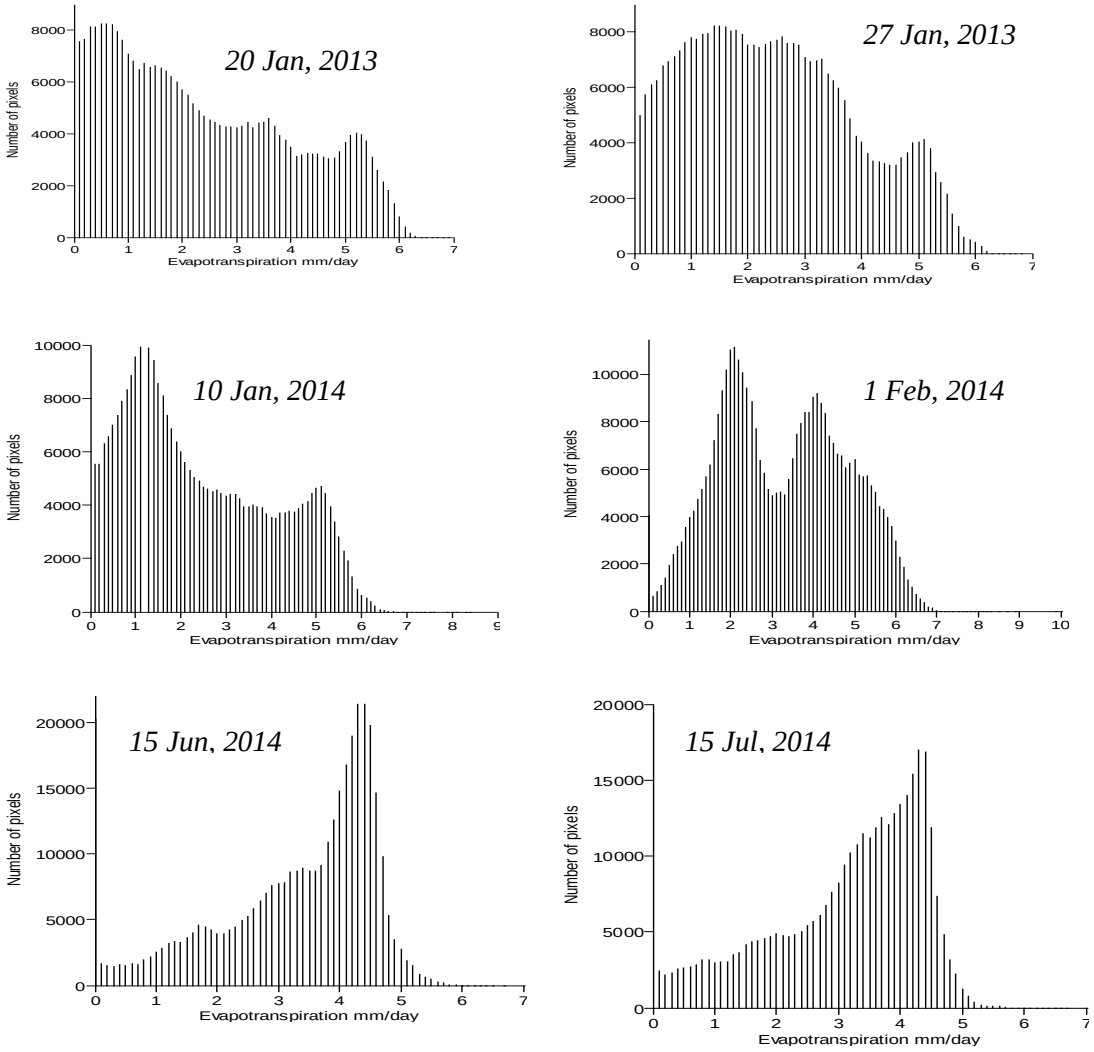

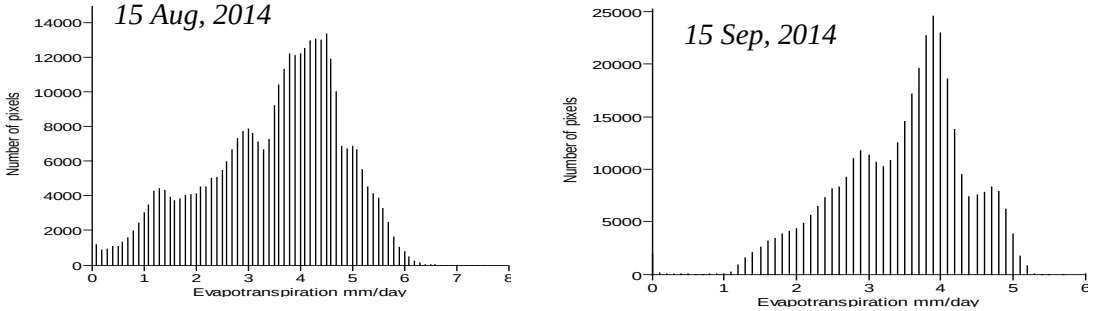

Figure 4.13: Histogram showing pattern of evapotranspiration in the study site

To provide a clue on how estimated daily evapotranspiration varies across space, it is presented on the following Figure 4.14.

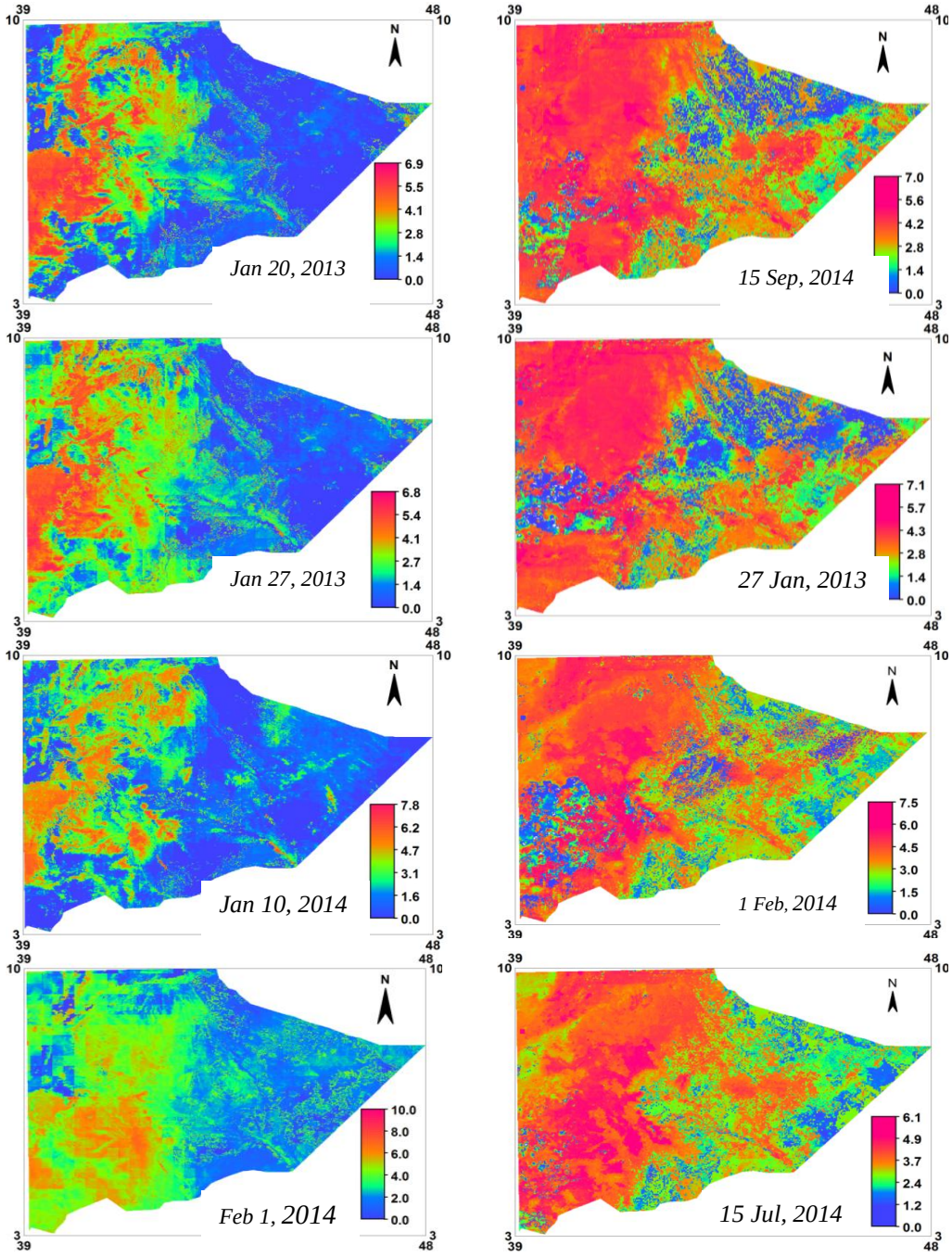

Figure 4.14: Spatial characteristics of SEBS based evapotranspiration

The values presented on Table 4.14 are aggregates for the whole study area. When we look into the spatial variability of evapotranspiration, it has shown large values in highland and water bodies. As lucidly presented in the Figure4.15, there is spatial variability that, the maximum evapotranspiration is observed at water body, wetland and forest land. Relatively the minimum value is observed in crop land, grass land, wood land and built-up environment.

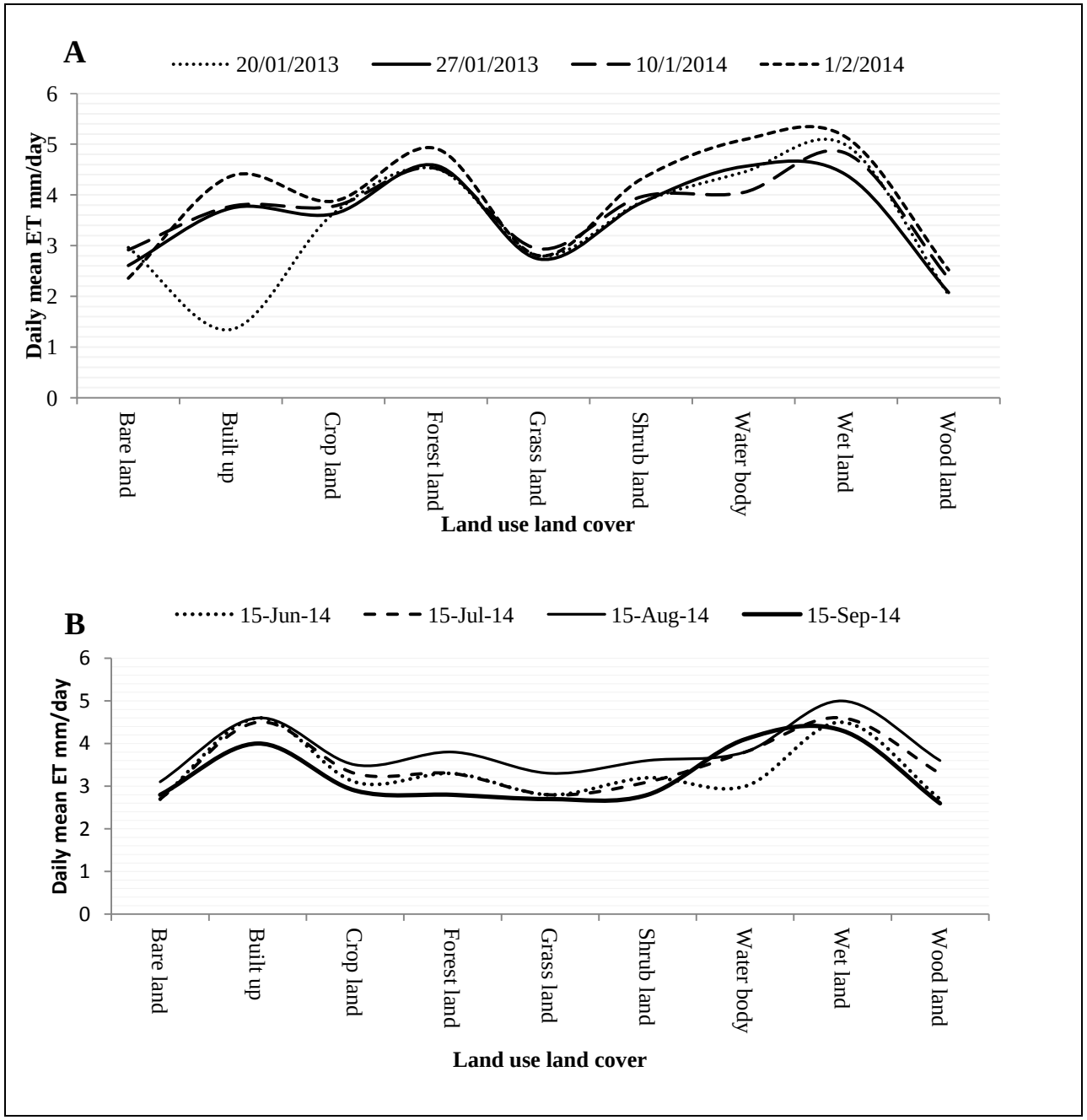

Figure 4.15: Daily SEBS based mean evapotranspiration across different land cover classes A). Dry season B). Wet season

As shown on the figure, upscaled daily evapotranspiration values follow almost similar patterns with evaporative fraction values presented in Table 4.12. Accordingly, forest land cover has experienced approximately equal evapotranspiration rate with water body and wet land. This can be attributed with canopy intercepted water evaporation coupled with transpiration immediately or after slightly shower rainfall at arid and semi arid environment. Similar to findings of this study, though under different study site in Ethiopia and with different estimation model, a study by Tenalem (2003), has reported maximum evapotranspiration rate at forest land cover in matured forest and afro-alpine ecosystem preceded by swamp and soda ash evaporative pans. A study by Tanaka *et al*. (2003) has reported that simulated cumulative evapotranspiration value has shown agreement with rainfall intercepted by canopy in evergreen forest. In our analysis, land covers where there exist surface and canopy intercepted water deficit in the dry season, crop land, shrub land and wood land, have experienced lower value.

More importantly, their minimal evapotranspiration rate can also be attributed with vegetation dryness and minimal leaf area index associated with semi desert vegetation canopy structure (Mo *et al*., 2004) in most parts of study site. The case for urban areas to have better evapotranspiration rate than grass land is attributed to presence of well watered vegetated surfaces in gardens, green parks and sides of streets that are greener than winter grass. As findings and respective arguments presented in Lin *et al*. (2006), though commonly known wisdom about evapotranspiration pattern in built-up area is minimal or null, with capability of remote sensing methods to catch existed mixed pixels there is evapotranspiration rate even that exceed other landscapes. With existence of vegetation cover at built-up areas, there is reduction in intensity of artificial concrete surface. As investigated by Liu *et al*. (2010), evapotranspiration rate in built-up environment is inversely proportional with level of built-up intensity.

Though water body have not experienced moister deficit for evapotranspiration, it has experienced mean evapotranspiration rate, which is less than wetland. This can be attributed to variations in surface albedo characteristics. As stated by Tenalem (2003), variations related with albedo, salinity and colloidal clay content can cause differences in evapotranspiration rate even at single lake surfaces at different spatial location. Observed evapotranspiration pattern in summer season is a lot different from dry season pattern across different land cover classes. Crop land, grass land and shrub land that have lower evapotranspiration rate than forest land in the dry

season have almost nearby values with forest land in wet season. This can be attributed to rejuvenation of vegetation greenness in summer season as vegetation indices like NDVI and LAI are reported well associated with rainfall (Zoungrana *et al*., 2015).

4.4. SEBS Model Results Comparative Analysis

4.4.1. FAO-Penman Evapotranspiration

Taking its relevance for validating remote sensing based SEBS model result in study area, evapotranspiration has been estimated from *in-situ* based meteorological stations on both days of the year taken from dry and wet season. As per these, point based evapotranspiration for both wet and dry season days has been estimated by FAO-PM method and presented in Figure 4.14.

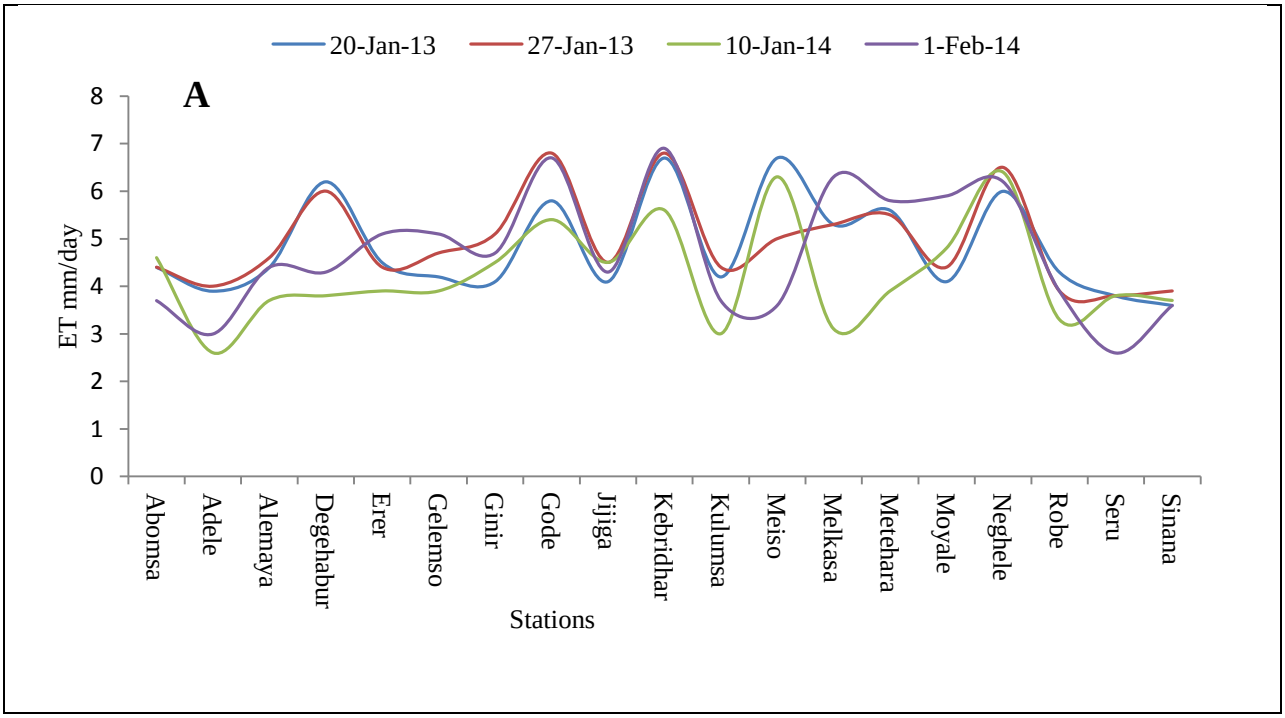

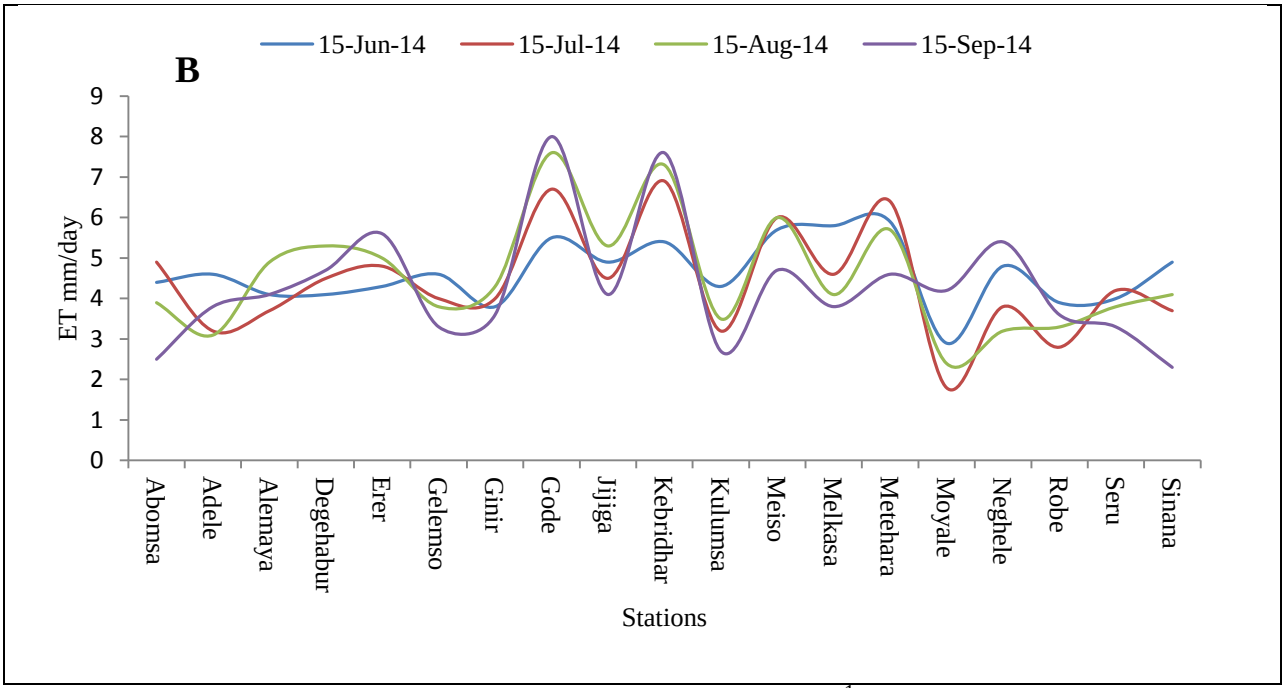

Figure 4.16: *In-situ* based FAO-PM evapotranspiration in mm d^{-1} (A). Dry season (B) Wet season)

As presented in Figure 4.16, in stations that found at arid and semi-arid environment like Neghele, Meiso, Kebridhar and Degehabur for the winter season evapotranspiration value is large enough. This is because of in-situ based meteorological stations are collected from well watered hypothetical grass surface which is a lot wetter and greener than surrounding environs in one way and FAO-PM model can be affected by temperature and wind characteristics of the area. This is also reported by Temesgen *et al*. (2014) on their study that has assessed the performance of different models in different agro-ecologies and landscapes of Ethiopia. More importantly, in the dry season there is relatively strong wind condition in arid and semi-arid environments. With existence of strong winds where there is no any energy shortage, FAO-PM model is reported sensitive and can inflate evapotranspiration (Hou *et al*., 2013; Debnath *et al*., 2015).

4.4.2. MSG Evapotranspiration

Before directly utilizing MSG evapotranspiration product for SEBS model comparative analysis, it is opted to provide descriptive analysis on its values. As per this, processed average, minimum, maximum and standard deviation of dry season MSG evapotranspiration for the whole study area has been presented on the following Table 4.15.

Table 4.15: Descriptive statistics of MSG evapotranspiration

DOY	20-Jan-13	27-Jan-13	10-Jan-14	1-Feb-14
Min	0	0	0	0
Max	3.7	4	3.4	3.2
Mean	1.5	1.4	1.3	1.2
Std	1	1	0.9	0.9
	15-Jun-14	15-Jul-14	15-Aug-14	15-Sep-14
Min	0	0	0	0
Max	3.9	3.4	4.6	4.7
Mean	2	1.7	2.2	2.4
Std	1.2	1	1.3	1.4

As explicitly presented on Table 4.15, the minimum evapotranspiration for all day under analysis is found 0, which means there is absence of evapotranspiration which is constrained by available water on the surface. The maximum value for some pixels ranges from 3.2 to 4 gm cm^{-2}. The mean evapotranspiration ranges from 1.2 (±1) mm day^{-2} to 1.5 (±0.9) mm day^{-2}. This value is an aggregate mean value for the whole study area. To provide a clue on how SAF MSG based evapotranspiration varies across different land cover characteristics, the mean values for each land cover class is given in the following Figure 4.15.

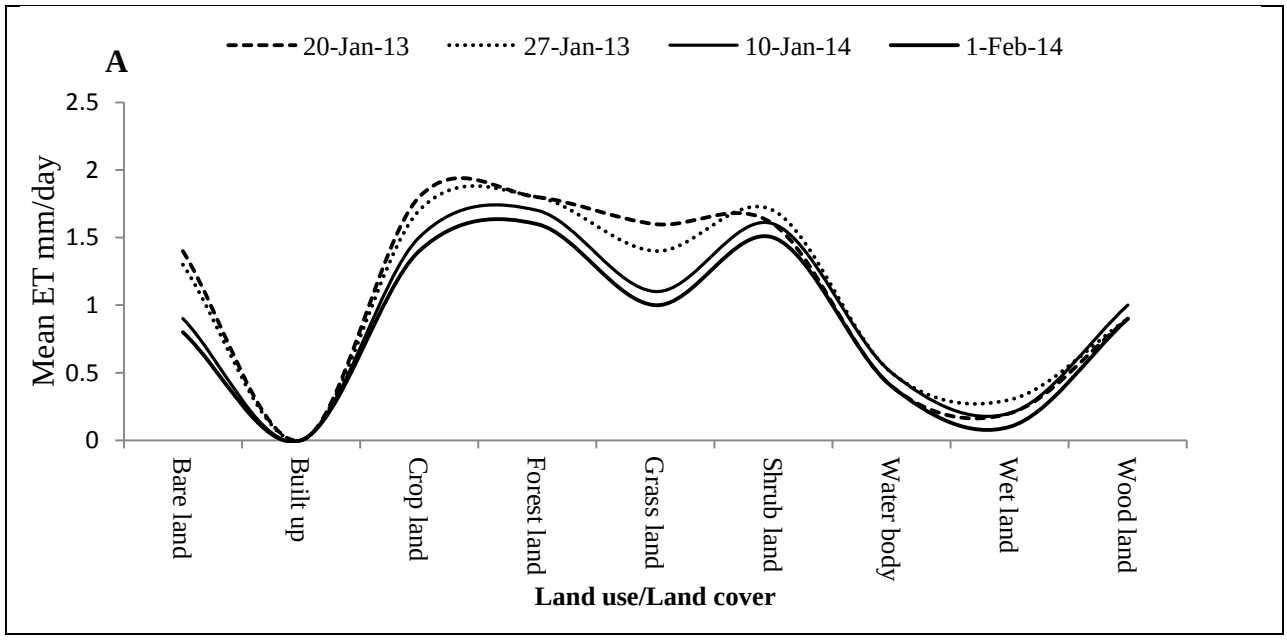

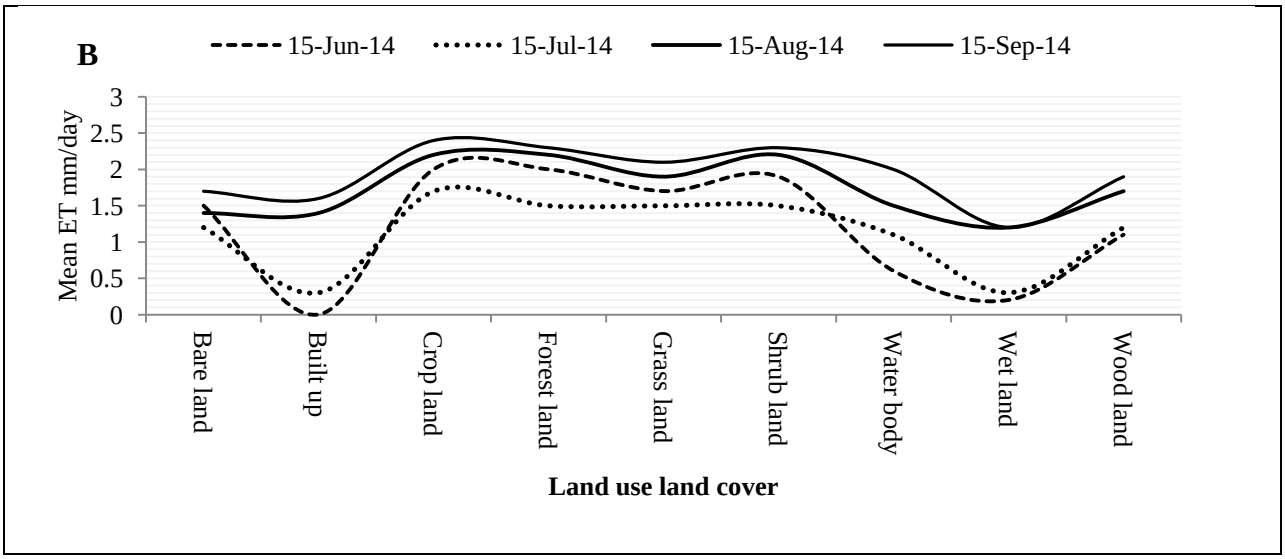

Figure 4.17: SAF MSG based evapotranspiration value across land cover classes A) dry season B). Wet season

As presented on Figure 4.18, forestland, crop land and shrub land have experienced better evapotranspiration rate that ranges from 1.5 to 2 mm day^{-2} followed by grassland. As investigated by Matin and Bourque (2013), vegetation abundance has a positive contribution for evapotranspiration that land cover types with sparse vegetation have experienced least evapotranspiration rate while with dense vegetation has experienced better evapotranspiration rate. Similarly, Simic *et al*. (2014) have reported implication of vegetation characteristics on evapotranspiration rate through LAI. More importantly, Henok *et al*. (2014) have reported implications of vegetation dynamics on evapotranspiration rate. Water body and wetland have also shown moderate to low evapotranspiration rate. There is no any amount of water lose through evapotranspiration. This is because of majority of energy reaching the surface at built-up environment is consumed to heat the surface, which consumes much amount of energy that can be partitioned to latent heat of vaporization in one way and immediate loss of water precipitated at built-up surface through run-off, which limits potential of evapotranspiration through moisture deficit. Water surfaces has experienced minimal evapotranspiration rate. This can happen primarily because of during product derivation SAF AET algorithm utilized ECOCLIM land cover database, which does not account water bodies in its classification scheme alone (SAF ATBD, 2010). This can be a problem while assigning aerodynamic roughness length for water body.

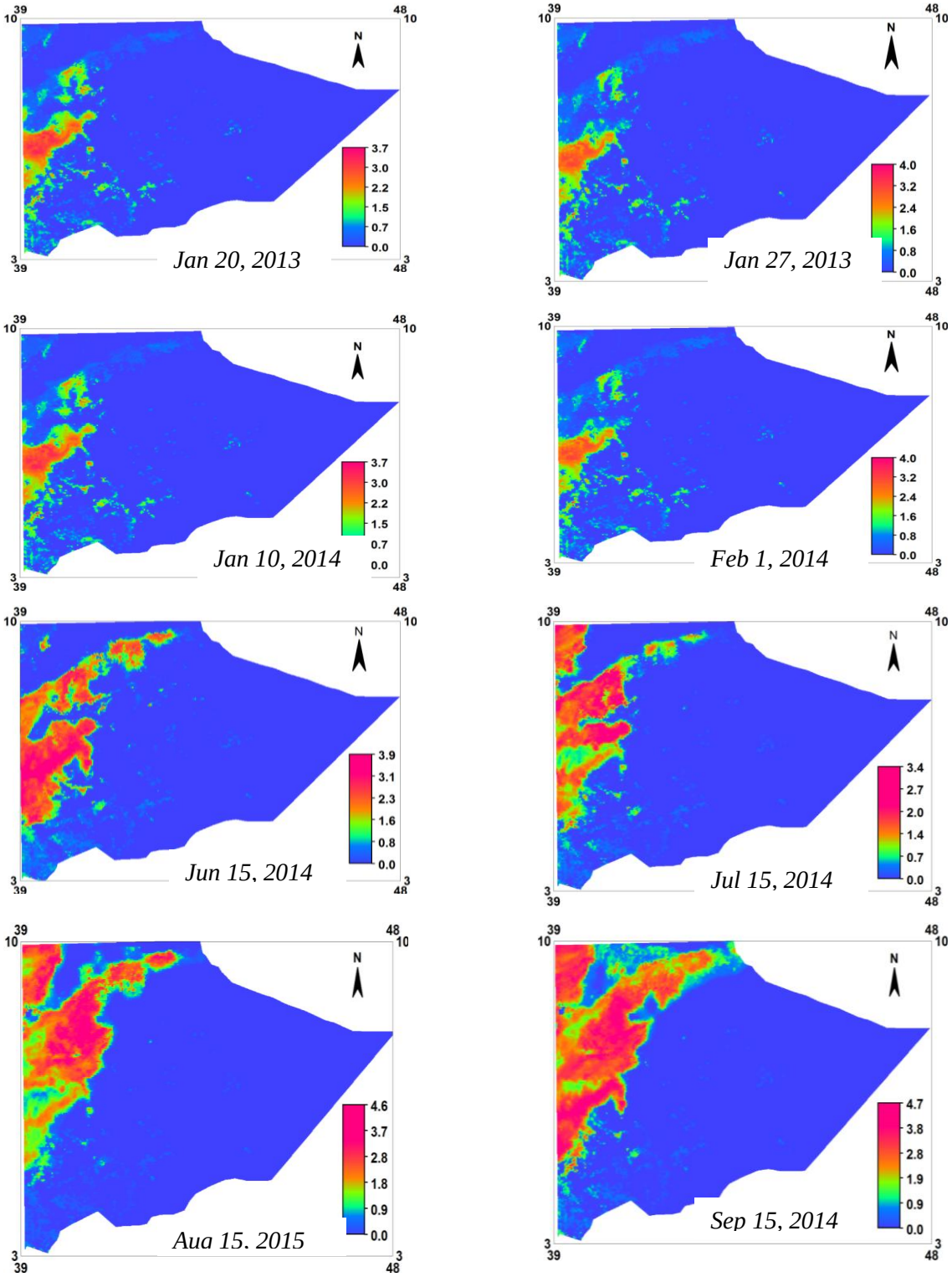

Figure 4.18: SAF MSG based evapotranspiration of the study site

In other way as presented in Figure 4.18 above, vast expanses of the study site in lowland area except highland areas that have better vegetation fraction, there is very low or almost null

evapotranspiration rate measured by MSG ET product. This can be attributed to SAF MSG ET algorithm capability to incorporate soil moisture and temperature at different layers (SAF PUM, 2015).

4.4.3. Comparative Analysis of SEBS Model Results

As stated in objective and methodology part of the study, estimated SEBS model evapotranspiration result is compared with SAF LSA evapotranspiration product and computed FAO-PM model results. Station based analysis has been undertaken and the result is presented in Figure 4.20.

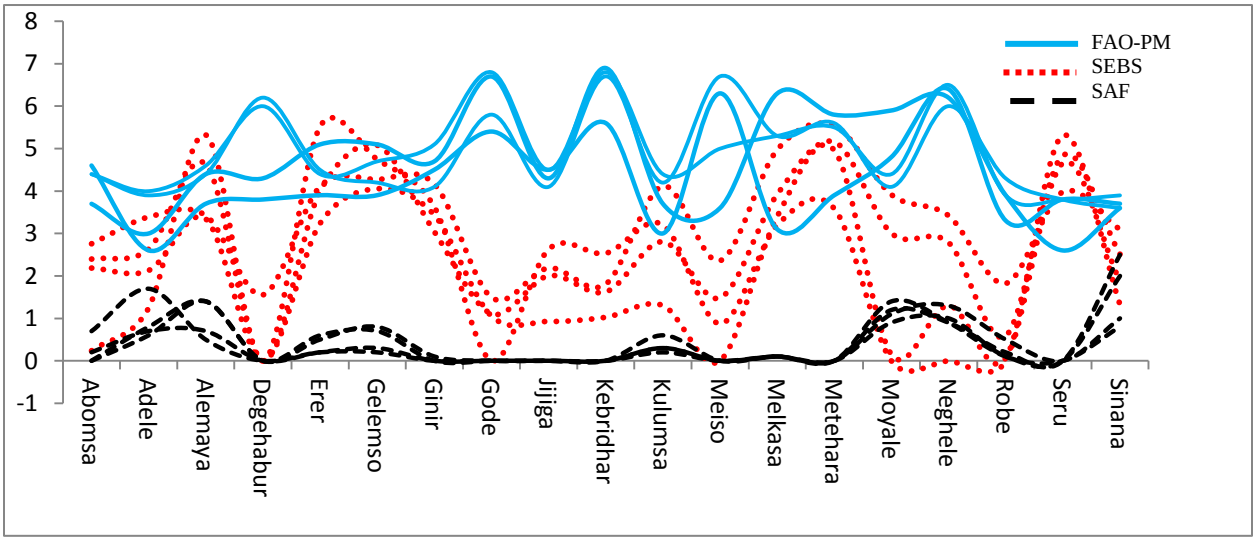

Figure 4.19: Point based comparison of SEBS ET with SAF MSG & FAO-PM for dry season

As tried to be presented on Figure 4.19, values extracted for locations where *in-situ* measurements were taken, in most stations SEBS model under estimates evapotranspiration values than FAO-PM model in general and specifically in stations located at arid and semi-arid sites of the study area. Seasonal vegetation dryness winter coupled with vegetation status of arid and semi-arid environment, remote sensing based SEBS model has yielded relatively lower values. In highland areas with relatively better humidity and vegetation cover like Adele, Alemaya, Ginir, Gelemso, Metehara, Melkasa and Seru, SEBS model has yielded approximate values with results of FAO-PM and SAF AET products. Similarly, station based estimated SEBS based and Meteosat Second Generation based evapotranspiration values, though their magnitude varies, has shown similar trends over different spatial locations within the study site. Though both SEBS based and SAF MSG evapotranspiration products have experienced nearly similar

trends, SEBS model has inflated the amount of evapotranspiration than SAF MSG evapotranspiration results. Patterns of underestimation over arid and semi arid areas have followed similar to SEBS model. As stated in Ghilain (2011) and SAF PUM (2015), this is because of evapotranspiration products that have good association but with a lot discrepancy is mainly the result of differences in model input datasets and biophysical variable derivation. Similarly, many empirical studies like Kwast *et al*. (2009), Gokmen *et al*. (2012) and Lu *et al*. (2012) have reported as SEBS model underestimates sensible heat flux in mixed landscapes where different land cover classes are aggregated to a single pixel. This underestimation of sensible heat flux intends the model to overestimate evapotranspiration.

As lucidly stated in Lu *et al*. (2012) under complex surface cover characteristics, SEBS model is reported to overestimate evaporative fraction. In addition to under estimation of sensible heat flux, deviations of SEBS based evapotranspiration and ET generated from *in-situ* measurements is resulted from inaccuracies in model inputs and lack of energy closure in *in-situ* measurements as *in-situ* measurements does not account canopy conditions. As investigated by Huang (2015), overestimation of evapotranspiration is large in arid and semi-arid environment because of prevailing water stress condition. Similar to this, Chen *et al*. (2013) have attributed cases related with roughness length parameterization for under estimation of sensible heat flux and over estimation of evapotranspiration. Simultaneously, their result has reported the case is land cover selective, of which bare land is the most vulnerable landscape. To provide a clue to what extent SEBS model can associate with station based FAO-PM and image based SAF MSG ET values, a correlation analysis has been done and the result is presented in the following Table 4.16.

Table 4.16: Correlation analysis of SEBS model results with FAO-PM and SAF ET values

	Wet season				Dry Season			
	FAO-SEBS		SAF-SEBS		FAO-SEBS		SAF-SEBS	
Stations	r	R^2	r	R^2	r	R^2	r	R^2
Abomsa	0.62	0.39	-0.09	0.01	-0.70	0.49	0.27	0.07
Adele	0.43	0.18	-0.48	0.23	0.28	0.08	-0.32	0.10
Alemaya	0.21	0.04	-0.68	0.46	-0.62	0.39	0.32	0.10
Degehabur	0.07	0.00	*	*	-0.43	0.18	*	*
Erer	-0.92	0.85	0.00	0.00	-0.59	0.34	0.59	0.35
Gelemso	0.98	0.96	-0.05	0.00	-0.04	0.00	0.11	0.01
Ginir	-0.90	0.81	0.86	0.74	-0.25	0.06	0.09	0.01
Gode	0.89	0.78	*	*	0.82	0.68	*	*
Jijiga	-0.47	0.22	0.61	0.37	0.85	0.72	*	*
Kebridhar	0.43	0.18	*	*	-0.77	0.59	*	*

Kulumsa	0.77	0.59	-0.53	0.28	-0.48	0.23	0.43	0.18
Meiso	0.31	0.09	-0.45	0.20	-0.97	0.94	*	*
Melkasa	0.54	0.29	-0.67	0.45	0.80	0.65	*	*
Metehara	0.90	0.80	*	*	0.98	0.96	*	*
Moyale	-0.73	0.53	-0.86	0.73	0.64	0.41	0.27	0.07
Neghele	0.27	0.07	-0.55	0.30	0.01	0.00	-0.68	0.47
Robe	0.25	0.06	-0.16	0.03	0.14	0.02	-0.63	0.40
Seru	-0.17	0.03	0.80	0.63	0.33	0.11	*	*
Sinana	-0.84	0.71	0.65	0.43	0.18	0.03	-0.63	0.40

* *Values not computed as SAF value remain zero for all observations*
Significance value not computed as station based observations are too small that it might provide inflated results

As presented on Table 4.16, for the wet season SEBS model has yielded evapotranspiration values with FAO-PM potential evapotranspiration values in stations where there is better vegetation cover and precipitation that are situated in highland and adjacent highlands like Abomsa, Adele, Kulumsa, Melkasa and Metehara while Gode has better association from arid and semi arid environment. This can be attributed with seasonal vegetation greenness and summer shower rains that can yield moisture to surface for evaporative demand (Henok *et al*., 2014). In remaining stations located in arid and semi arid environment, there is inverse association (negative correlation coefficient) which is resulted from SEBS model under and over estimation of evapotranspiration value in association with reference FAO-PM model. The correlation analysis done with SAF MSG evapotranspiration for stated stations has only shows better association for three stations – Seru, Sinana and Ginir. In stations where there is negative correlation coefficient, it does not connote the models does not provide any value rather the presence of discrepancy in ET pairs for analysis, which is resulted from under and over estimations. That is why rather than simply relying on quantitative aspects, graph scatter plot is opted to have a clear clue as how the models provide ET estimates (Figure 4.20 below)

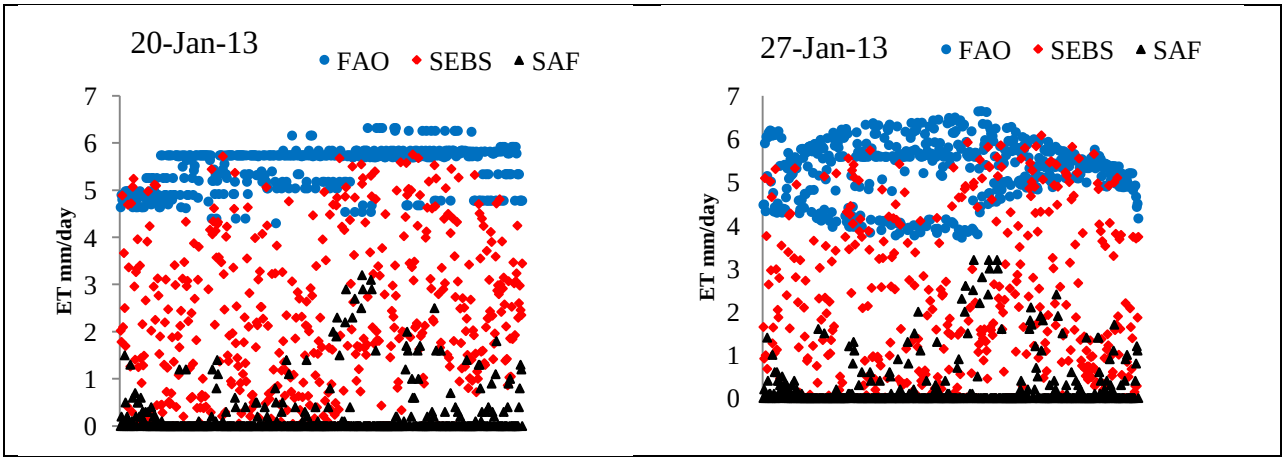

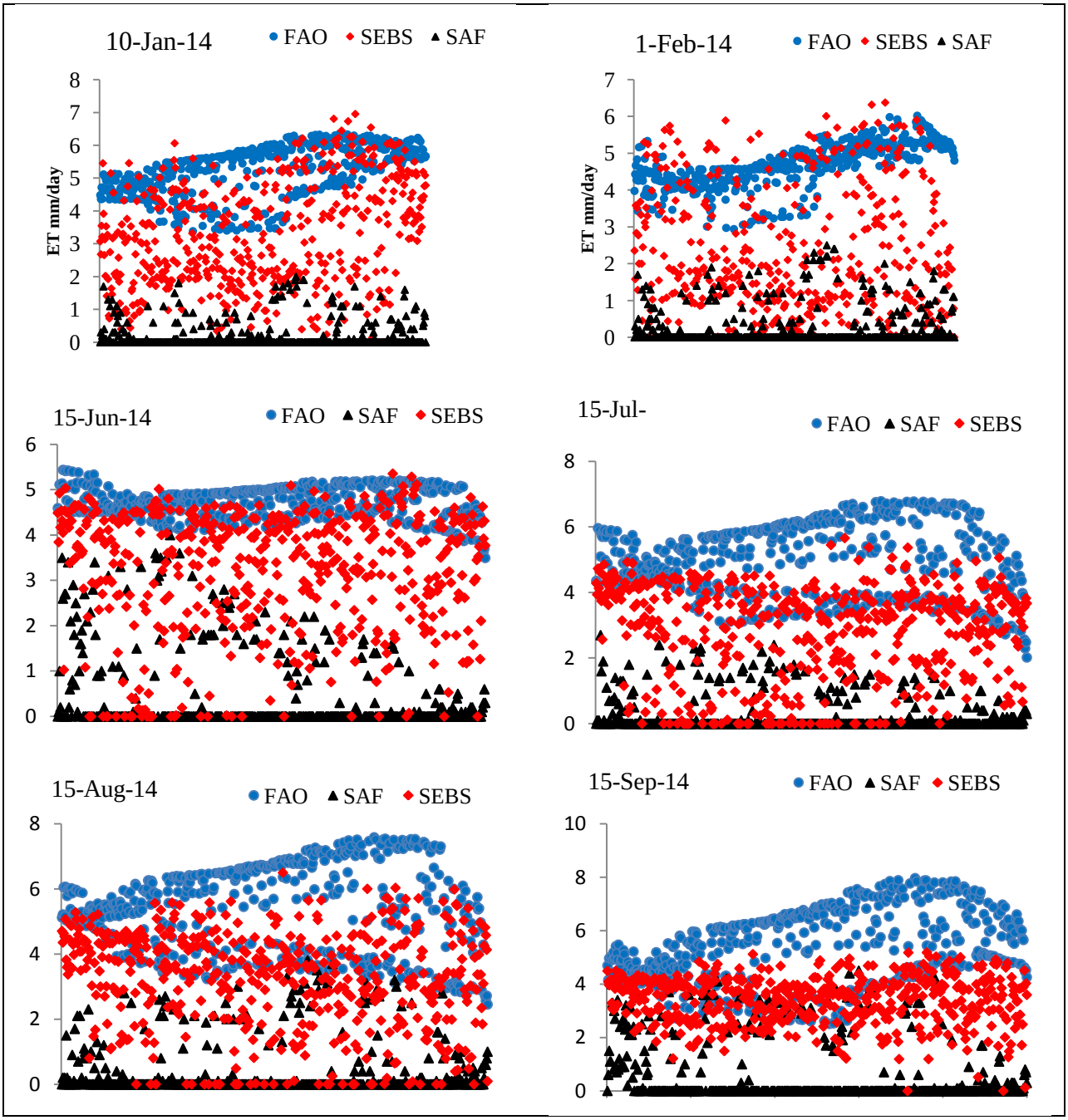

Figure 4.20: Comparison of randomly selected SEBS, FAO-PM and SAF MSG ET

After interpolation of *in-situ* based FAO-PM evapotranspiration values, randomly generated sample values has been extracted from SEBS, FAO and SAF MSG products at similar locations and the values is presented on Figure 4.18. As lucidly presented, SEBS has yielded relatively moderate results that is higher than SAF MSG product value which is distributed across the study area and lower than FAO-PM values in dry season. Similar to dry season, SEBS model underestimates ET than FAO-PM and overestimates than SAF MSG values but there is a better

tendency of association in some pixels taken randomly selected values. The level of over and under estimation is not uniform across study area. Taking the importance of agro-ecological considerations in water management and its attribution from climatic, water and solar energy (Oldeman & Velthuyzen, 1991), aggregate values are segregated to different agro-ecologies in the study site. As per this, segregated value by agro-ecologies for the day 15 June 2014 is presented in Figure 4.21 below.

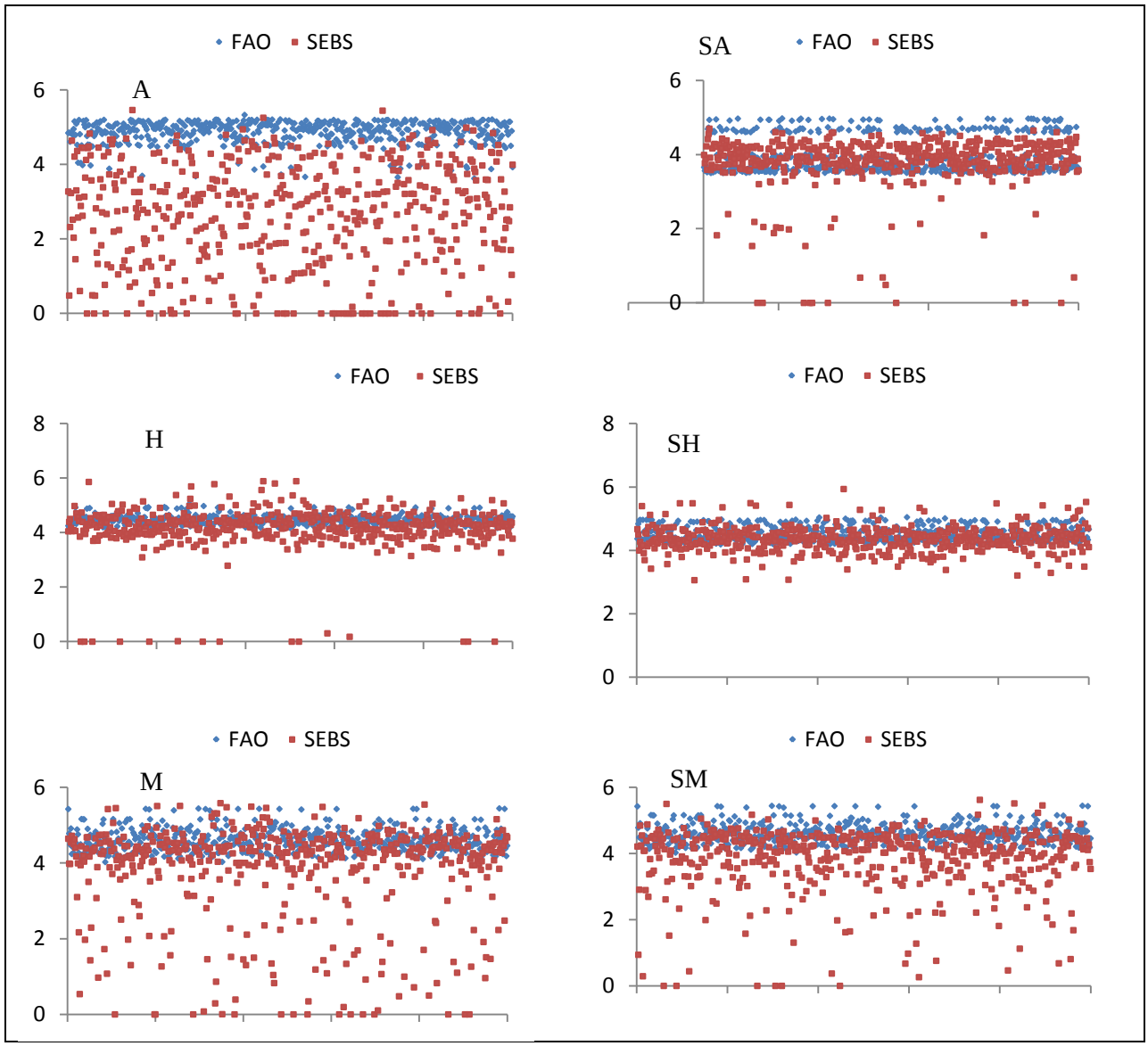

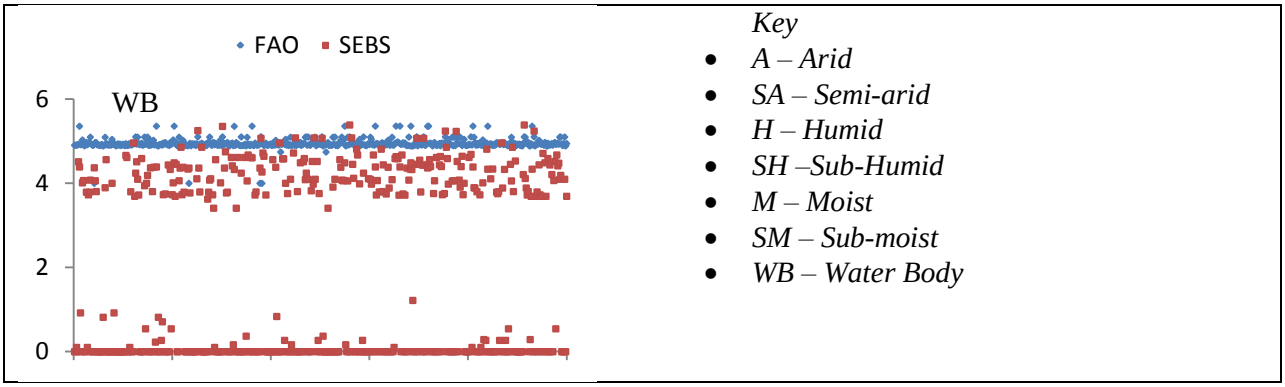

Figure 4.21: Comparative analysis of SEBS with FAO-PM results in June 15, 2015

As shown on figure 4.21, SEBS model has yielded better evapotranspiration estimates at humid, sub-humid, moist and sub-moist and semi-arid agro-ecologies in the winter season. Bigger disparity is observed in arid agro-ecology which is the vast expanse of the study site and water body, an extremely little spatial extent in the study site. In the dry season, the SEBS model has relatively provided better estimates with FAO-PM model outputs only in moist, humid and sub-humid agro-ecologies (*see* Appendix II). From this comparative analysis, it is straight forward to claim SEBS model underestimates evapotranspiration in vegetation and moisture deficit landscapes. These under estimation can be related to FAO-PM results is reference potential evapotranspiration which is not account crop coefficients. Therefore as potential values are greater that actual one, it is possible to claim as SEBS model can bring reasonable results.

4.4.4. SEBS Model Sensitivity Analysis

As presented in above sections, remote sensing based SEBS model has given reasonable results in relation to FAO-PM and Meteosat Second Generation evapotranspiration product. Taking availability of datasets and respective derivation mechanisms in one way and existence of surrogate variables for some model parameters, it is essential to check sensitivity of remote sensing based SEBS model for different inputs. Emphasis is given for derivation of SEBS flux terms and evapotranspiration by using land cover and NDVI based aerodynamic roughness length. As per these, evapotranspiration and related energy flux terms generated by using these terms is presented on the following Table 4.16.

Table 4.17: Sensitivity of SEBS model for land cover related inputs

	Mean ET values in DOY(mm day^{-1})			
Z_{om} source	20-Jan-13	27-Jan-13	10-Jan-14	1-Feb-14
Land cover class	2.92	2.85	2.94	3.24
NDVI	3.78	3.75	3.83	4.05
Change in ET (mm day^{-1})	+0.85	+0.90	+0.89	+0.81
% Δ in ET	29.18	30.81	30.52	27.88
	15-Jun-14	15-Jul-14	15-Aug-14	15-Sep-14
Land cover class	3.4	3.5	3.8	2.9
NDVI	3.2	3.5	3.5	2.6
Change in ET (mm day^{-1})	-0.2	0	-0.3	-0.3
% Δ in ET	-20	0	-30	-30

As presented in Table 4.17, evapotranspiration estimated by using land cover class based roughness length and vegetation index based roughness length has shown deviation in its output which is manifestation of SEBS model sensitivity for aerodynamic roughness length value. Dry season evapotranspiration value estimated by using NDVI based roughness length inflated by a percentage that ranges from 27.88% to 30.52% than evapotranspiration values estimated by using fixed roughness length values assigned for each land cover class on all days under analysis in dry season. As investigated by Kwast *et al*. (2009), though SEBS model has a capability of yielding proxy values of sensible heat flux with field estimated values, it is reported as it underestimates at mixed landscape which can result in overestimation of latent heat flux and evapotranspiration. In the wet season the trend is reversed that evapotranspiration estimated by using NDVI for aerodynamic roughness length derivation under estimates from 20 to 30%. This is mostly resulted because in the summer season there is large NDVI values which further can increase aerodynamic roughness length values. Though results presented in Table 4.16 has shown aggregate values for all study area, the extent of model sensitivity at different land cover class varies. As per this, model sensitivity for aerodynamic roughness length input among different land cover classes has been presented on Table 4.18.

In addition to presenting descriptive statistics, to claim on model sensitivity for aerodynamic roughness length input derivation, it is opted to undertake statistical test on significant mean evapotranspiration variations. As per this, paired sample t-test has been undertaken and results have been presented on the following Table 4.18.

Table 4.18: Statistical test for SEBS model sensitivity analysis

	Paired Differences					
DOY	ET Pairs Z_{om} derived from Land cover & NDVI	Mean	Std. dv	Std. Error	t	Sig(2 tailed)
20-Jan-13	Land cover based NDVI based	0.52	1.28	0.05	9.17	0.00
27-Jan-13	Land cover based NDVI based	0.29	1.38	0.06	4.70	0.00
10-Jan-14	Land cover based NDVI based	0.66	1.29	0.05	11.47	0.00
1-Feb-14	Land cover based NDVI based	0.49	1.46	0.06	7.49	0.00
15-Jun-14	Land cover based NDVI based	-0.05	0.83	0.03	-1.58	0.11
15-Jul-14	Land cover based NDVI based	-0.08	0.77	0.03	-2.35	0.01
15-Aug-14	Land cover based NDVI based	-0.46	0.96	0.04	-10.8	0.00
15-Sep-14	Land cover based NDVI based	-0.68	0.76	0.03	-19.9	0.00

As presented in Table 4.18, in all days under analysis, SEBS model is sensitive for aerodynamic roughness length derivation while estimating evapotranspiration. As presented on the table overall mean difference that ranges from 0.29 to 0.66 while evapotranspiration is estimated by using fixed land cover based aerodynamic roughness length and empirical derivations using NDVI values. In a paired sample test, the t statistic is positive if there is an increment in mean values from first to second data set in a pair test. As shown, within a pair, there is a positive mean difference when evapotranspiration is estimated from fixed land cover based aerodynamic roughness length and using NDVI through empirical relations as mean difference t statistic is positive. At 95 percent confidence level, 499 degree of freedom (N-1), for all DOY in dry season there is a statistically significant mean difference that SEBS model is sensitive for aerodynamic roughness length derivations while estimating energy fluxes and evapotranspiration. Similar to dry season, there is a statistically significant mean evapotranspiration value difference for evapotranspiration estimated by using aerodynamic roughness length from fixed land cover based values and empirical derivation from NDVI. This is with exception of 15th June 2014 where there is no statistically significant mean difference in evapotranspiration pairs (499, degree of freedom, significance (*P*) value 0.11 that denotes the null hypothesis works). Results

presented in Table 4.18, can clearly imply as prepackaged SEBS model is sensitive for aerodynamic roughness length input if other things remain constant.

Table 4.19: SEBS model sensitivity for aerodynamic roughness length across land cover class

DOY	20-Jan-13			27-Jan-13			10-Jan-14			1-Feb-14		
Z_{om} source	LC	NDVI	% Δ in ET	LC	NDVI	% Δ in ET	LC	NDVI	% Δ in ET	LC	NDVI	% Δ in ET
Bare land	2.43	2.96	21.76	2.29	2.61	14.03	2.39	2.92	22.04	2.42	2.36	-2.70
Built up	1.80	1.34	-25.40	3.21	3.74	16.58	3.12	3.77	21.01	4.06	4.37	7.72
Crop land	3.21	3.63	13.18	2.94	3.63	23.20	3.15	3.78	19.84	3.33	3.88	16.55
Forest land	3.27	4.52	38.20	3.39	4.58	35.06	3.29	4.52	37.40	3.85	4.91	27.82
Grass land	2.52	2.80	11.24	2.49	2.74	9.88	2.58	2.94	13.97	2.77	2.81	1.09
Shrub land	3.10	3.85	24.36	3.05	3.84	25.86	3.23	3.96	22.74	3.51	4.31	22.83
Water body	3.77	4.45	18.03	4.59	4.56	-0.63	3.76	4.05	7.57	5.04	5.09	1.01
Wet land	4.90	4.98	1.73	4.19	4.40	4.92	4.67	4.82	3.14	5.15	5.14	-0.18
Wood land	2.32	2.03	-12.49	2.31	2.08	-10.05	2.24	2.35	5.20	2.79	2.52	-9.57
	15-Jun-2014			15-Jul-2014			15-Aug-2014			15-Sep-2014		
Bare land	2.7	2.7	0	2.7	2.7	0	3.1	3.4	30	2.8	3.6	80
Built up	4.6	4.4	-20	4.5	4.4	-10	4.6	4.7	10	4	4	0
Crop land	3.1	3	-10	3.3	3.4	10	3.5	3.5	0	2.9	2.6	-30
Forest land	3.3	3	-30	3.3	3.4	10	3.8	3.5	-30	2.8	2.6	-20
Grass land	2.8	2.9	10	2.8	3	20	3.3	3.1	-20	2.7	2.9	20
Shrub land	3.2	3.2	0	3.1	3.3	20	3.6	3.5	-10	2.8	2.6	-20
Water body	3	4.3	130	3.8	4.1	30	3.8	4.4	60	4.1	4	-10
Wet land	4.5	4.5	0	4.6	4.6	0	5	4.8	-20	4.3	4.2	-10
Wood land	2.7	2.6	-10	3.3	2.8	-50	3.6	3	-60	2.6	2.8	20

As clearly presented on Table 4.19, the sensitivity of SEBS model for aerodynamic roughness length values varies as per respective land cover characteristics. In the dry season the biggest sensitivity is observed in forest land cover class. The model inflates evapotranspiration when aerodynamic roughness length is determined from NDVI, which accounts a percentage change ranges from 27.82% to 38.2%. Minimum sensitivity is observed in water body and wet land. In some land cover classes like built-up and woodland, estimating evapotranspiration by using aerodynamic roughness length determined from NDVI deflates evapotranspiration value within the landscape.

CHAPTER V: CONCLUSION AND RECOMMENDATIONS

5.1. Conclusion

In heterogeneous landscape where either there exist acute *in-situ* data scarcity or field measurement become impractical, remote sensing based evapotranspiration estimation methods are capable of providing intended pixel level ET estimates. As per this argument, remote sensing based SEBS model has been examined weather it can provide proxy ET values in eastern Ethiopian landscape.

While it is proposed to utilize MODIS and ASTER level 1B images for derivation of surface parameters used for SEBS model, it is mandatory to preprocess raw images before analysis operation is undertaken. As per this, format conversion, reflectance and radiance conversion and atmospheric correction for reflectance bands have been done. As SMAC model utilizes atmospheric variables under radiative transfer, it has resulted in improvement in MODIS reflectance bands though observed improvement in reflectance is not unidirectional. For some bands it has an additive implication on reflectance values while on some bands it has subtractive impacts. Atmospheric variables interact in a different manner with each reflectance bands at the spectrum. Before derivation of land surface temperature, brightness temperature and atmospheric water vapor is demanded in prepackaged SEBS model. Brightness temperature of MODIS bands 31 and 32 are computed and their value varies as per surface characteristics. Computed atmospheric water vapor value in all day of the year also varies spatially as moisture yielding parameters and aerodynamic characteristics vary from location to location.

From the basic processing and analysis opportunities in utilizing prepackaged SEBS model is there is a possibility of ingesting either land surface parameters processed from MODIS level 1B calibrated products or processed secondary composites at any temporal resolution. As per this by utilizing atmospherically corrected reflectance bands for the dry season, brightness temperature and atmospheric ware vapor, surface parameters that are demanded by SEBS model as biophysical inputs has been derived. These are NDVI, LAI, fraction of vegetation cover, land surface temperature, surface emissivity and albedo. For the summer season, the indices are utilized from secondary composites. As the study site, where current study is undertaken is heterogeneous in-terms of land cover and agro-ecology, these variables also vary as per surface

characteristics especially on land cover characteristics. One of the basic advantages of using prepackaged SEBS model in ILWIS platform is that users have a flexibility of either deriving these surface parameters from Level 1B MODIS or ASTER products or directly utilizing processed composites at any intended spatio-temporal resolution from other sources with minor processing effort.

With integration of surface parameters derived and meteorological datasets, SEBS model estimates surface energy fluxes, instantaneous evapotranspiration which is termed as evaporative fraction and daily evapotranspiration. As results of estimated energy flux results for dry season shown, there is maximum amount of energy partitioned for heating the ground (Ground Heat Flux). Contrary to this, energy portioned for water phase change (Latent Heat of Vaporization) is found minimal for the whole study area. When this pattern is clustered to different land cover classes, it has different interactions. In some land cover classes where latent heat of vaporization is minimal, ground heat flux booms and the vice verse is true. Estimated mean evaporative fraction for the whole study area, at dry season, is found 0.5(±0.3) mm $hour^{-1}$ while mean evapotranspiration ranges from 3.7(±1.6) mm day^{-1} to 4(±1.7) mm day^{-1}. For both parameters, there is an extreme spatial variability attributed from heterogeneity in interactions of surface parameters that govern evapotranspiration like vegetation cover, aerodynamic roughness characteristics and surface moisture yield and energy availability. Deviation of mean evapotranspiration value in the summer season from dry season is not pronounced. This is because of in the winter season there are little pixels with high ET values concentrated at some hot spots while in the summer season there is large number of pixels with moderate evapotranspiration values distributed across the study site associated with vegetation condition of the area.

Any model that is used to estimate surface characteristics should be analyzed either by comparing with other model outputs or validating model outputs with direct measurement values. As comparative analysis done, in the dry season, SEBS model result has yielded under estimated evapotranspiration values than FAO-PM potential evapotranspiration and overestimated values than SAF MSG evapotranspiration values. The scale of deviation varies as per agro-ecology and land cover characteristics of a site in the study area. In moisture deficit drought prone areas the deviation in FAO-PM and SEBS model results is extreme. Image based

SEBS and SAF MSG evapotranspiration models result either extremely lower values of evapotranspiration or almost absence of evapotranspiration process. Contrary to image based models, FAO-PM has results extremely higher evapotranspiration values at these arid and semi-arid areas. In areas where there is better vegetation cover and moisture is reliable like humid, sub-humid and moist agro-ecology, SEBS model has yielded relatively proxy values with FAO-PM values. Though, there is no fixed standards to judge the model performance, it is possible to claim as the model can bring reasonable and moderate values, which are completely neither inflated nor deflated evapotranspiration estimates.

More than model performance evaluation, model sensitivity issue is also an issue that has equal concern in environmental modeling. Aerodynamic roughness length has been derived from land cover based fixed aerodynamic roughness length values and derivation from NDVI using its empirical relationships. The model is found sensitive for these inputs that there is a statistically significant change in mean evapotranspiration value. When aerodynamic roughness length value is derived from land cover based values adopted from literatures, it has yielded mean evapotranspiration value lower than estimated by using NDVI based aerodynamic roughness length value. Observed sensitivity is also varying among land cover classes and DOY. In some instances it has been observed that there is a reversed sensitivity trend.

5.2. Recommendations

Though current study has evaluated the capability of SEBS model in yielding proxy evapotranspiration estimates with other models at complex landscape, there are some issues to be incorporated in further research work. Accordingly, the following research areas are recommended for future research.

- To undertake comparative analysis, there should also be extended study that validates the model by using direct evapotranspiration measurements by sentilometres, which can minimize or nearly can cease errors propagated from data sets used for comparative analysis.
- In summer season where cloud cover constrained the utilization of both MODIS and ASTER level 1B products, hinging towards decadal and monthly composites is inalienable option like current study has utilized decadal composites from different sources for summer season. Therefore, though the products are reported valid on their

product algorithm theoretical baseline documents (ATBD), there should be comparative analysis of parameters derived from level 1B products and decadal composites for clear certainty before ingesting in SEBS model.

- For modeling land cover related aerodynamic roughness characteristics, vegetation height and displacement height is estimated by using empirical relationships with NDVI and fixed land cover based aerodynamic roughness length values adopted from literatures. To have firm certainty on model capability, there should be integration of accurate satellite measurement values for vegetation height generated from LiDAR point cloud measurements and fine resolution photogrammetric outputs.
- Undertaken model sensitivity assessment of current study only focused on aerodynamic roughness length. There should be other detailed studies that assess model sensitivity for Leaf Area Index, hours of bright sunshine and constant and dynamic scalar displacement length with its variability simultaneous to land cover characteristics of a site. The sensitivity study should also test for similar variables like LAI with different derivation mechanisms.
- As the model is found sensitive for aerodynamic roughness length derivations, while reporting the results of SEBS model, there should be explicit description as how roughness length is derived to provide a clue for users before they directly utilize outputs of SEBS model evapotranspiration products.
- Other than hydrological modeling for water balance assessment, other studies has developed robust drought assessment tools such as Evapotranspiration Deficit Index (ETDI)(Narasimahan & Srinivasan, 2005; Eden, 2012) and ratio of actual and potential evapotranspiration (Anderson *et al*., 2011), Water Stress Index (WSI) (Narasimahan & Srinivasan, 2005) through incorporate evapotranspiration. Except in some instances this is done by using in-situ metrological observations. As established reality remote sensing based evapotranspiration outputs can bring pixel level evapotranspiration values. Therefore, there need a further research that utilized SEBS based evapotranspiration outputs for spatially distributed hydrological drought modeling application.

References

Alebachew Abreham (2009). Open Water Evaporation Estimation Using ground Measurements and Satellite Remote Sensing. A Case Study of Lake Tana, Ethiopia. Unpublished Master's Thesis Submitted to University of Twente Faculty of Geoinformation Science and Earth Observation.

Allen, R., Pereira, L., Raes, D., & Smith, M. (1998).Crop Evapotranspiration: Guidelines for Computing Crop Water Requirements. FAO Irrigation and Drainage Paper 56, Rome-Italy: FAO

Allen, R., Irmark, A., Trezza, R., Hendrickx, H.M.,, Bastianssen, W. & Kjaersgaard, J. (2011). Satellite based ET Estimation in Agriculture using SEBAL and METRIC. *Hydrological Processes*, 25: 4011-4027

Ambrose, M.S. & Sterling, M.S. (2014). Global Patterns of Annual Actual Evapotranspiration With Land-cover Type: Knowledge Gained from a New Observation-Based Database. *Hydrological Earth System Science*, 11: 12103–12135

Anderson, C.M., Hain, C., Wardlow, B., Pimstein, A., Mecikalski, R.J., Kustas, P.W. (2011). Evaluation of Drought Indices Based on Thermal Remote Sensing of Evapotranspiration over the Continental United States. *Journal of Climate*, 24: 2025- 2044.

Anderson, C.M., Norman, M.J., Mecikalski, R.J., Torn, D.R., Kustas, P.W. & Basara, B.J. (2004). A Multiscale Remote Sensing Model for Disaggregating Regional Fluxes to Micrometeorological Scales. *Journal of Hydrometeorology*, 5: 343-363

Anderson, C.M., Norman, M.J., Mecikalski, R.J., Otkin, A.J. & Kustas, P.W. (2007). A Climatological Study of Evapotranspiration and Moisture Stress across the Continental United States based on Thermal Remote Sensing: Model Formulation. *Journal of Geophysical Research*, 112(D10117), doi: 10.1029/2006JD007506

Anderson, C.M., Norman, M.J., Diak, R.G., Kustas, P.W., Mecikalski, R.J. (1997). A Two-Source Time-Integrated Model for Estimating Surface Fluxes Using Thermal Infrared Remote Sensing. *Remote Sensing of Environment*, 60:19.5-216.

Anderson, C.M., Kustas, P.W., Norman, M.J., Hain, R.C., Mecikalski, R.J., Schultz, L., Gonz ´ alez-Dugo, P.M., Cammalleri, C., d'Urso, G., Pimstein, A. & Gao, F. (2011). Mapping aily Evapotranspiration at Field to Continental Scales Using Geostationary and polar Orbiting Satellite Imagery. *Hydrology and Earth System Science*, 15: 223–239.

Anderson, C.M., Kustas, P.W., Alfieri, G.J., Gao, F., Hain, C., Prueger, H.J., Evett, S., Colaizzi, D.P., Howell, T., Chávez, L.J. (2012). Mapping Daily Evapotranspiration at Landsat Spatial Scales During the BEAREX'08 field campaign. *Advances in Water Resources*, 50: 162–177.

Ashraf, A.M., Maah, J.M. & Yusoff, I. (2011). Introduction to Remote Sensing of Biomass, Biomass and Remote Sensing of Biomass. Pp 130-170. In Atazadeh, I. (ed). Biomass and Remote Sensing of Biomass. InTech. *Accessed* from http://www.intechopen.com/books/biomass-and-remote-sensing-ofbiomass/introduction-to-remote-sensing-of-biomass

Asner, P.C., Scurlock, M.J., Hicke, A.J. (2003). Global Synthesis of Leaf Area Index Observations: Implications for Ecological and Remote Sensing Studies. *Global Ecology & Biogeography*, 12: 191– 205.

Assefa Melesse, Wossenu Abtew & Tibebe Dessalegne (2009). Evaporation Estimation of Rift Valley Lakes: Comparison of Models. *Sensors*, 9: 9603-9615. doi:10.3390/s91209603

Bai, Y., Feng, M., Jiang, H., Wang, J., Zhu, Y. & Liu, Y. (2014). Assessing Consistency of Five Global Land Cover Data Sets in China. *Remote Sensing*, 6: 8739-8759. doi:10.3390/rs6098739

Barati, S., Rayegani, B., Saati, M., Sharifi, A. & Nasri, M. (2011). Comparison the Accuracies of Different Spectral Indices for Estimation of Vegetation Cover Fraction in Sparse Vegetated Areas. *The Egyptian Journal of Remote Sensing and Space Sciences*, 14:49-56.

Barbagallo, S., Consoli, S. & Russo, A. (2009). A One-Layer Satellite Surface Energy Balance for Estimating Evapotranspiration Rates and Crop Water Stress Indexes. *Sensors*, 9: 1-21. doi:10.3390/s90100001

Bala, A., Singh, K.R. & Gayathri, V. (2013). Review on Different Surface Energy Balance Algorithms for Estimation of Evapotranspiration through Remote Sensing. *International Journal of Emerging Technology and Advanced Engineering*, 3(7): 582-588

Balogun, C. (1974). The Influence of Some Climatic Factors on Evaporation and Potential Evapotranspiration at Ibadan, Nigeria. *Ghana Journal of agricultural Sciences*, 7: 45-49

Bastiaanssen, M.G., Menenti, M., Feddes, A.R. & Holtslag, M.A. (1998). A Remote Sensing Surface Energy Balance Algorithm for Land (SEBAL) 1: Formulation. *Journal of Hydrology*, 212-213: 198–212.

Belete Berhanu, Yilma Seleshi & Assefa Melese (2014). Surface Water and Groundwater Resources of Ethiopia: Potentials and Challenges of Water Resources Development. In Assefa Melese, Wossenu Abtew & Shimelis Setegn (eds). *Nile River Basin: Ecohydrological Challenges, Climate Change and Hydropolitics*. Springer: Switzerland. Pp. 97-117.

Bicheron, P., Defourny P., Brockmann, C., Schouten, L., Vancutsem, C., Huc M., Bontemps, S., Leroy, M., Achard, F., Herold, M., Ranera, F. & Arino, O. (2008). GlobCover Products Description and Validation Report. MEDIAS-France: Berlin.

Billi, P. & Caparrini, F. (2006). Estimating Land Cover Effects on Evapotranspiration with Remote Sensing: A Case Study in Ethiopian Rift Valley. *Journal of Hydrological Sciences*, 51: 4, 655-670, doi: 10.1623/hysj.51.4.655

Birky, A.A. (2001). NDVI and a Simple Model of Deciduous Forest Seasonal Dynamics. *Ecological Modeling*, 143: 43 – 58.

Bruin, R.A., Trigo, E.I., Jitan, A.M., Temesgen Enku, Tol, D.V. & Gieske, M.S. (2010). Reference Crop Evapotranspiration Derived from Geo-Stationary Satellite Imagery: A Case Study for the Fogera Flood Plain, NW-Ethiopia and the Jordan Valley, Jordan.

Brunsell, A.N. & Gillies, R.R. (2000). The Effect of Emissivity on Evaporation. *A conference paper presented on theme "Remote Sensing and Hydrology 2000" at Proceedings of a symposium held at Santa Fe, New Mexico, USA*

Burt, E.J., Barber, M.G., Rigby, L.D. (2009). *Elementary Statistics for Geographers*. The Guilford Press: New York.

Carlson, N.T. & Ripley, A.D. (1998). On the Relation between NDVI, Fractional Vegetation Cover, and Leaf Area Index. *Remote Sensing of Environment*, 62: 241-252.

Casa, A. & Ovando, G, (2012). Development of a Tool to Monitor Crop Growth and Grain Yield. In Maathuis, P.H & Mannaerts, M.M. (*eds*). GEONETCast-DevCoCast Application Manual. University of Twente: The Netherlands. Pp. 82-106.

Cihlar, J., Ly, H., Li, Z., Chen, J., Pokrant, H. & Huang, F. (1997). Multitemporal, Multichannel AVHRR Datasets for Land Biosphere Studies: Artifacts and Corrections. *Remote Sensing of Environment*, 60:35-57.

Cleugh, A.H., Leuning, R., Mu, Q., Running, W.S. (2007). Regional Evaporation Estimates from Flux Tower and MODIS Satellite Data. *Remote Sensing of Environment*, 106: 285–304

Chesworth, W., Macías, F. & Arbestain, C.M. (2008). Alkaline Soils. In Chesworth, W. (eds). *Encyclopedia of Soil Sciences*. Dordrecht, The Netherlands: Springer. pp. 37-38.

Colaizzi, D.P., Kustas, P.W., Anderson, C.M., Agam, N., Tolk, A.J., Evett, R.S., Howell, A.T., Gowda, H.P., O'Shaughnessy, A.S. (2012). Two-source Energy Balance Model Estimates of Evapotranspiration Using Component and Composite Surface Temperatures. *Advances in Water Resources*, 50: 134–151

Courault, D., Seguin, B. & Olioso, A. (2003). Review to Estimate Evapotranspiration from Remote Sensing Data: Some Examples from the Simplified Relationships to the Use of Mesoscale Atmospheric Models. ICID Workshop on Remote Sensing of Evapotranspiration for Large Regions, September 17, 2003.

Cristobal, J., Poyatos, R. Ninyerola, M., Llorens, P., & Pons, X. (2011).Combining Remote Sensing and GIS Climate Modelling to Estimate Daily Forest Evapotranspiration in a Mediterranean Mountain Area. *Hydrology and Earth System Sciences, 15*, 1563–1575.

CSA (2013). Seasonal Climate Forcast. *CSA Buletine, 24*(23)

CSA, EDRI & IFPRI (2006). Atlas of the Ethiopian Rural Economy. Addis Ababa: CSA, Addis Ababa: EDRI & Washington DC: IFPRI.

CSA, EDRI & IFPRI (2010). Population & Housing Census: Atlas of Ethiopia 2007. Addis Ababa: CSA & EDRI & Washington DC, IFPRI.

CSA & IFPRI (2013). Atlas of Agricultural Statistics 2006/07 - 2010/11. Addis Ababa: CSA

Ethiopian Geological Survey & Ministry of Mines (2009). Opportunities for Clay Resources Development in Ethiopia. Addis Ababa Ethiopian Geological Survey, Geoscience Data Centere.

Debnath, S., Adamala, S. & Raghuwanshi, S.N. (2015). Sensitivity Analysis of FAO-56 Penman-Monteith Method for Different Agro-ecological Regions of India. *Environmental Process*, 2:689–704. doi: 10.1007/s40710-015-0107-1

Dessie Nedaw (2010). Water Balance and Groundwater Quality of Koraro Area, Tigray, Northern Ethiopia. *MEJS*, 2 (2): 110-127.

Disney, M., Lewis, P., Thackrah, G. Quaife, T. & Barnsley, M. (2004). Comparison of MODIS Broadband Albedo over an Agricultural Site with Ground Measurements and Values Derived from Earth Observation Data at a Range Of Spatial Scales. *International Journal of Remote Sensing*, 25(23): 5297–5317.

Dobos, E. (2006). Albedo. In Lal. R. (ed). *Encyclopedia of Soil Science (volume 1)*. CRC Press: pp. 64-66

Eden, U. (2012). Drought Assesment by Evapotranspiration Mapping in Twente, The Netherlands. Unpublished Masters Thesis Submitted University of Twente Faculty of Geoinformation Science and Earth Observation.

Elhag, M., Psilovikos, A., Manakos, I. & Perakis, K (2011). Application of the SEBS Water Balance Model in Estimating Daily Evapotranspiration and Evaporative Fraction from Remote Sensing Data over the Nile Delta. *Water Resources Management*, doi: 10.1007/s11269-011-9835-9

European Space Agency (2009). GlobCover data set. Accessed on Jan 15, 2016 from http://due.esrin.esa.int/files/Globcover2009_V2.3_Global_.zip

FAO (2012). ETo Calculator: Land and Water Digital Media Series No 36. FAO, Rome: Italy

Ferreira, E., Dentas, A.A. & Garcia, G.A (2012). Estimation of Evapotranspiration in Minas Gerais State, Brazil. In Maathuis, P.H & Mannaerts, M.M. (eds). GEONETCast-DevCoCast Application Manual. University of Twente: The Netherlands. Pp. 45-47.

Fuller, O.D. and Ottke, C. (2002). Land Cover, Rainfall and Land-Surface Albedo in West Africa. *Climatic Change*, 54: 181–204

Ghilain, H., Arboleda, A. & Gellens-Meulenberghs, F. (2011). Evapotranspiration Modeling at Large Scale Using Near-Real Time MSG SEVIRI Derived Data. *Hydrological and Earth System Science*, 15: 771–786

Gibson, L., Münch, Z., Engelbrecht, J., Petersen, N. & Conrad, J. (2009). Remote Sensing as a Tool for Resources Assessment towards the Determination of the Legal Compliance of Surface and Groundwater Use. Report Submitted to South African Water Research Commission. WRC Report No. 1690/1/09.

Gibson, L., Jarmain, C., Su, Z. & Eckardt, E.F. (2013). Estimating Evapotranspiration Using Remote Sensing and the Surface Energy Balance System – A South African Perspective. *Water SA*, 39(4). *Accessed* from http://dx.doi.org/10.4314/wsa.v39i4.5 on August 5, 2015

Goode, R.P., Qiu, J., Yurchyshyn, V., Hickey, J., Chu, M.C., Kolbe, E., Brown, C.T. & Koonin, S.E. (2001). Earthshine Observations of the Earth's Reflectance. *Geophysical Research Letters*, 28(9):1671-1674

Gokmen, M., Vekerdy, Z., Verhoef, A., Verhoef, W., Batelaan, O. & Tol, C. (2012). Integration

of Soil Moisture in SEBS for Improving Evapotranspiration Estimation under Water Stress Conditions. *Remote Sensing of Environment*, 121: 261–274

Hadjimitsis, G.D., Papadavid, G., Agapiou, A., Themistocleous, K., Hadjimitsis, M.G., Retalis, A., Michaelides, S., Chrysoulakis, N., Toulios, L. & Clayton, I.R.C. (2010). Atmospheric Correction for Satellite Remotely Sensed Data Intended for Agricultural Applications: Impact on Vegetation Indices. *Natural Hazards Earth System Science*, 10: 89–95.

Hain, R.C., Mecikalski, R.J. & Anderson, C.M. (2009). Retrieval of an Available Water-Based Soil Moisture Proxy from Thermal Infrared Remote Sensing. Part I: Methodology and Validation. *Journal of Hydrometeorology*, 10: 665-683

Hajj, E.M., Begue, A., Lafrance, B., Hagolle, O., Dedieu, G. & Rumeau, M. (2008). Relative Radiometric Normalization and Atmospheric Correction of a SPOT 5 Time Series. *Sensors*, 8: 2774-2791.

Han, L., Li, X., Wang, J., Liu, S. & Jiao, Z. (2004). A Simple Interpretation of NDVI-Ts Space Combining LAI and Evapotranspiration. *IEEE*.

Hareef, B.S. (2013). Surface Reflectance Retrieval from the High Resolution Multispectral Satellite Image Using 6S Radiative Transfer Model. *International Journal of Remote Sensing and GIS*, 2(3): 130-137

Harris, S.F. & Robinson, S.J. (1916). Factors Affecting the Evaporation of Moisture from the Soil. *Journal of Agricultural Research*, VII (1): 439-461.

Hengl, T. (2009). A Practical Guide to Geostatistical Mapping. Luxembourg: Office for Official Publications of the European Communities.

Henok Alemu, Gabriel, B., Kaptue, T.A. & Kovalskyy, V. (2014). Evapotranspiration Variability and Its Association with Vegetation Dynamics in the Nile Basin, 2002–2011. *Remote Sensing*, 6: 5885-5908. doi:10.3390/rs6075885

Hou, L., Zou, S., Xiao, X. & Yang Y. (2013). Sensitivity of the Reference Evapotranspiration to Key Climatic Variables during the Growing Season in the Ejina Oasis Northwest China. *SpringerPlus*, 2(Suppl 1):S4. Accessed from http://www.springerplus.com/content/2/S1/S4

Huang, C., Li, Y., Gu, J., Lu, L. & Li, X. (2015). Improving Estimation of Evapotranspiration under Water-Limited Conditions Based on SEBS and MODIS Data in Arid Regions. *Remote Sensing*, 7: 16795–16814. doi:10.3390/rs71215854

Huntingford, C., Verhoef, A. & Stewart, J. (2000). Dual versus Single Source Models for Estimating Surface Temperature of African Savannah. *Hydrology and Earth System Sciences*, 4(*1*), 185-191.

Huntington, L.J. and Allen, G.R. (2010).Evapotranspiration and Net Irrigation Water Requirements for Nevada.

ITC-ILWIS (2001). Geostatstics in ILWIS 3.0 Academic User's Guide. International Institute for Aerospace Survey and Earth Sciences (ITC) Enschede, the Netherlands

Jasechko, S., Sharp, D.Z., Gibson, J.J., Birks, J.S., Yi, Y. & Fawcett, J.P. (2013). Terrestrial Water Fluxes Dominated by Transpiration, *Nature*, 349. doi doi:10.1038/nature11983

Jia, L., Su, Z., Hurk, B., Menenti, M., Moene, A., Bruin, H., Yrisarry, B., Ibanez, M. & Cuesta, A. (2003). Estimation of Sensible Heat Flux Using the Surface Energy Balance System (SEBS) and ATSR Measurements.*Physics and Chemistry of the Earth*, 28: 75–88

Jia, X., Scherer, F.T. & Steele, D.D. (2007). Crop Water Requirement for Major Crops in North Dakota and its Vicinity Area. Paper presented at An ASABE Section Meeting, Paper No. RRV-07133. Accessed on September 22, 2015 from https://www.ndsu.edu/fileadmin/aben/Papers/Crop_Water_Requirement_ND.pdf

Jia, Z, Liu, S., Xu, Z., Chen, Y. & Zhu, M. (2012). Validation of Remotely Sensed Evapotranspiration over the Hai River Basin, China. *Journal of Geophysical Research*, 117(D13113). doi:10.1029/2011JD017037

Jiang, Q., Tang, C., Ma, E., Yuan, Y. & Zhang, W. (2014). Variations of Near Surface Energy Balance Caused by Land Cover Changes in the Semiarid Grassland Area of China. Advances in Meteorology, 2014(894147). http://dx.doi.org/10.1155/2014/894147

Jimnez-Munoz, J. C. and Sobrino, J. A. (2005). Atmospheric Water Vapour Content Retrieval from Visible and Thermal Data in the Framework of the DAISEX Campaigns. *International Journal of Remote Sensing*, 26(*15*), 3163-3180, DOI: 10.1080/01431160500127484

Kaufman, G. & Gao, B. (1992). Remote Sensing of Water Vapor in the Near IR from EOS/MODIS. *IEE Translation of Geosciences and Remote Sensing*, 30(105)

Katsaros, B.K., Mcmurdie, A.L., Lind, J.R. & Devault, E.J. (1985). Albedo of a Water Surface, Spectral Variation, Effects of Atmospheric Transmittance, Sun Angle and Wind Speed. *Journal of Geophysical Research*, 90(C4):7313-732.

Karabulut, M. & Ceylan, N. (2005). The Spectral Reflectance Responses of Water with Different Levels of Suspended Sediment in The Presence of Algae. *Turkish Journal of Engineering and Environmental Sciences*, 29, 351 – 360.

Karimi, P. & Bastiaanssen, M.W. (2015). Spatial Evapotranspiration, Rainfall and Land Use Data in Water Accounting – Part 1: Review of the Accuracy of the Remote Sensing Data. *Hydrology and Earth System Science*, 19: 507–532

Karimi, P., Bastiaanssen, M.G.W., Sood, A., Hoogeveen, J., Peiser, L., Bastidas-Obando, E., Dost, J.R. (2015). Spatial Evapotranspiration, Rainfall and Land Use Data in Water Accounting – Part 2: Reliability of Water Accounting Results for Policy Decisions in the Awash Basin. *Hydrology and Earth System Science*, 19: 533–550.

Kergoat, L. (1998). A Model for Hydrological Equilibrium of Leaf Area Index on a Global Scale. *Journal of Hydrology*, 212–213: 268–286

Ketema, T. & Merkel, J.B. (2009). Estimation of Groundwater Recharge Using a GIS-based Distributed Water Balance Model in Dire Dawa, Ethiopia. *Hydrogeology Journal*, 17: 1443-1457. doi: 10.1007/s10040-009-0455-x

King, M.D., Kaufman, J.Y., Menzel, P.W. & Tanre, D. (1992). Remote Sensing of Cloud, Aerosol and Water Vapor Properties from the Moderate Resolution Imaging Spectrometer (MODIS). *IEEE Transactions on Geosciences and Remote Sensing*, 3(1): 1-27

Kumar, N.D. & Reshmidevi, V.T. (2013). Remote Sensing Applications in Water Resources. *Journal of the Indian Institute of Science*, 93(2): 163-187.

Kustas, P.W. (1990). Estimation of Evapotranspiration with One and Two Layer Model. *Journal of Applied Meteorology*, 29: 704-715

Kustas, P.W., Humes, S.K., Norman, M.J. & Moran, S.M. (1996).Single and Dual Source Modeling of Energy Fluxes with radiometric Surface Temperature.*Journal of Applied Meteorology*, 35:110-120.

Kwast, J., Timmermans, W., Gieske, A., Su, Z., Olioso, A., Jia, L., Elbers, J., Karssenberg, D. & Jong, S. (2009). Evaluation of the Surface Energy Balance System (SEBS) Applied to ASTER Imagery with flux-Measurements at the SPARC 2004 Site (Barrax, Spain). *Hydrological and Earth System Science Discussion*, 6: 1165–1196

Li, F., Jupp, B.D., Thankappan, M., Wang, W.L., Sixsmith, J., Lewis, A., & Held, A. (2015).

Land Surface Brightness Temperature Retrieved from Landsat Data. Paper Presented at 21st International Congress on Modelling and Simulation, Gold Coast, Australia, 29 Nov to 4 Dec 2015.

Li, Q., Kustas, P.W., Anderson, C.M., Prueger, H.J. & Scott, L.R. (2008). Effect of Remote Sensing Spatial Resolution on Interpreting Tower-Based Flux Observations. *Remote Sensing of Environment*, 112: 337–349

Li, Z., Jia, L., Su, Z., Wan, Z., Zhang, R. (2003). A New Approach for Retrieving Perceptible Water from ATSRZ Split-Window Channel Data over Land Area. *International Journal of Remote Sensing*, 24(24): 5095-51 17.

Li, Z., Tang, R., Wan, Z., Bi, Y., Zhou, C., Tang, B., Yan, G. & Zhang, X. (2009).A Review of Current Methodologies for Regional Evapotranspiration Estimation from Remotely Sensed Data. *Sensors*, 9: 3801-3853.doi:10.3390/s90503801

Liang, S. (2001). Narrowband to Broadband Conversions of Land Surface Albedo I: Algorithms. *Remote Sensing of Environment*, 76:213-238

Liang, S. (2003). A Direct Algorithm for Estimating Land Surface Broadband Albedos from MODIS Imagery. *IEEE Transactions on Geoscience and Remote Sensing*, 41(*1*):136-145.

Lin, W., Velde, R. & Su, Z. (2006). Satellite Based Regional-Scale Evapotranspiration in the Hebei Plain, Northeastern China. *Proceedings of the 1st EPS/MetOp RAO Workshop, 15-17 May 2006, ESRIN, Frascati, Italy*

Liu, S., Hu, G., Lu, L. & Mao, D. (2007). Estimation of Regional Evapotranspiration by TM/ETM Data over Heterogeneous Surfaces. *Photogrammetric Engineering & Remote Sensing*, 73(10): 1169-1178.

Liu, W., Hong, Y., Khan, I.S., Huang, M., Vieux, B., Caliskan, S. & Grout, T. (2010). Actual Evapotranspiration Estimation for Different Land Use and Land Cover in urban Regions Using Landsat 5 Data. *Journal of Applied Remote Sensing*, 4(041873).

Liou, Y. Kar, K.S. (2014). Evapotranspiration Estimation with Remote Sensing and Various Surface Energy Balance Algorithms – A Review. *Energies*, 7: 2821-2849. doi:10.3390/en7052821

Landsat Project Science Office (2002). Landsat 7 Science Data User's Handbook. Goddard Space Flight Center, NASA, Washington, DC *Accessed* from http://ltpwww.gsfc.nasa.gov/IAS/handbook/handbook_toc.html on Sunday, July 26, 2015

Lillesand, M.T., Kiefer, W.R. Chipman, W.J. (2005). *Remote Sensing and Image Interpretation* (5th *ed*). John Wiley & Sons: USA.

Lu, D., Mausel, P., Brondizio, E. & Moran, E. (2002). Assessment of Atmospheric Correction Methods for Landsat TM Data Applicable to Amazon Basin LBA Research. *International Journal of Remote Sensing,* 23(13): 2651-2671.

Lu, L., Li, Z.L., Tang, R., Tang, H.B., Wu, H., Yang, F., Labed, J. & Zhou, G. (2012). Evaluating the SEBS-estimated Evaporative Fraction from MODIS Data for a Complex Underlying Surface. *Hydrological Processes*, Accessed from Wiley Online Library on July 25, 2015, doi: 10.1002/hyp.9440

Ly, S., Charles, C. & Degr, A. (2011). Geostatistical Interpolation of Daily Rainfall at Catchment Scale: The Use Of Several Variogram Models in the Ourthe and Ambleve Catchments, Belgium. *Hydrology and Earth System Science*, *15*, 2259–2274.

Ma, E., Deng, X., Zhang, Q. & Liu, A. (2014). Spatial Variation of Surface Energy Fluxes Due to Land Use Changes across China. *Energies*, 7:2194-2206. doi:10.3390/en7042194

Ma, W., Ma, Y. & Ishikawa, H. (2014). Evaluation of the SEBS for Upscaling the Evapotranspiration Based on In-Situ Observations over the Tibetan Plateau. *Atmospheric Research*, 138: 91-97

Macias, F. Arbestain, CM, & Chesworth, W. (2008). Acid Soils. PP 7-11. In Chesworth, W. (eds). *Encyclopedia of Soil Sciences*. Dordrecht, The Netherlands: Springer

Mao, K., Qin, Z., Shi, J. & Gong, P. (2005). A practical Split-Window Algorithm for Retrieving Land-surface Temperature from MODIS Data. *International Journal of Remote Sensing*, 26(15): 3181–3204

Mair, A. & Fares, A. (2011). Comparison of Rainfall Interpolation Methods in a Mountainous Region of a Tropical Island. *Journal of Hydrologic Engineering*, 371-383

Matin, A. & Bourque, P.C. (2013). Influence of Vegetation Cover on Regional Evapotranspiration in Semi-Arid Watersheds in Northwest China. *InTech open Science*, 97-125.

Matinfar R.H. & Soorghali, M. (2014). Estimate Evapotranspiration using SEBS Model based on Landsat 5 (TM) Thermal Data and GIS. *Indian Journal of Fundamental and Applied Life Sciences*, 4 (*3*): 2231-6345

Manninen, T., Korhonen, L., Voipio, P., Lahtinen, P. & Stenberg, P. (2009): Leaf Area Index

(LAI) Estimation of Boreal Forest Using Wide Optics Airborne Winter Photos. *Remote Sensing*, 1(4): 1380–1394.

McCabe, F.M. & Wood, F.E. (2006). Scale Influences on the Remote Estimation of Evapotranspiration Using Multiple Satellite Sensors. *Remote Sensing of Environment*, 105: 271–285

Mengesha Tefera, Tadiwos Chernet & Workineh Haro (1996). *Geological Map of Ethiopia* (2nd ed). Addis Ababa: Geological Survey of Ethiopia and Ministry of Mines.

Mkhwanazi, M., Chávez, L.J. & Rambikur, H.E. (2012). Comparison of Large Aperture Scintillometer and Satellite-based Energy Balance Models in Sensible Heat Flux and Crop Evapotranspiration Determination. *International Journal of Remote Sensing Applications*, 2(*1*): 24-30.

Mo, X., Liu, S., Lin, Z. & Zhao, W. (2004). Simulating Temporal and Spatial Variation of Evapotranspiration over the Lushi Basin. *Journal of Hydrology*, 285: 125–142

Moradizadeh, M., Momeni, M. & Saradjian, M.R. (2008). Estimation of Atmospheric Column and Near Surface Water Vapor Using the Radiance Values of MODIS. *The International Archives of the Photogrammetry, Remote Sensing and Spatial Information Sciences*. XXXVII (Part B8): 523- 528.

Moradizadeh, M., Momeni, M. & Saradjian, M.R. (2010). Enhancing the Accuracy of Water Vapor Estimation by Considering Wet and Dry Conditions in Ratio Technique. Commission VI, WG VI /4, Paper presented at I Canadian Geomatic Conference, June 18th to 19th, 2010 Calgary Canada.

Moore, J.C. (1976). A Comparative Study of Radiation Balance above Forest and Grassland. *Quarterly Journal of the Royal Meteorological Society*, 102(434): 889-899.

Morgan, C.P.R. (2005). *Soil Erosion and Conservation* (3rd *ed*). UK: Blackwell Publishing.

National Water Resources Commision (1972). Geological urvey of the Wabishebele Basin. A Map of Wabishebele Basin with a Scale of 1/1000000 and 1/250000 with Explicit Notes. National Water Resources Commision in collaboration with French Ministry of Foreign Affairs.

Naoki, K., Ukita, J., Nishio, F., Nakamura, K. & Nakayama, K. (2010). Comparison Between

Brightness Temperature and Reflectivity to Thickness of Sea-Ice. International Archives of the Photogrammetry, Remote Sensing and Spatial Information Science, Volume XXXVIII, Part 8, Kyoto Japan 2010

Narasimahan, B. & Srinivasan, R. (2005). Development and Evaluation of Soil Moisture Deficit Index (SMDI) and Evapotranspiration Deficit Index (ETDI) for Agricultural Drought Monitoring. *Agricultural and Forest Meteorology*, 133:69-88.

Norjamaki, I. & Tokola, T. (2007). Comparison of Atmospheric Correction Methods in Mapping Timber Volume with Multi-temporal Landsat Images in Kainuu, Finland. *Photogrammetric Engineering & Remote Sensing*, 73(2): 155–163.

Nouri, H., Beecham, S., Kazemi, F., Hassanli, M.A. & Anderson, S. (2013). Remote Sensing Techniques for Predicting Evapotranspiration from Mixed Vegetated Surfaces, *Hydrology and Earth System Science*, 10: 3897–3925

Nutini, F., Boschetti, M., Candiani, G., Bocchi, S. & Brivio, A.P. (2014). Evaporative Fraction as an Indicator of Moisture Condition and Water Stress Status in Semi-Arid Rangeland Ecosystems. *Remote Sensing*, 6: 6300-6323. doi:10.3390/rs6076300

Oldeman, R.N. & Velthuyzen, T.H (1991).Aspects and Criteria of the Agroecological Zoning Approach of FAO. Working Paper and Preprint 91/07.

Ortega-Farias, S., Irmark, S. & Cuenca, H.R. (2009). Special Issue on Evapotranspiration Measurement and Modeling. *Irrigation Science*, 28: 1–3

Oliver, E.J. (2005). Evapotranspiration. In Oliver, E.J. (ed). *Encyclopedia of World Climatology*. pp 370-373. Springer: Dordrecht, the Netherlands.

Pallant, J. (2007). SPSS *Survival Manual: A Step by Step Guide to Data Analysis Using SPSS for Windows* (3rd ed). Open University Press: New York.

Parodi, G. (2007). SEBS for ILWIS Open 3.4: An Interface for Surface Energy Balance in ILWIS Open Source. A Lecture not Presented in ITC Department of Water Resources Management

Paulson, A.C. (1970). The Mathematical Representation of Wind Speed and temperature Profiles in the Unstable Atmospheric Surface Layer. *Journal of Applied Meteorology*, 9:857-861

Peng, J., Liu, Y., Zhao, X. & Loew, A. (2013). Estimation of Evapotranspiration from MODIS TOA Radiances in the Poyang Lake Basin, China. *Hydrological Earth System Science*, *17*: 1431–1444.

Peng, J., Fan, W., Xu, X., Wang, L., Liu, Q., Li, J. & Zhao, P. (2015). Estimating Crop Albedo in the Application of a Physical Model Based on the Law of Energy Conservation and Spectral Invariants. *Remote Sensing*, 7: 15536-15560. doi:10.3390/rs71115536

Pereira, A. & Pires, L. (2011). Evapotranspiration and Water Management for Crop Production. In Gerosa, G. (ed). Evapotranspiration - From Measurements to Agricultural and Environmental Applications. Accessed from http://cdn.intechopen.com/pdfs-wm/22694.pdf on January 11, 2016

Petitcolin, F. & Vermote, E. (2002). Land Surface Reflectance, Emissivity and Temperature from MODIS Middle and Thermal Infrared Data. *Remote Sensing of Environment*, 83:112 – 134

Petropoulos, P.G., Carlson, N.T. & Griffiths, M.H. (2014). Turbulent Fluxes of Heat and Moisture at the Earth's Land Surface: Importance, Controlling Parameters, and Conventional Measurement Techniques. In Petropoulos, P.G.(ed). *Remote Sensing of Energy Fluxes and Soil Moisture Content*. CRC Press: London.

Pinheiro, T.C., Descloitres, J., Privette, L.J., Susskind, J., Iredell, L. & Schmaltz, J. (2008). Near-real Time Retrievals of Land Surface Temperature within the MODIS Rapid Response System. *Remote Sensing of Environment*, 106: 326–336

Proud, R.S., Rasmussen, O.M., Fensholt, R., Sandholt, I., Shisanya, C., Mutero, W., Mbow, C. & Anyamba, A. (2010). Improving the SMAC atmospheric correction code by analysis of Meteosat Second Generation NDVI and surface reflectance data. *Remote Sensing of Environment*, 114: 1687–1698

Qin, Z., & Berliner, A. & Karnieli, P. (2001). A Mono-Window Algorithm for Retrieving Land Surface Temperature from Landsat TM Data and Its Application to the Israel-Egypt Border Region. *International Journal of Remote Sensing*, 22(*18*): 3719– 3746

Raes, D. (2009). The ET_o Calculator – Evapotranspiration from a Reference Surface: Reference Manual. Food and Agriculture Organization of the United Nations Land and Water Division, FAO: Rome, Itlay.

Rahman, H. and Dedieu, G. (1994). SMAC: A Simplified Method for the Atmospheric Correction of Satellite Measurements in the Solar Spectrum. *International Journal of Remote Sensing*, 15(I):123-143.

Richter, R. & Schlifer, D. (2015). Atmospheric/Topographic Correction for Satellite Imagery:

ATCOR 2/3 User Guide, Version 9.0.0. DLR-IB 565-01/2015, Wessling, Germany.

Riihela, A., Manninen, T. & Anderson, K. (2013). Algorithm Theoretical Basis Document SAF MSG Surface Albedo: Edition 1.

Roerink, J.R., Su, Z., Menenti, M. (2000). S-SEBI: A Simple Remote Sensing Algorithm to Estimate the Surface Energy Balance. *Physics and Chemistry of Earth*, 25(2): 147-157

Ruhoff, R.A., Paz, L.A., Collischonn, W., Aragao, C.L., Rocha, R.H. & Malhi, S.Y. (2014). A MODIS-Based Energy Balance to Estimate Evapotranspiration for Clear-Sky Days in Brazilian Tropical Savannas. *Remote Sensing*, 4: 703-725. doi:10.3390/rs4030703

Sailor, J.D. (1995). Surface Climate Response to Modifications in Surface Albedo and Vegetation Cover. *Journal of Applied Meteorology*, 34:1694-1704

SAF ATBD (2010). SAF for Land Surface Analysis (LSA SAF): Algorithm Theoretical Basis Document. Version 1.2. Accessed from

SAF PUM (2015). The EUMETSAT Satellite Application Facility on Land Surface Analysis (LSA SAF): Evapotranspiration (ET) Product User Manual. Version 2.5. *Accessed* from

Santos, D.C., Bezerra, G.B., Silva, B.B. & Rao, R.T. (2010). Assessment of Daily Actual Evapotranspiration with SEBAL and S-SEBI Algorithms in Cotton Crop. *Revista Brasileira de Meteorologia*, 25(3), 383 – 392.

Schaaf, B.C., Gao, F., Strahler, H.A., Lucht, W., Li, X., Tsang, T. *et al*. (2002). First Operational BRDF, Albedo Nadir Reflectance Products from MODIS. *Remote Sensing of Environment*, 83: 135 – 148.

Schaaf, B.C. (2009). *Albedo and Reflectance Anisotropy*. Global Terrestrial Observing System: Rome

Sekertekin, A., Kutoglu, H.S., Kaya, S. & Marangoz, M.A. (2015). Analysing the Effects of Different Land Cover Types on Land Surface Temperature Using Satellite Data. *The International Archives of the Photogrammetry, Remote Sensing and Spatial Information Sciences*, Volume XL-1/W5. doi:10.5194/isprsarchives-XL-1-W5-665-2015

Senay, G. (2015). Drought monitoring and Impact Assessment Using Satellite-derived Evapotranspiration. *NASA IDS: Seasonal Prediction of Hydro-Climatic Extremes in the Greater Horn of Africa (GHA): The Second Participatory Research Workshop and Project Meeting; July 28-29, 2015; Addis Ababa Ethiopia*

Sharma, R.A., Badarinath, V.K. & Roy, S.P. (2008). Corrections for Atmospheric and Adjacency

Effects on High Resolution Sensor Data - A Case Study Using IRS-P6 LISS-IV Data. *The International Archives of the Photogrammetry, Remote Sensing and Spatial Information Sciences*. XXXVII (Part B8): 497- 501

Shoko, C., Dube, T., Sibanda, N. & Adelabu, S. (2015). Applying the Surface Energy Balance System (SEBS) Remote Sensing Model to Estimate Spatial Variations in Evapotranspiration in Southern Zimbabwe. *Transactions of the Royal Society of South Africa*, 70(*1*): 47–55

Silva, J., Ribeiro, C., Guedes, R. (n.d). Roughness Length Classification of Corine Land Cover Classes. *Accessed* on december 3, 2015 from http://www.megajoule.pt/img_upload/Publications/545_Ewec2007fullpaper1.pdf

Simic, A., Fernandes, R. & Wang, S. (2014). Assessing the Impact of Leaf Area Index on Evapotranspiration and Groundwater Recharge across a Shallow Water Region for Diverse Land Cover and Soil Properties. *Journal of Water Resource and Hydraulic Engineering*, 3(4): 60-73.

Smets, B., Jacobs, T. & Swinnen, E. (2015). Normalized Difference Vegetation Index (NDVI): Product User Manual. *Accessed* from

Spaargaren, O. (2008). Vertisols. Pp 807-809. In In Chesworth, W. (eds). *Encyclopedia of Soil Sciences*. Dordrecht, The Netherlands: Springer

Sobrino, A.J. and Kharraz, J. E. & Li, Z.L. (2003). Surface Temperature and Water Vapor Retrieval from MODIS Data. *International Journal of Remote Sensing*, 24(24): 5161–5182

Su, Z. (2002). The Surface Energy Balance System (SEBS) for Estimation of Turbulent Heat Fluxes. *Hydrology and Earth System Sciences*, 6(1): 85-99

Su, Z. (2005). Estimation of the Surface Energy Balance. In Anderson, G.M. & McDonnell, J.J. (eds). *Encyclopedia of Hydrological Sciences*. John Wiley & Sons Ltd: West Sussex, England. Pp.731-752

Su, Z. (2005). SEBS Surface Energy Balance System for Estimation of Turbulent heat Fluxes and Evapotranspiration. Lecture Note for Advanced Training Course on Land Remote Sensing. Lecture No. D1La6. International Institute for Geo-Information Science and Earth Observation (ITC), Enschede, The Netherlands.

Su, Z. (2009). SEBS: Surface Energy Balance System for Estimation of Turbulent Heat Fluxes

and Evapotranspiration. *A Lecture note for ESA Advanced Training Course on Land Remote Sensing. 28 June to 3 July, 2009. Accessed from*

Su, Z. and C. Jacobs. (2011). ENVISAT: actual evaporation. BCRS Report 2001: USP-2 Report 2001 01-02, Beleidscommissie Remote Sensing (BCRS), Delft, 2001.

Tabachnick, G.B. & Fidell, S.L. (2013). *Using Multivariate Statistics* (6th *ed*). Pearson Education, Inc: USA.

Taha, H. (1997). Urban Climates and Heat Islands: Albedo, Evapotranspiration, and Anthropogenic Heat. *Energy and Buildings*, 25: 99-103

Takashima, Y. & Masuda, K. (1987). Emissivities of Quartz and Sahara Dust Powers in the Infrared Region (7 – 17Am). *Remote Sensing of Environment*, 23:51 – 63.

Tanaka, K., Takizawa, H., Tanaka, N., Kosaka, I., Yoshifuji, N., Tantasirin, C., Piman, C., Suzuki, M. & Tangtham, N. (2003).Transpiration Peak over a Hill Evergreen Forest in Northern Thailand in the Late Dry Season: Assessing the Seasonal Changes in Evapotranspiration Using a Multilayer Model. *Journal of Geophysical Research*, 108, (D17), 4533. doi:10.1029/2002JD003028

Tang, R., Li, Z., Jia, Y., Li, C., Chen, K., Sun, X. & Lou, J. (2013). Evaluating One and Two Source Energy Balance Models in Estimating Surface Evapotranspiration from Landsat-derived Surface Temperature and Field Measurements. *International Journal of Remote Sensing*, iFirst: 1–15

Teklebirhan Arefaine, Dessie Nedaw,Tesfamichael Gebreyohannes (2012). Groundwater Recharge, Evapotranspiration and Surface Runoff Estimation Using WetSpass Modeling Method in Illala Catchment, Northern Ethiopia. *Momona Ethiopian Journal of Science*, 4(*2*): 96-110

Temesgen Enqu, Tol, C., Assefa Melesse, Semu Moges & Gieske, A. (2014).Multi-model Approach for Spatial Evapotranspiration Mapping: Comparison of Models Performance for Different Ecosystems. In Assefa Melesse, Wossenu Abtew Shimelis & Setegn, G. (eds). *Nile River Basin: Ecohydrological Challenges, Climate Change and Hydropolitics*. Springer: Switzerland. Pp. 285-305

Tenalem Ayenew (2003). Evapotranspiration Estimation Using Thematic Mapper Spectral Satellite Data in the Ethiopian Rift and Adjacent Highlands. *Journal of Hydrology*, 279: 83–93.

Tenalem Ayenew (2004). Surface Kinetic Temperature Mapping Using Satellite Spectral Data in Central Main Ethiopian Rift and Adjacent Highlands. *SINET: Ethiopian Journal of Sciences*, 24(1): 51-68.

Temesgen Enku, Tol, C., Assefa Mekonnen., Semu A. & Gieske, A. (2014). In Assefa Mekonnen, Wossenu Abtew & Shimelis G. (eds). *Nile River Basin: Ecohydrological Challenges, Climate Change and Hydropolitics*. Springer: New York. Pp. 285-305.

Tewelde Yideg (2012). Assessing the Potential of Geonetcast Earth Observation and *In-situ* Data for Drought Early Warning and Monitoring in Tigray, Ethiopia. Unpublished Master's Thesis Submitted to University of Twente Faculty of Geoinformation Science and Earth Observation.

Timmermans, J., Su, Z., Tol, C., Verhoef, A. & Verhoef, W. (2013).Quantifying the Uncertainty in Estimates of Surface–atmosphere Fluxes through Joint Evaluation of the SEBS and SCOOPE Models. *Hydrological and Earth System Sciences*, 17: 1561–1573

Tinebeb Yohannes (2012). Remote Sensing Evapotranspiration Using Geonetcast and In-situ Data Streams for Drought Monitoring and early Warning: Case Study for Amhara Regional State in Ethiopia. Unpublished Masters Thesis Submitted University of Twente Faculty of Geoinformation Science and Earth Observation.

Toller, G. N., Isaacman, A., Kuyper, J. & Salomonson, V. (2006). MODIS Level 1B Product User's Guide, Greenbelt, MD: NASA/Goddard Space Flight Center

Trenberth, E.K., Smith, L., Qian, T., Dai, A. & Fasulo, J. (2006). Estimates of the Global Water Budget and Its Annual Cycle Using Observational and Model Data. *Journal of Hydrometeorology - Special Section*, 8, 758- 769.

Trishchenko, P.A., Cihlar, J. & Li, Z. (2002). Effects of Spectral Response Function on Surface Reflectance and NDVI Measured with Moderate Resolution Satellite Sensors. *Remote Sensing of Environment*, 81:1–18.

Troen, I., & Lundtang Petersen, E. (1989). *European Wind Atlas*. Roskilde: Risø National Laboratory

Tsouni, A., Kontoes, C., Koutsoyiannis, D., Elias, P. & Mamassis, N. (2008). Estimation of Actual Evapotranspiration by Remote Sensing: Application in Thessaly Plain, Greece. *Sensors*, 8: 3586-3600; doi: 10.3390/s8063586

Wang, L., Parodi, G.N. & Su, Z. (2008). SEBS Module BEAM: A Practical Tool for Surface

Energy Balance Estimates from Remote Sensing Data. Proceedings of the 2nd MERIS / (A) ATSR User Workshop, Frascati, Italy 22–26 September 2008 (ESA SP-666, November 2008).

Wilson, R.T., Milton, E.J. & Nield, J.M. (2014). Spatial Variability of the Atmosphere over Southern England, and Its Effect on Scene-based Atmospheric Corrections. *International Journal of Remote Sensing*,

Wossenu Abtew & Assefa Melese (2013). *Evaporation and Evapotranspiration: Measurements and Estimations*. Springer: Dordrech, The Netherlands.

Ukkola, M.A. & Prentice, C.I. (2013). A Worldwide Analysis of Trends in Water-Balance Evapotranspiration. *Hydrology and Earth System Science*, 17: 4177–4187

USAID Biodiversity Analysis and Technical Support Team (2008). Ethiopia Biodiversity and Tropical Forests Assessment Report 118/119. USAID

Valor, E. and Caselles, V. (1996). Mapping Land Surface Emissivity from NDVI: Applications to European, African and South American Areas. *Remote Sensing of Environment*, 57:167-184.

Verhoef, A., McNaouton, K.G. & Jacobs, G.F. (1997). A Parameterization of Momentum Roughness Length and Displacement Height for a Wide Range of Canopy Densities. *Hydrology and Earth System Science*, 1: 81-91.

Vorosmarty, C.J., Federer, A.C. & Schloss, A.L. (1998). Potential Evaporation Functions Compared on US Watersheds: Possible Implications for Global-Scale Water Balance and Terrestrial Ecosystem Modeling. *Journal of Hydrology*, 207: 147–169

Waters, R., Allen, R., Tasumi, M., Trezza, R. & Bastiaanssen, W. (2002). SEBAL (Surface Energy Balance Algorithms for Land) - Idaho Implementation: Advanced Training and Users Manual. Version 1.0. *Accessed* on 28 October 2015 from http://www.usask.ca/watershed/pdf/Aberdeen_lab_readings_2015/sebal_Manual_2000.pdf

Weng, Q., Lu, D. & Schubring, J. (2004). Estimation of Land Surface Temperature – Vegetation Abundance Relationship for Urban Heat Island Studies. *Remote Sensing of Environment*, 89: 467-483

Wolters, E., Dierckx, W., Dries, J. & Swinnen, E. (2014). PROBA-V Products User Manual v1.1. *Accessed* from

Wondimagegn, S. (2006). Remote Sensing Analysis of Summer Time Evapotranspiration Using SEBS Algorithm: A Case Study in Regge and Dinkel, The Netherlands. Unpublished Masters Thesis Submitted University of Twente Faculty of Geoinformation Science and Earth Observation

Williams, G.R. (1984). *Introduction to Statistics for Geographers and Earth Scientists*. Macmillan Publishers Ltd: London.

Yale Center for Earth Observation (2014). Obtaining and Processing MODIS Data. Retrived from http://www.yale.edu/ceo/Documentation/*MODIS*_data.pdf on 24 July 2015.

Yan, W.J., Liu, Y.J., Chen, Z.B., Feng, M., Fang, F.S., Xu, G., Zhang, H.F. *et al*. (2014). Changes in the Land Surface Energy Budget in Eastern China over the Past Three Decades: Contributions of Land-Cover Change and Climate Change. *Journal of Climate, 27*: 9233- 9252.

Yang, Y. (2015).*Evapotranspiration over Heterogeneous Vegetated Surfaces*. Springer-Verlag: Berlin.

Zeng, N. & Woon, J. (2009). Expansion of the World's Deserts Due to Vegetation-Albedo Feedback under Global Warming. *Geophysical Research Letters*, 36(L17401). doi:10.1029/2009GL039699

Zerihun Woldu (1999). Forests in the Vegetation Types of Ethiopia and their Status in the Geographical Context. Paper presented at Forest Genetic Resources Conservation Strategy Development Workshop, June 1999. Addis Ababa, Ethiopia.

Zhang, K., Kimball, S.J., Mu, Q., Jones, A.L., Goetz, J.S. & Running, W.S. (2009). Satellite Based Analysis of Northern ET Trends and Associated Changes in the Regional Water Balance from 1983 to 2005. *Journal of Hydrology*, 379: 92–110

Zhang, K., Kimball, S.J., Nemani, R.R. & Running, W.S. (2010). A Continuous Satellite-derived Global Record of Land Surface Evapotranspiration from 1983 to 2006. *Water Resources Research*, 46(W09522). doi:10.1029/2009WR008800

Zhang, H., Lu, L., Liu, Y. & Liu, W. (2015). Spatial Sampling Strategies for the Effect of Interpolation Accuracy. *ISPRS International Journa*l of *Geo-Information, 4*: 2742-2768; doi:10.3390/ijgi4042742

Zhang, T., Wen, J., Velde, R., Meng, X., Li, Z., Liu, Y. & Liu, R. (2008). Estimation of the Total

Atmospheric Water Vapor Content and Land Surface Temperature Based on AATSR Thermal Data. *Sensors*, 8: 1832-1845.

Zotarelli, L., Dukes, D.M., Romero, C.C., Migliaccio, W.K. & Morgan, T.K. (2009). Step by Step Calculation of the Penman-Monteith Evapotranspiration (FAO-56 Method). Agricultural and Biological Engineering Department, Florida Cooperative Extension Service, Institute of Food and Agricultural Sciences, University of Florida. *Accessed* from http://edis.ifas.ufl.edu on August 2, 2015

Zoungrana, B.B., Conrad, C., Amekudzi, K.L., Thiel, M. & Da, D.E. (2015). Land Use/Cover Response to Rainfall Variability: A Comparing Analysis between NDVI and EVI in the Southwest of Burkina Faso. *Climate*, 3, 63-77; doi:10.3390/cli3010063

APENDICES

I. Merged GlobCover

Code	Key	Merged to
14	Rain-fed croplands	Crop land
20	Mosaic cropland (50-70%) / vegetation (grassland/shrub land/forest) (20-50%)	
30	Mosaic vegetation (grassland/shrub land/forest) (50-70%) / cropland (20-50%)	Grass land
120	Mosaic grassland (50-70%) / forest or shrub land (20-50%)	
140	Closed to open (>15%) herbaceous vegetation (grassland, savannas or lichens/mosses)	
40	Closed to open (>15%) broadleaved evergreen or semi-deciduous forest (>5m)	Forest
60	Open (15-40%) broadleaved deciduous forest/woodland (>5m)	
130	Closed to open (>15%) (broadleaved or needle leaved, evergreen or deciduous) shrub land (<5m)	
150	Sparse (<15%) vegetation	Wood land
170	Closed (>40%) broadleaved forest or shrub land permanently flooded - Saline or brackish water	Wet land
180	Closed to open (>15%) grassland or woody vegetation on regularly flooded or waterlogged soil - Fresh, brackish or saline water	
190	Artificial surfaces and associated areas (Urban areas >50%)	Built up
200	Bare areas	Bare land
210	Water bodies	Water bodies
110	Mosaic forest or shrub land (50-70%) / grassland (20-50%)	Shrub land

II. Merged Agro-ecology

Cod	Detailed Agro-ecology	Merged to
A1	Hot to Warm Arid Lowland Plains	Arid
A2	Tepid to Cool Arid Mid Highlands	
H2	Tepid to Cool Humid Mid Highlands	Humid
H3	Cold to Very Cold Humid Mid Highlands	
M1	Hot to Warm Sub-Moist Lowlands	moist
M2	Tepid to Cool Moist Mid Highlands	
M3	Cold to Very Cold Moist Sub-Afroalpine to Afroalpine	
SA1	Hot to Warm Semi-Arid Lowlands	Semi-arid
SA2	Tepid to Cool Semi-Arid Mid-Highlands	
SH1	Hot to Warm Sub-Humid Lowlands	Sub-humid
SH2	Tepid to Cool Sub-Humid Lowlands	
SH3	Tepid to Cool Sub-Humid Sub-Afroalpine to Afroalpine	
SM1	Hot to Warm Sub-Moist Lowlands	Sub moist
SM2	Tepid to Cool Sub-Moist Mid-Highlands	
SM3	Cold to Very Cold Sub-Moist Sub-Afroalpine to Afroalpine	